Mohamed Khider University, Biskra

Faculty of Science and Technology

Department of Electrical Engineering

MASTER'S THESIS

Science and Technology

Electrical Engineering

Renewable energy in electrical engineering

Ref:

Presented and supported by:

CHAREF KHODJA Imane & ELHAMDI Fatima Zohra

On: Monday 26 Mai 2025

Power optimization of a floating PV station -Part 01

Jury:

Pr. MAHDAD Belkacem	PR	University of Biskra	Chairman
Pr. SAADI Aicha	MCA	University of Biskra	Examiner
Pr. MOUSSI Ammar	PR	University of Biskra	Supervisor

Academic year: 2024/2025

Mohamed Khider University, Biskra

Faculty of Science and Technology

Department of Electrical Engineering

MASTER'S THESIS

Science and Technology

Electrical Engineering

Renewable energy in electrical engineering

Ref:

On: Monday 26 Mai 2025

Power optimization of a floating PV station-Part 01

Presented by:

CHAREF KHODJA Imane & ELHAMDI Fatima Zohra

Favorable opinion of the supervisor:

Pr. MOUSSI Ammar

Signature Favorable opinion of the Chairman of the Jury

Stamp and signature

Acknowledgements:

First of all, we would like to express our deep gratitude to our supervisor, **Pr. MOUSSI Ammar**, for his advice, expertise and support throughout our research journey.

We would like to thank the distinguished follow-up committee chaired by **Professor Mehdad Belkacem** and discussant **Professor Saadi Aisha** for their excellent guidance.

We would also like to thank **Mr. Mohammed LAAOUAD** for his help.

We would also like to thank our parents, siblings and friends for their support and encouragement.

Our sincere thanks also go to the staff of the Electrical Engineering, Renewable Energy Laboratories in Biskra for their assistance during the experimental phase.

Finally, we salute the authors and researchers whose work has influenced our study. To all those who contributed in any way, we sincerely thank you for your invaluable support.

الإهداء

"العلِم زادُ الأرواح، ورفيقُ الطريق لمن أراد أن يسمو بنَفسه ويترك أثراً لا يزول"...

الحمد لله الذي علّم الإنسان ما لم يعلم، ورفع بالعلم أهله، وقرن طلبه بالعبادة والسعي. الحمد لله على النعم التي لا تُعد، وعلى العطاء الذي لا ينضب، وعلى اللطف الذي يرافقنا حين تثقل الخُطى، وعلى الأحبة الذين كانوا لنا نورًا في طريق طويل.

إلى **أبي** ...من زرع فينا حب العلم، وآمن بنا قبل أن ندرك حجم الطريق، كنت السند الصامت والدعاء الدائم، وكنت الأمان حين ضاقت السُبل... فلك كل الشكر والدعاء.

إلى **أمي** ...النور الذي لا يخبو، والدفء الذي لا يبرد، كنتِ الحاضنة لأحلامي، والملهمة لعزيمتي، علمتني أن النجاح يُولد من الصبر والدعاء. إليكِ أهدي كل فرحة، وكل لحظة وصلتُ فيها إلى هدفي.

إلى **أختي وفاء** ...يا رفيقة الطفولة والضحكات الخفيفة، يا يد الخير والمساندة، كنتِ دائمًا النبض الجميل في أيامي .

إلى **أخي وليد** ...الداعم بصمت، الحاضر بقلبه الكبير، شكرًا لأنك كنت الأمان حين احتجت السند .

إلى **أخي جابر** ...الذي أفتخر به، صاحب القلب النقي والبسمة الطيبة، حضورك في حياتي نعمة لا تقدّر بثمن.

إلى صديقتي الأقرب، **فطيمة** ...كنتِ أكثر من رفيقة، كنتِ أختًا للروح، كنتِ الحضن الذي لا يخذل، فلكِ من القلب ألف محبة وامتنان.

إلى **روضة**، الجميلة اسمًا وصفة... يا من جمعتني بها الحياة بمحبة صادقة ونية خالصة، أرجو من الله أن يديم وصلنا ويكتب لنا لقاءً في جناتّه كما جمعنا في الدنيا.

إلى **منار**، التي كانت للروح طمأنينة، ولبالي سكينة... يا من تحملين الخير في ملامحكِ ، لكِ كل التقدير والدعاء.

إلى **مروى**، الزهرة التي لا تذبل، الحضور الهادئ المشرق، يا من كانت صحبتكِ من أجمل ما وهبتني الأيام.

إلى **كوثر**، الأديبة الحنونة، التي تكتب الحب في ملامحها قبل كلماتها، يا من كنتِ لقلبي ملاذاً من السكينة والدعم.

وإلى **نسيمة**، الحاضرة في القلب دائمًا، يا من كنتِ رفيقة المحبة والدعاء، ووجهًا مشرقاً في محطات التعب والفرح.

وإلى كل من شاركني الرحلة، في لحظة تعب، أو ابتسامة، أو دعاء خفي...

هذا النجاح ليس لي وحدي، بل هو امتداد لكل من كان لي سندًا... شكرًا من القلب، حتى يرضى الله

الإهداء:

"العلم ما كان في القلبِ نوره و الجهل ماكان في القلب ظُلماه"...

الحمد لله .. الذي علّم بالقلم ، و رَفع بالعِلمِ اقواما .. حمدًا يليق بجلال وجهه وعظيم سلطانه، على نعمٍ لا تُعد، وعلى عطاءٍ لا ينضب،حمدًا على القوّة حين خارت عزائمنا، وعلى السند حين ثقلت الخطى، وعلى نعمة الأحبة الذين كانوا لنا وطنًا قبل أن نصل.

إلى أبي .. من حمل همّ العلم عنّا قبل أن نعرف اسمه ، يُراقب ، يُساند و يزرع فينا قناعة ان طلب العلم عبادة و أَنّ النجاح لا يُهدى ، بل يُنتزع بالكدّ و الدعاء و العمل ، فله من القلب شكرا لا تفيه الحروف و دعاء لا يغيبُ عن السّجود

إلى أمي التي تُشبه الصباح حين يبتسم ، التي كانت و لا تزال منارةُ حياتي صناعة احلامي و ملهمة عزيمتي لكِ أُهدي نجاحي و أهدي لكِ قلبي كلّه ..

إلى أختي الكبرى مجدة، أمّي الثانية، في حنانكِ ملاذ، وفي قوتكِ درع، كنتِ ظلًا لا يغيب.

إلى أختي دعاء، المهندسة التي تحمل في عينيها بريق المستقبل، يا رفيقة القلب والنفس، يا حلمًا آمنًا...

إلى أخي مصعب، السند .. دمت لي اخا و أمانا

إلى الصغار روعة وشمس وغيث، يا عناقيد الفرح، ويا بهجة الأيام، وجودكم هو أجمل المعاني التي عرفها قلبي.

وإلى الصديقة الرفيقة إيمان، التي شاركتني العمل، الحلم، والكدّ خطوة بخطوة، كنتِ سندًا لا يُعوّض، ووجهًا للوفاء لا يغيب..

وإلى مروة، الدكتورة صاحبة القلب الكبير والروح الإيجابية التي تبعث الأمل أينما حلّت،

وإلى روضة الجميلة كما اسمها، أدعو الله أن يجمعنا في روضةٍ من رياض الجنة كما جمعتنا الحياة بمحبة صادقة.

وإلى كوثر، الأديبة التي خطّت دواوين الدفء بوجودها، ونسجت من الكلمات مرافئ للسكينة.

منار .. الممرضة المُهندسة و كما أسميتك دائماالمجاهدة

وإلى خالتي العزيزة، التي احتوتني كالوطن، وكانت لي حضنًا من الراحة والدعاء، أسأل الله لها الشفاء التام والسعادة التي تليق بقلبها الطيب.وإلى كل زملائي الذين شاركوني أيام الجدّ والسهر والتحدي،وكل من ترك أثرًا جميلًا في مسيرتي، ولو بكلمة، بابتسامة، أو حتى بصمتٍ مُطمئن...لكم جميعًا...

هذا النجاح ليس لي وحدي، بل هو قطعة منكم، وامتداد لجميلكم، فشكرًا حتى يرضى الله

Abstract

With the growing adoption of solar energy as a photovoltaic source, challenges related to large land occupation have emerged, potentially affecting residential and agricultural areas. As an alternative, the concept of floating photovoltaic power plants were developed. Initially this procedure was implemented on dams and reservoirs, and later expanded to high-capacity installations. In this work, we designed an experimental prototype of a floating photovoltaic station, alongside a thermal simulation model designed using Simulink to compare the performance of ground-mounted and floating solar panels**.** The results highlighted the superior thermal performance of floating systems, due to the natural cooling effect of water, providing more cooling than ground-mounted systems. In addition, the tracking effect was also investigated. It was show that the tracking offers higher power output.

Keywords : Floating solar power plants, Natural cooling, Photovoltaic, Thermal performance.

الملخص

مع تزايد الاعتماد على الطاقة الشمسية كمصدر كهروضوئي ، ظهرت تحديات تتعلق بإستهلاكها لمساحات واسعة ، مما قد يؤثر على الأراضي السكنية و الزراعية ، كحل بديل . تم تطوير مفهموم الطاقة الكهروضوئية العائمة ، حيث نفذت أولى المشاريع فوق السدود و الخزانات ، و تطورت لاحقا لتشمل محطات بقدرات عالية . في هذا العمل ؛ قمنا بإنجاز نموذج تجريبي لمحطة كهروضوئية عائمة إلى جانب محاكاة لنموذج حراري يقارن بين خلايا الشمسية الأرضية و العائمة ، و أظهرت النتائج أن الأداء الحراري للخلايا الشمسية العائمة أفضل بفضل تأثير التبريد الطبيعي للماء مقارنة بالخلايا الكهروضوئية في الأرض . بالإضافة إلى ذلك، تم أيضًا فحص تأثير عملية تتبع القيمة القصوى MPPT, وقد تبين أن التتبع يوفر خرج طاقة أعلى.

الكلمات المفتاحية : الطاقة الشمسية العائمة، التبريد الطبيعي، الطاقة الكهروضوئية، الأداء الحراري .

Résumé

Avec l'essor de l'énergie solaire comme source photovoltaïque**,** des défis liés à l'occupation de vastes espaces ont émergé, impactant les zones résidentielles et agricoles**.** En réponse, le concept de centrales photovoltaïque flottantes a été développé, initialement installé sur des barrages et réservoirs, avant d'évoluer vers des installations de grande capacité. Dans ce travail, nous avons réalisé un modèle expérimental d'une station photovoltaïque flottante, ainsi qu'une simulation thermique à l'aide de Simulink, comparant les performances de cellules solaires terrestres et flottantes**.** Les résultats ont mis en évidence une meilleure efficacité thermique des cellules flottantes, grâce à l'effet de refroidissement naturel de l'eau, offrant un refroidissement par rapport aux systèmes terrestres. En outre, l'effet de poursuite (MPPT) a également été étudié et il a été démontré que cette procédure offre une puissance de sortie plus élevée.

Mots clés : Centrales Photovoltaïques flottantes, Refroidissement naturel, Photovoltaïque, Efficacité thermique.

Table of Contents

Chapter II: Floating Photovoltaic Systems and Power Optimization

Chapter IV: Practical Implementation /simulation and results

List of figures

List of Tables

General Introduction

General Introduction:

With the global demand for clean energy steadily rising and climate change becoming an urgent concern, solar energy has established itself as a vital pillar in the transition to renewable sources. However, deploying large-scale solar technologies has not been without its obstacles. Limited land availability, high land acquisition costs, and the environmental footprint of terrestrial solar installations have all posed major challenges. On average, ground-mounted solar power plants require 1.5 hectares per megawatt of installed capacity, often competing with agricultural and urban land use.[1]

In light of these limitations, the concept of Floating Photovoltaic (FPV) systems emerged. First introduced in Japan in 2007, FPV systems utilize unused water surfaces—such as reservoirs, lakes, and dams to host solar panels. This novel approach not only preserves valuable land but also enhances energy efficiency, with studies showing up to 15% higher output due to the natural cooling effect of water. Moreover, FPV systems can significantly reduce water evaporation by up to 70%[2], making them a dual-purpose solution in regions facing water scarcity. While promising, this technology also introduces new engineering and maintenance challenges related to structural stability, corrosion, and the operation of electrical systems in aquatic environments.

This thesis aims to explore the potential, design, and performance of floating photovoltaic power systems from both theoretical and experimental perspectives. It is structured into four interconnected chapters:

The first chapter provides a foundational understanding of solar energy, including the nature of solar radiation, solar angles, types of solar energy (thermal and photovoltaic), and the basic electrical characteristics of PV cell systems.

The second chapter explores the domain of floating photovoltaic energy, offering a detailed look at the definition and classification of FPV systems, suitable water bodies, technical components, and the thermal, electrical, environmental, and economic benefits. It also examines real-world FPV projects and traces their development from 2007 to the present day. The third chapter focuses on the simulation of photovoltaic panel performance in floating environments. It emphasizes the thermal modeling of the solar cell, accounting for environmental variables such as ambient temperature, solar irradiance, and wind speed.

Finally, the fourth chapter is dedicated to the practical implementation of the proposed system and is divided into two main sections. The first section outlines the design and construction of a scaled-down floating photovoltaic (FPV) system, covering the mechanical floating structures, electrical circuitry, and integrated sensors. The second section presents a comparative analysis between the simulated and experimental results, emphasizing the performance differences between ground-based and floating PV systems. As part of this analysis, we also examined the impact of incorporating a solar tracking mechanism. This comprehensive evaluation provides valuable insights into improving the efficiency, adaptability, and overall performance of floating solar installations.

Chapter I
Solar Photovoltaic Energy Fundamentals

I-1 Introduction:

The intensive use of fossil fuels, which were an essential resource for the previous industrial revolutions in the past centuries, raised a number of problems for the very long term nowadays. Firstly, one is dealing with exhaustible resources which are essential and on which, therefore, one may not expect that a very long-term growth be founded. Secondly, the use of these fossil fuels leads to long term environmental problems, such as acid rains and greenhouse effects, which are typically negative externalities.

Under these conditions, there is growing interest for renewable and environment-friendly energy sources such as solar energy, on which some kind of sustainable growth may be based. Solar energy is indeed a renewable source of energy, the use of which avoids most of the negative repercussions due to the use of fossil fuels. For our country, the most promising issue is The solar photovoltaic systems, in which energy is produced as a direct result of the conversion of the energy of the solar ray, using the so-called photovoltaic effect.

I-2 Solar radiation:

All radiant energy originates from the Sun, that enormous ball of fire that has been there for 4.5 billion years. It is situated around 150 million kilometers away from Earth and is seen in our sky as a calm and bright disk. The sun is 100 times bigger than our planet and has a radius of 696,000 km. Its mass is equivalent to 333,000 Earths put together.

The Sun, which is mostly made of hydrogen and helium, is a real energy factory. It releases electromagnetic radiation with a maximum intensity in the visible light spectrum that travels at an astounding 300,000 km/s across a spectrum of frequencies as wide as it is interesting.

The Sun releases an enormous 3.85 × 10^26 W of power every second. However, only 1.9 × 10^{17} W, or a very little portion of this energy reaches our planet. Even though it is little, this energy is what keeps life on Earth going.

The solar star is our planet's primary companion as it orbits the Sun in a somewhat elliptical pattern. The distance between them fluctuates by ±1.69% throughout the course of the year, like a cosmic dance that is determined by the eccentricity of our orbit. [2]

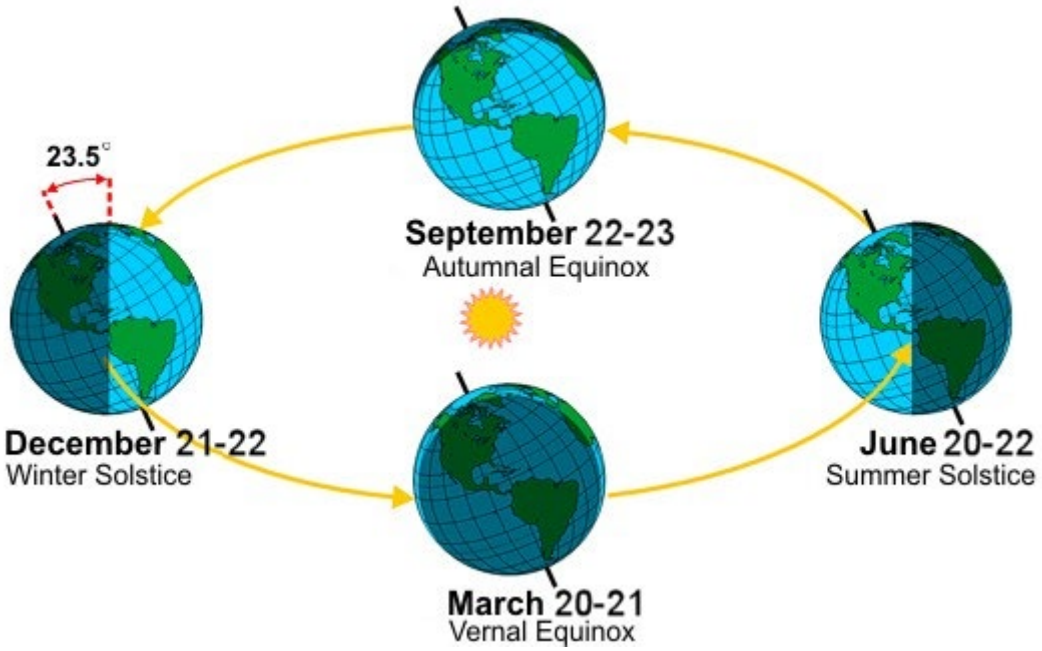

Figure I-1: Earth-Sun motion

In its annual movement around the Sun, the Earth completes a full rotation on itself every 24 hours, spinning around its polar axis. This north-south axis is tilted at an angle of 23°27' relative to the perpendicular of its orbital plane, maintaining this elegant tilt throughout its journey around the Sun. This steadfast inclination is the direct reason behind the changing seasons.

During winter months in the northern hemisphere, the days grow shorter, and the Sun, shy and low, barely climbs high in the sky. Meanwhile, the southern hemisphere basks in the warmth of summer. But when summer returns to the northern hemisphere, the situation reverses: the Earth tilts its northern pole toward the Sun, stretching the days and bringing the Sun’s rays closer to vertical. [2, 3]

I.2.1 Spectrum of Solar radiation:

As an energy source, sunlight is a climatic factor that should be harnessed—either passively, through glazed openings, or actively, for energy production. At the same time, it may be necessary to mitigate its effects to prevent overheating during the summer months. Effectively managing solar energy thus requires a precise understanding of the sun's position (in terms of both altitude and azimuth) as well as the intensity of solar radiation at any given moment.

The Sun emits electromagnetic radiation, and the white light that reaches Earth does so in a remarkably short time—approximately 8 minutes and 19 seconds on average—since it travels at the speed of light, about 299,792,458 meters per second. This radiation forms a continuous spectrum that ranges from ultraviolet to infrared wavelengths, with its peak intensity occurring in the visible range. However, as this radiation passes through the Sun's chromosphere and the Earth's atmosphere, certain photons are absorbed by the atoms present in these layers [2].

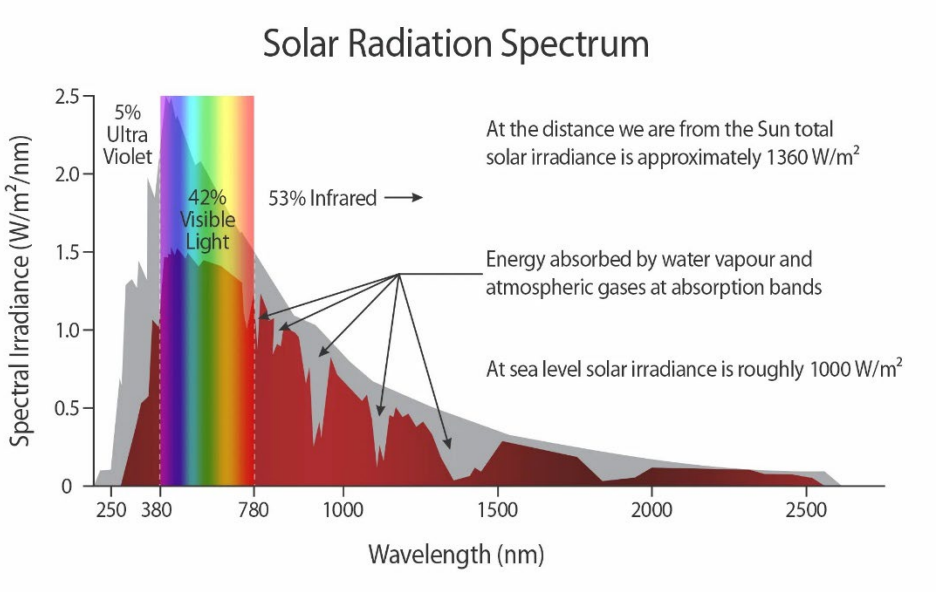

Figure I-2: Spectrum of solar radiation

I.2.2 Components of solar radiation:

Direct radiation and diffuse radiation are the two main components of solar radiation that reach the earth; these two elements combine to generate what is referred to as global radiation. Albedo is a third player that we add to these two elements. [1]

A. Direct Radiation:

The amount of solar energy that travels straight from the Sun's disk to a surface is known as direct radiation. It is the Sun's unadulterated light, moving across space unhindered.

B. Diffuse Radiation:

On the other side, diffuse radiation happens when sunlight is scattered by objects like buildings, the ground, or clouds. It creates a soft, pervasive light because, in contrast to direct radiation, it comes from all directions. Figure I.3 depicts these two radiation kinds, diffuse, direct and albedo.

Diffuse radiation is equally important, even though direct radiation is what solar modules use most of the time.

C. Albedo:

The percentage of incoming radiation that a surface reflects or scatters is known as albedo. This phrase is frequently used to characterize how reflective clouds or the ground are. It is an average number that takes into consideration every angle of incidence that might exist. A black body has zero albedo by definition as it absorbs all light.

D. Radiation from the Earth:

Simply put, the total of these three contributions is global radiation:

$$\textit{Global Radiation} = \textit{Albedo} + \textit{Diffuse} + \textit{Direct Radiation}$$

The entire amount of solar energy that is accessible at the Earth's surface is determined by this combination.

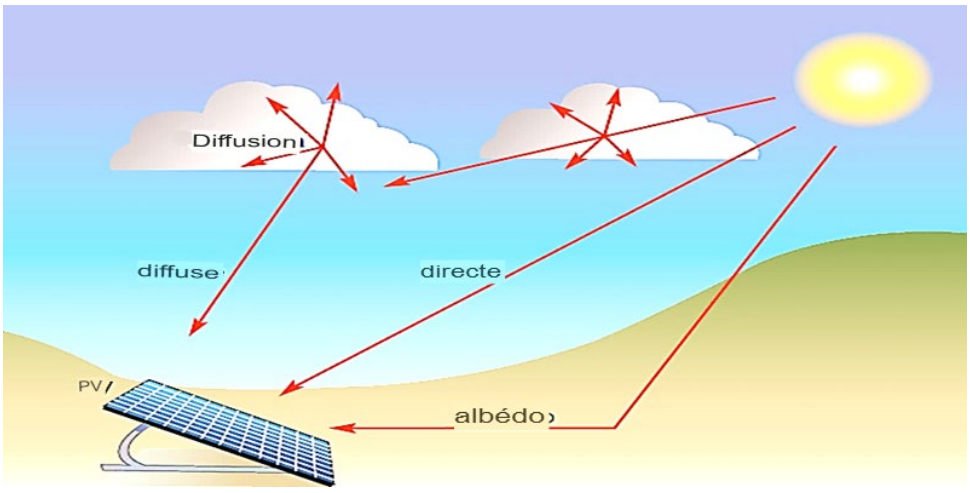

Figure I-3: Different components of global radiation

I.2.3 Solar radiation measuring instrument:

The classic principle for measuring solar irradiance relies on the thermoelectric effect: a black body absorbs solar radiation, and the resulting temperature increase is measured using thermocouples. This temperature change generates an electromotive force, which is then recorded. However, these measurements remain challenging, especially when devices are exposed to outdoor conditions.

Nowadays, Various instruments are used to measure direct, diffuse, reflected, or global radiation, expressed in watts per square meter (W/m^2).

Campbell-Stokes heliograph:

This device, equipped with a glass sphere acting as a magnifying lens, measures sunshine duration—the time during which direct solar radiation is strong enough (practically, over 120 W/m^2) to burn or discolor a strip of paper replaced daily. The length of the burned sections allows for the calculation of sunlight duration.

Pyranometer:

The pyranometer measures global radiation (direct + diffuse) from the entire celestial hemisphere, within a wavelength range of 0 to 3 μm. It generates an electrical voltage proportional to solar irradiance. This voltage is produced by a thermopile, where the upper part heats up under radiation, while the shielded lower part serves as a reference. These devices, however, are costly. [4]

Diffuse radiation pyranometer:

Similar to the standard pyranometer, this device features a metal band that blocks the Sun, eliminating the direct component of incident radiation. The band adjusts seasonally to track solar declination.

Pyrheliometer:

This instrument measures exclusively the direct component of solar radiation. It requires a solar tracker and a collimator to keep the Sun’s disk perfectly focused while blocking the rest of the sky.

Photovoltaic Cells:

Global irradiance can also be measured elegantly using a crystalline silicon solar cell. The cell is loaded onto a low resistance, ensuring it operates near it's short-circuit point, where the current is directly proportional to irradiance.

I.2.4 Solar Angles:

Solar angles are essential parameters for calculating solar radiation.

Longitude (λ):

The longitude of a location is the angle between two meridional planes (passing through the polar axis): one being the reference meridian (Greenwich, 0°), and the other being the meridian of the location in question.

Latitude (Φ):

The latitude of a location is the angle between the equatorial plane and the line connecting the Earth's center to that location. The equator has a latitude of 0°, the North Pole +90°, and the South Pole -90°. This convention assigns a positive sign to the Northern Hemisphere and a negative sign to the Southern Hemisphere.

Altitude (L):

The altitude of a point corresponds to its vertical distance from a reference surface, typically mean sea level.

Declination (ω):

Declination is the angle between the equator and the line connecting the Earth's center to the Sun's center. Due to the Earth's axial tilt (23.45°), declination varies between ±23.45° throughout the year. It reaches its maximum in summer and winter and becomes zero during the spring and autumn equinoxes.

Declination is calculated using the formula:

$$\omega = 23.45 * \sin(2\pi(284 + n) / 365) \quad \text{(I.1)}$$

Where:

n : is the number of days elapsed since January 1st (ranging from 1 to 365 or 366, depending on leap years).

Sun's hour angle (δ):

The solar hour angle, denoted as δ, tracks the Sun's position in its daily rotation, as if it were moving along an imaginary cone with an opening angle of δ'. It represents the angle between two meridional planes: one passing through the observer and the other containing the Sun. This angle, constantly changing, maps the Sun's apparent path across the sky throughout the day.

In principle, a full solar day corresponds to a variation of δ ranging from -180° to +180°, equivalent to 24 hours. At solar noon, when the Sun is at its zenith, the hour angle is zero. Before noon, it is negative, indicating that the Sun lies east of the local meridian. After noon, it becomes positive, marking the Sun's progression toward the west. Thus, the hour angle allows us to trace the Sun's celestial dance, hour by hour.

$$\delta = 15 \times (UTC\ hours\ - 12 + 15\lambda) \quad \text{(I.2)}$$

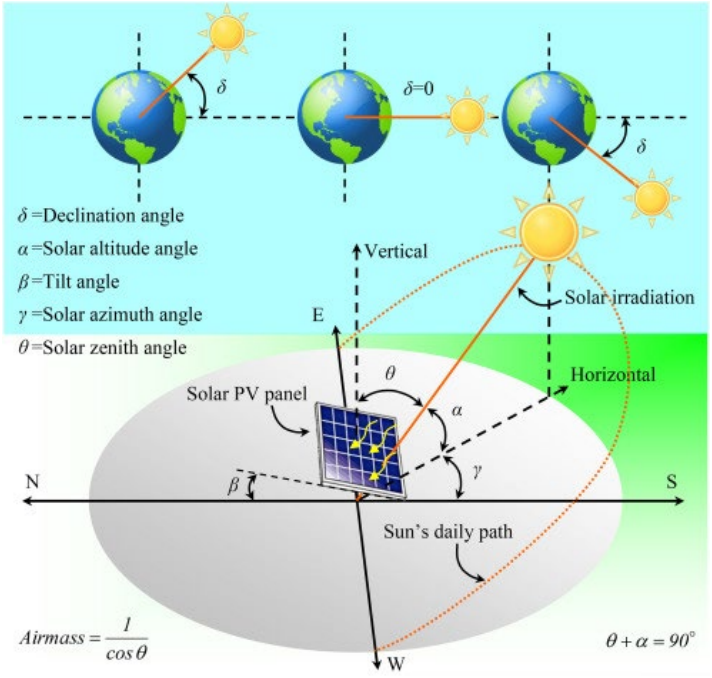

Figure I-4: Schematic diagram of the earth and angles used in the calculation.

I.2.5 Radiometric data in Algeria:

Algeria has great solar potential and is blessed with an abundance of sunshine. The southern areas have an average of 2,650 hours of sunlight each year, according to meteorological statistics. Global irradiation levels vary from 2,100 kWh/m² in the North to 2,400 kWh/m² in the South each year.

Algeria has the greatest solar potential in the whole Mediterranean basin, according to an analysis done by the German Aerospace Agency (DLR) using satellite data. According to estimates, this potential is 13.9 TWh/year for photovoltaic solar energy and 169,000 TWh/year for solar thermal energy. Algeria's solar potential is comparable to eleven significant natural gas reserves, including Hassi R'mel, to put this into context. [2]

I-3 Energy conversion:

The requirement for telecommunications firms to establish equipment in remote locations, away from cities and conventional power grids, initially fueled the development of photovoltaic technology. The ≪ space race ≫ provided the second boost. Solar cells soon emerged as the best way to deliver the energy needed for extended space travel at a reasonable price and with the least amount of weight.

Finally, the 1973 energy crisis renewed and expanded interest in terrestrial applications of solar energy. Photovoltaic energy, obtained by converting light into electricity through the photovoltaic effect, emerged as a promising alternative. [5] This steady evolution was made possible by fundamental research on photovoltaic materials, as well as the gradual improvement of energy management systems. Indeed, photovoltaic electricity is an intermittent energy source, non-linear and dependent on numerous factors, such as irradiance and temperature.

I-4 Different solar technologies:

Thermodynamic, thermal and photovoltaic are the three primary methods of directly harnessing solar energy.

I.4.1 Concentrated thermodynamic solar energy:

Concentrated solar power (CSP) is an ingenious technology that uses mirrors to focus solar energy onto a tube containing a heat-transfer fluid. The captured heat is then transferred to a

water circuit, turning the water into steam. This pressurized steam drives a turbine connected to a generator, producing electricity. [7]

Figure I-5: Thermodynamic solar power (concentrated solar power)

I.4.2 Solar thermal energy:

The main function of solar thermal energy is to convert sunlight into heat. It uses solar-exposed panels with a fluid flowing through them to absorb and transfer heat. This is particularly convenient because it may be used for something as basic as boiling water for daily usage. But if one wants to take it a step further and generate electricity, you'll need to add a generator, like a hot air engine, to convert that heat into power. [7, 8]

Figure I-6: Examples of thermal modules

I.4.3 Photovoltaic solar energy:

Solar photovoltaic energy captures sunlight, as opposed to solar thermal energy, which uses the sun as a heat source. It produces electricity from the photon energy that reaches the Earth's surface by permitting sunshine photons energy to electrons in a semiconductor, which is what a photovoltaic cell is made of. [9] .

This process, called the photovoltaic effect, is rather remarkable since it occurs without the need for fuel, noise, pollution, or moving components. It's a really effective, quiet, and clean technology.

Figure I-7: Sunflowers in Korea

I-5 Photovoltaic effect:

The sun gives us so much, especially energy—it’s the primary source of it. Thermal energy, delivered by solar radiation (through the transformation of hydrogen nuclei into helium nuclei), is absolutely essential for survival. Without it, our world would just be a frozen wasteland. Humans might survive an ice age, but without the sun, the human body simply couldn’t adapt.

Beyond its vital role, thermal energy is also harnessed by humans to generate electricity. How? Through photovoltaic panels. Sunlight hits these panels and is converted into electricity via the photovoltaic effect.

The photovoltaic effect, discovered by Alexandre Edmond Becquerel in 1839, is a fascinating phenomenon. It occurs when photons are absorbed by a semiconductor material, creating an electrical voltage. Photovoltaic cells produce direct current from solar radiation, which can then power devices or recharge batteries. [1]

I.5.1 Operating principle:

In essence, a photovoltaic cell is a light-sensitive diode. The characteristics of semiconductor materials determine how it functions. In essence, two thin semiconductor layers, each doped differently, make up a cell. Doping the N-layer results in an excess of electrons, whereas doping the P-layer results in a deficit. A possible barrier between the two layers is created by this disparity. [1] The energy of light photons is transferred to the N-layer electrons when they strike the cell. A direct electric current is then produced when these energized electrons pass through the potential barrier.

To collect this current, electrodes are printed onto both layers of the semiconductor. The top electrode is a fine grid that allows light to pass through, and an anti-reflective coating is added on top to maximize light absorption. This setup ensures the cell captures as much solar energy as possible.

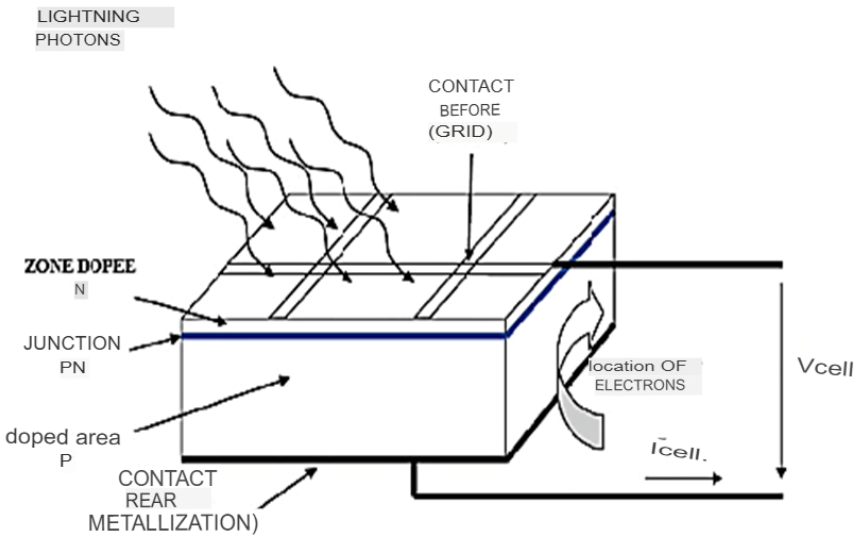

Figure I-8: Diagram of a photovoltaic cell

I.5.2 Photovoltaic cells:

The use of solar cells began in the space industry. Research helped improve their performance and reduce their size, but it was the 1973 energy crisis that really pushed governments and industries to invest heavily in photovoltaic technology and its terrestrial applications.

A solar cell is made of a semiconductor material that absorbs light energy and converts it directly into electric current. A semiconductor is a material with far fewer free charges compared to metals. For an electron, normally bound to its atom (in the valence band), to break free and contribute to current conduction, it needs a minimum amount of energy. This energy allows it to jump to higher energy levels (the conduction band).

This minimum energy is called the "band gap" (Eg), measured in electron-volts (eV). This threshold value is unique to each semiconductor material. For photovoltaic applications, it typically ranges between 1.0 and 1.8 eV. For example, it's 1.1 eV for crystalline silicon and 1.7eV for amorphous silicon. Figure I.10 illustrates this conduction phenomenon in semiconductor materials. [6]

I.5.3 Single-diode photovoltaic cell model:

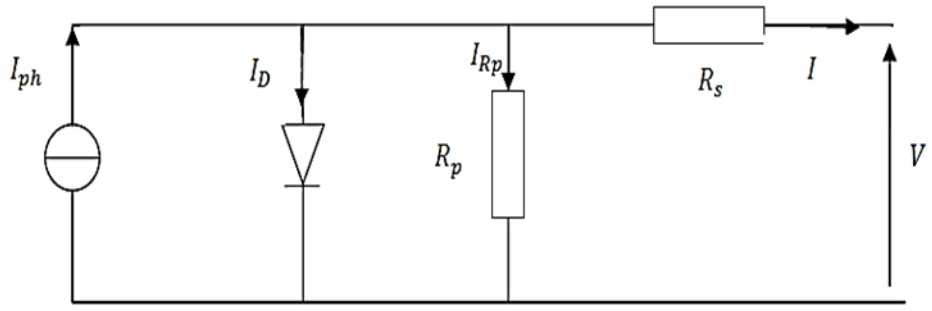

Figure I-9: Equivalent diagram of a single-diode solar cell

The five-parameter model is chosen because it allows for a very realistic analysis and evaluation of photovoltaic module performance. This model represents the solar cell as a current source that simulates the conversion of light into electrical energy. It includes a series resistance (Rs) to account for contact and connection resistances, as well as a parallel resistance (Rp),

called the shunt resistance, to model leakage currents. A parallel diode is also included to represent the PN junction. [10]

From the equivalent circuit shown in Figure I-9, we can write the following equations:

1. The total current is the sum of the currents through the diode, shunt resistance, and load:

$$Iph = Id + I + IRp \quad (I.3)$$

The current through the shunt resistance (Rp) is given by:

$$IRp = \left(\frac{V+Rs.I}{Rp}\right) \quad (I.4)$$

2. The diode current is described by the diode equation:

$$Id = I0.\left(\exp\left(\frac{V+Rs.I}{nVt}\right) - 1\right) \quad (I.5)$$

where I0 is the diode saturation current, given by:

$$I0 = AT^3 \exp\left(\frac{Eg}{Kt}\right) \quad (I.6)$$

with:

- $V_t = \left(\frac{Kt}{q}\right)$: the thermal voltage at temperature T*T*,
- q: the electron charge (1.602×10−19 C),
- K: Boltzmann's constant (1.381×10−23 J/K),
- A: a constant (1.2 A/cm2K3),
- n: the junction non-ideality factor,
- T: the effective cell temperature in Kelvin,
- Eg: the bandgap energy (for crystalline silicon, Eg=1.12 eV).

Combining these equations, we get the I(V) characteristic of the photovoltaic module:

$$I=I_{ph} - I_{0.}\left(e\left(\frac{V+Rs.I}{nVt}\right) - 1\right) - \left(\frac{V+Rs.I}{Rp}\right) \quad (I.7)$$

I.5.4 Power of a PV cell:

Under fixed ambient conditions (such as light intensity, temperature, air speed, etc.), the electrical power **P** (in watts) available at the terminals of a photovoltaic (PV) cell is given by the simple formula:

$$P=V\cdot I \tag{I.8}$$

where:

- P (in watts) is the power supplied by the PV cell,
- V (in volts) is the voltage measured across the cell.
- I (in amperes) is the current delivered by the cell.

This equation shows that the power depends directly on the voltage and current produced by the cell. It's the foundation for understanding how solar energy is converted into usable electricity.

I.5.5 Maximum power of a PV cell:

For an ideal solar cell, the maximum power "Pmax ideal" would simply be the open-circuit voltage Voc multiplied by the short-circuit current Isc:

$$P_{max\ ideal}=V_{oc}\cdot I_{sc} \tag{I.9}$$

where:

- Pmax ideal (in watts) is the theoretical maximum power supplied by the PV cell.
- Voc (in volts) is the open-circuit voltage measured across the cell.
- Isc (in amperes) is the short-circuit current delivered by the cell.

In experimental, the characteristic curve of a PV cell isn't perfect—it's more "rounded." The voltage at the maximum power point Vmpp is therefore lower than the open-circuit voltage Voc, and the current Impp is also lower than the short-circuit current Isc. The actual maximum power is then given by:

$$P_{max}=V_{mpp}\cdot I_{mpp} \tag{I.10}$$

This equation reflects the maximum power the cell can realistically deliver under practical conditions.

I.5.6 Electrical characteristics of solar cells:

Properties

Under a given level of illumination, a photovoltaic cell exhibits a non-linear I(V) characteristic (see Figure I.10), which represents all possible electrical configurations of the cell. This curve expresses equation 1.7 and is defined by three key physical quantities:

Open-circuit voltage (Voc) :

This value corresponds to the voltage generated by an illuminated cell that is not connected to a circuit. The open-circuit voltage (Voc) of a PV cell typically ranges between 0.3 V and 0.7 V, depending on the material used.

Short-circuit current (Isc):

This value represents the current generated by an illuminated cell that is connected to itself (short-circuited). The short-circuit current (Isc) depends mainly on the level of illumination, the technology used, and the size of the cell. For example, for crystalline silicon, it generally ranges between 5 A and 8 A. [11]

These two parameters, along with the shape of the I(V) curve, help us understand how the photovoltaic cell behaves under different electrical conditions.

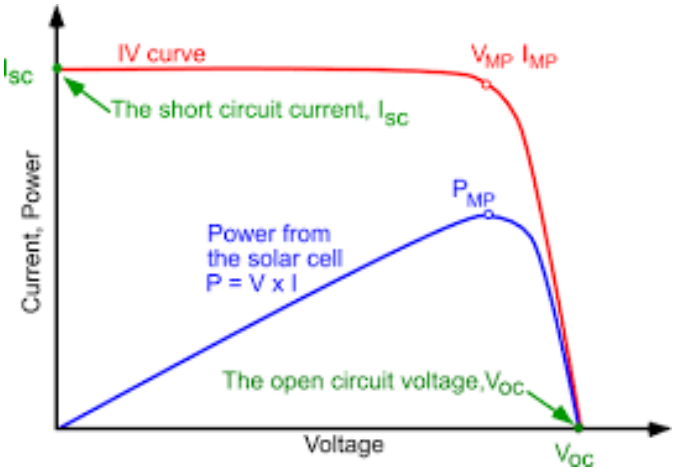

Figure I-10: Current-voltage characteristics of a photovoltaic cell

I.5.7 Cell association:

Series Connection:

When N photovoltaic cells are connected in series, the same current flows through all the cells. Figure I.11 shows the resulting characteristic (Isc, Voc) of such a configuration under ideal conditions. For N identical cells (each with a short-circuit current Isc and an open-circuit voltage Voc, the overall characteristic is obtained by summing the voltages of each cell while keeping the current constant. The total open-circuit voltage of the series connection (Vsco) is therefore given by:

$$Voc = Ns \cdot Voc$$

Where: Ns: is the number of cells in series.

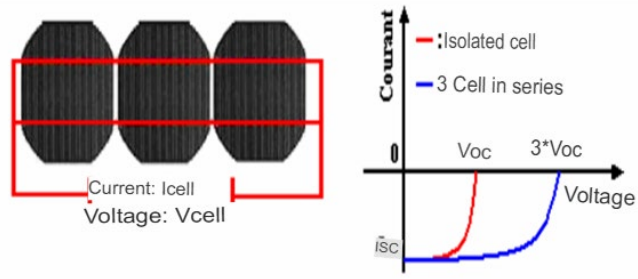

Figure I.11 Grouping characteristic Series of a photovoltaic cell

Parallel Connection:

When Np identical photovoltaic cells are connected in parallel, all the cells share the same voltage, but their currents add up. The total short-circuit current of the parallel connection (Ipco) is therefore given by: $Ipco = Np \cdot Isc$

Where: - Np is the number of cells in parallel

- Isc is the short-circuit current of a single cell.

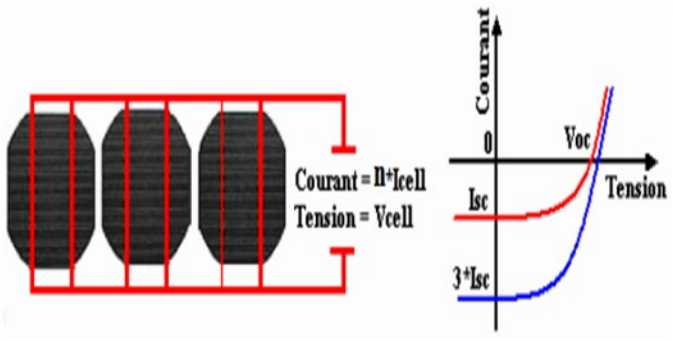

Figure I-12: Parallel grouping characteristic of a photovoltaic cell

Parallel/Series Connection:

Significant current and high voltage are frequently achieved with this kind of connection. When photovoltaic cells are connected in series, the current stays the same but the separate voltages add up to one cell's value. The total output of current is increased when the currents are coupled in parallel.

The following illustrates the characteristics of a pair of solar modules; this arrangement may be extended to a set of Ns modules connected in series. This configuration offers a versatile way to satisfy certain energy requirements by permitting both higher voltage and current.

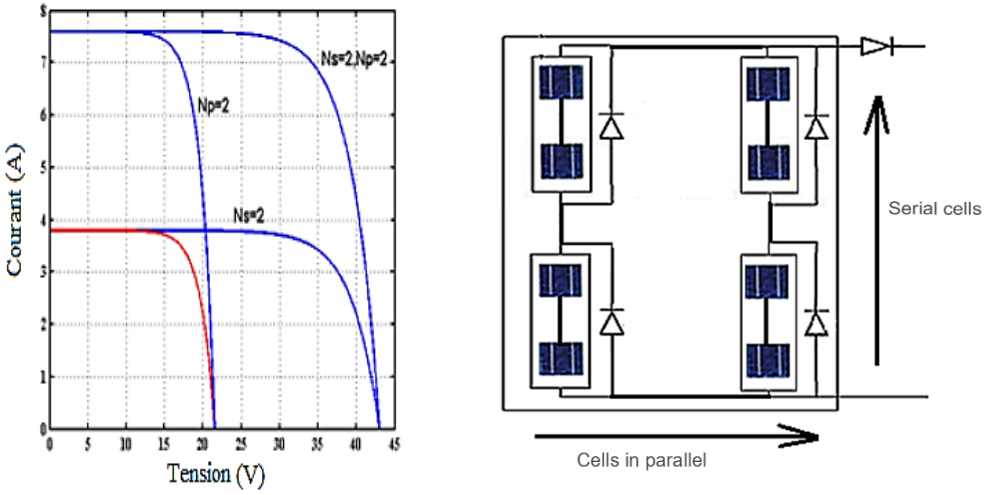

Figure I-13: Serial/Parallel grouping characteristic of a photovoltaic cell

I.5.8 Conventional Protection of a PV System:

To ensure a long lifespan for a photovoltaic installation designed to produce electrical energy, it is essential to add electrical protections to commercial modules. These protections help prevent destructive failures, often caused by the connection of cells in series and panels in parallel. For this purpose, two types of conventional protections are commonly used in current installations (see Figure I.14).

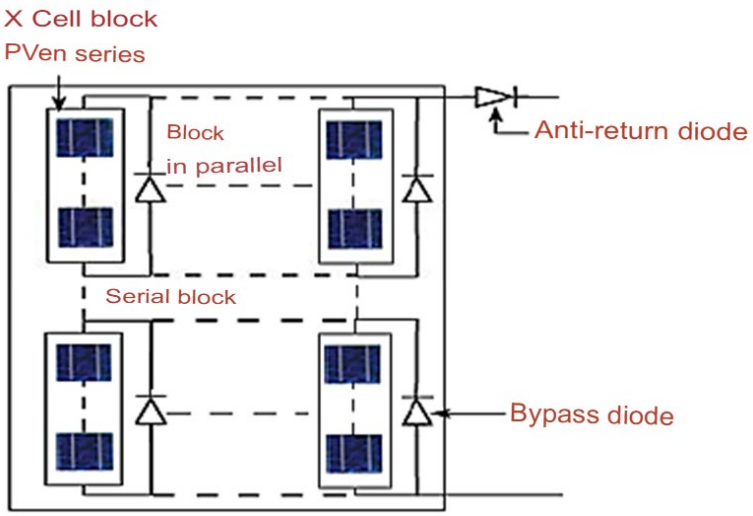

Figure I-14: Diagram of a photovoltaic module

The blocking diode plays a crucial role in preventing reverse current in photovoltaic systems (GPV). This phenomenon can occur in two scenarios: either when multiple modules are connected in parallel, or when a directly connected load (such as a battery) switches from receiver mode to generator mode, for example, at night.

On the other hand, bypass diodes are used to isolate a subset of cells when the lighting is uneven. This prevents the formation of hot spots and protects poorly illuminated cells from potential damage.

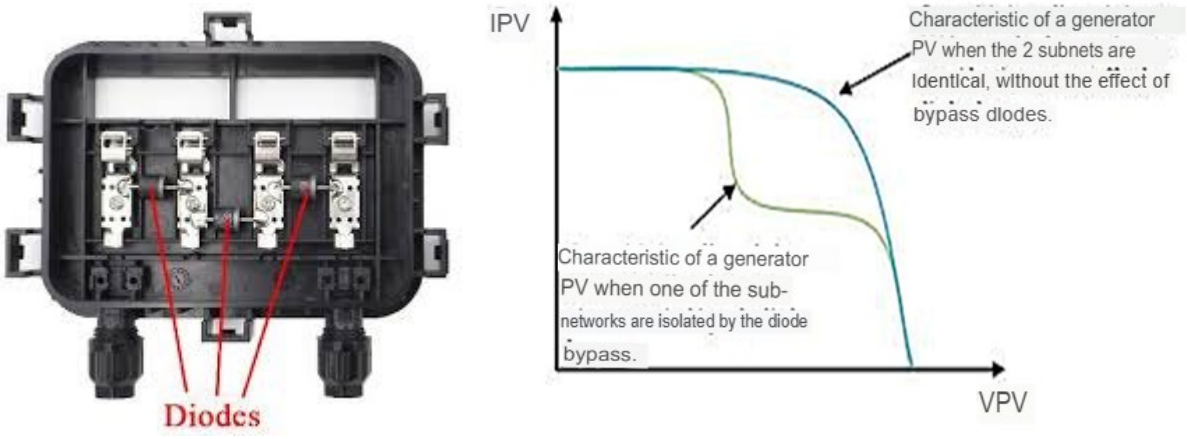

Figure I-15: Effect of the bypass diode on the I(V) characteristic of a GPV

The conduction of these diodes affects the generator output characteristic, as shown in Figure I.15, by the loss of part of the energy protection and by the presence of two power maxima.

I.5.9 Maximum power operation:

In an electrical system with a source and a load, it is important to extract the maximum power of the PV module for optimal operation and economic efficiency of the system. Thus, finding the optimal operating point using optimization techniques is crucial. For photovoltaic (PV) systems, this task is more complex because the performance of solar cells depends heavily on factors like sunlight and ambient temperature. To address this, we need a device that can continuously drive the system to operate at the optimal point, ensuring maximum efficiency.

There are several methods for maximizing power in PV systems, which can be divided into two main categories:

Indirect methods:

These rely on databases containing the characteristics of PV panels under various climatic conditions (temperature, sunlight, etc.) and use empirical mathematical equations to determine the maximum power point.

Direct methods:

These use real-time voltage and current measurements from the panels. The algorithms in this category adjust working parameters based on variations in these measurements, without needing a prior knowledge of the PV panel characteristics. Examples of direct methods include the differentiation method, Perturb & Observe (P&O) method, and the incremental conductance method.

The advantage of direct methods is their adaptability and independence from pre-existing data, making them highly effective in dynamic environmental conditions.

I-6 Influence of temperature and illumination:

The performance of a photovoltaic cell (or a PV generator) is directly influenced by sunlight and temperature. The variations in current and power as a function of voltage, for different levels of sunlight at a constant temperature of 25°C, are shown in Figure I.16. These curves clearly reveal the presence of maxima on the power curves, corresponding to the Maximum Power Points (Pmax).When irradiation changes at a given temperature, the short-circuit current Isc varies proportionally with the irradiation. However, the open-circuit voltage Voc (at no load) changes very little, remaining almost stable despite variations in sunlight.

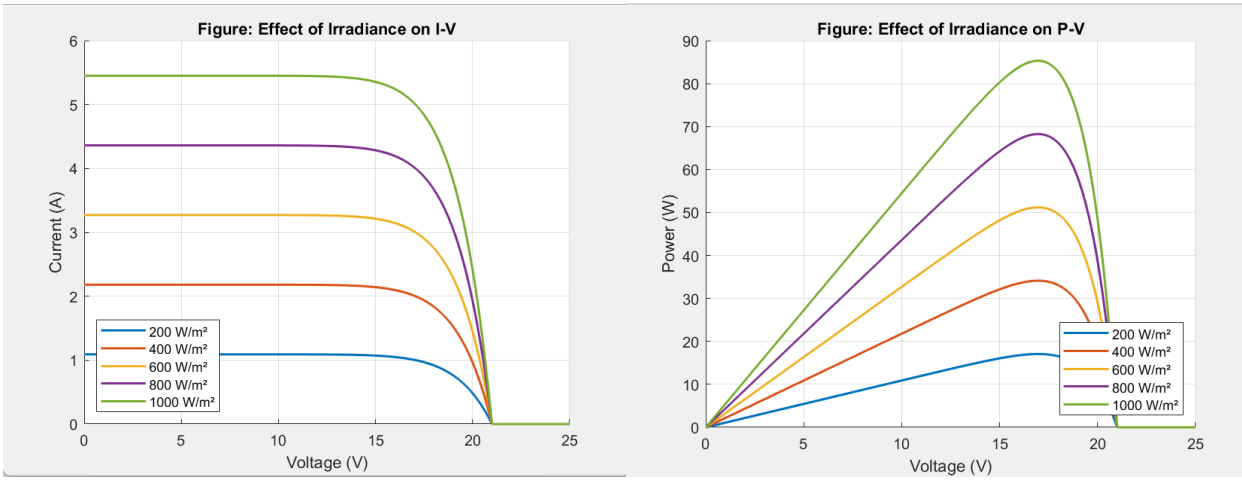

Figure I-16: Evolution of the I(V) and P(V) characteristics for different solar radiations (T=25˚C).

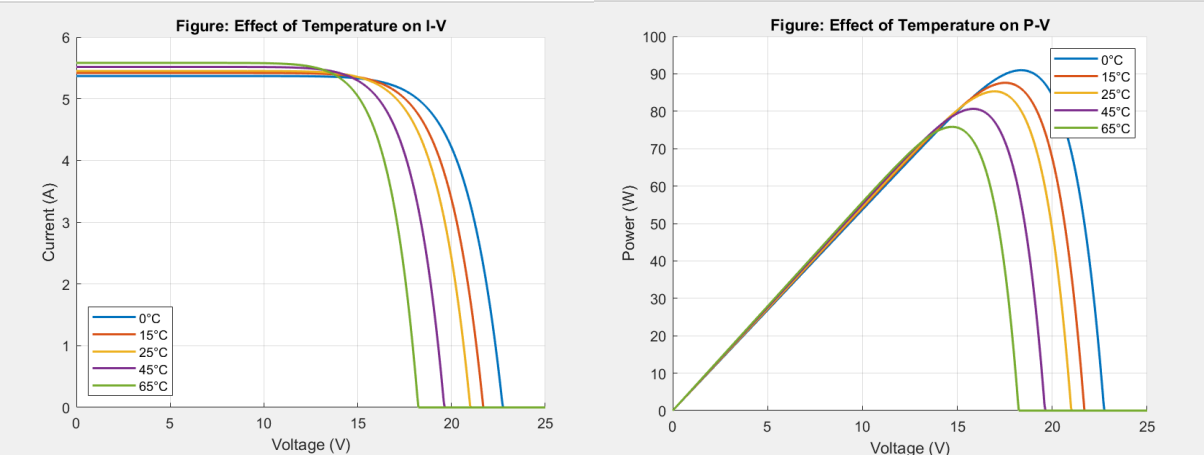

Figure I-17: I(V) and P(V) characteristics Evolution for different temperatures (E= 1000w/m^2)

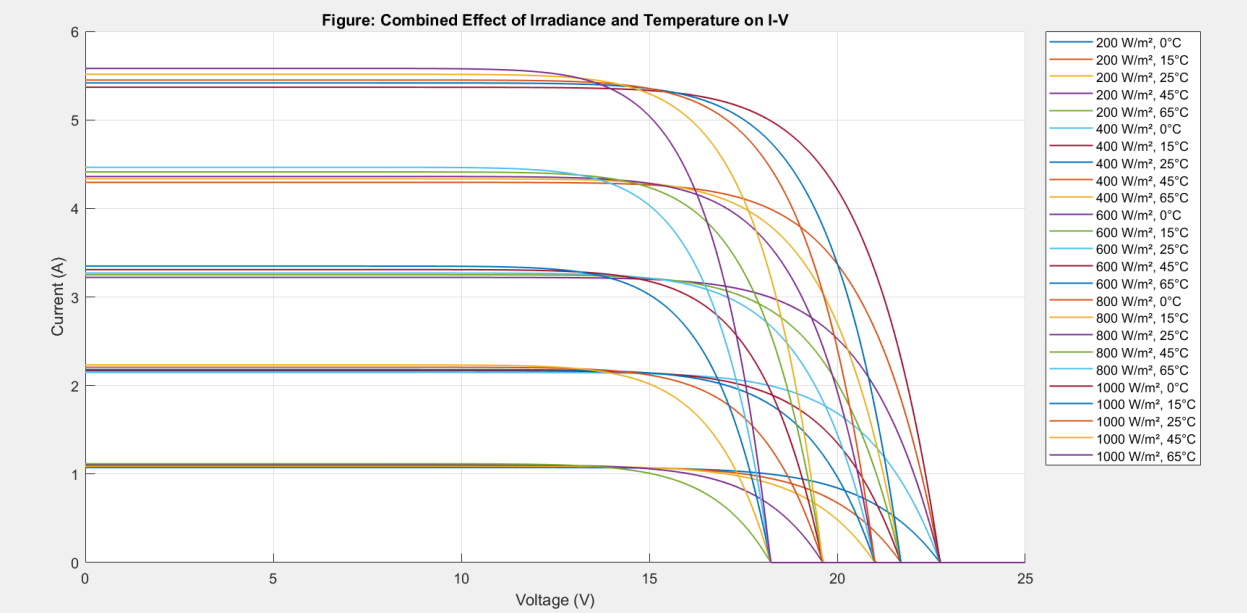

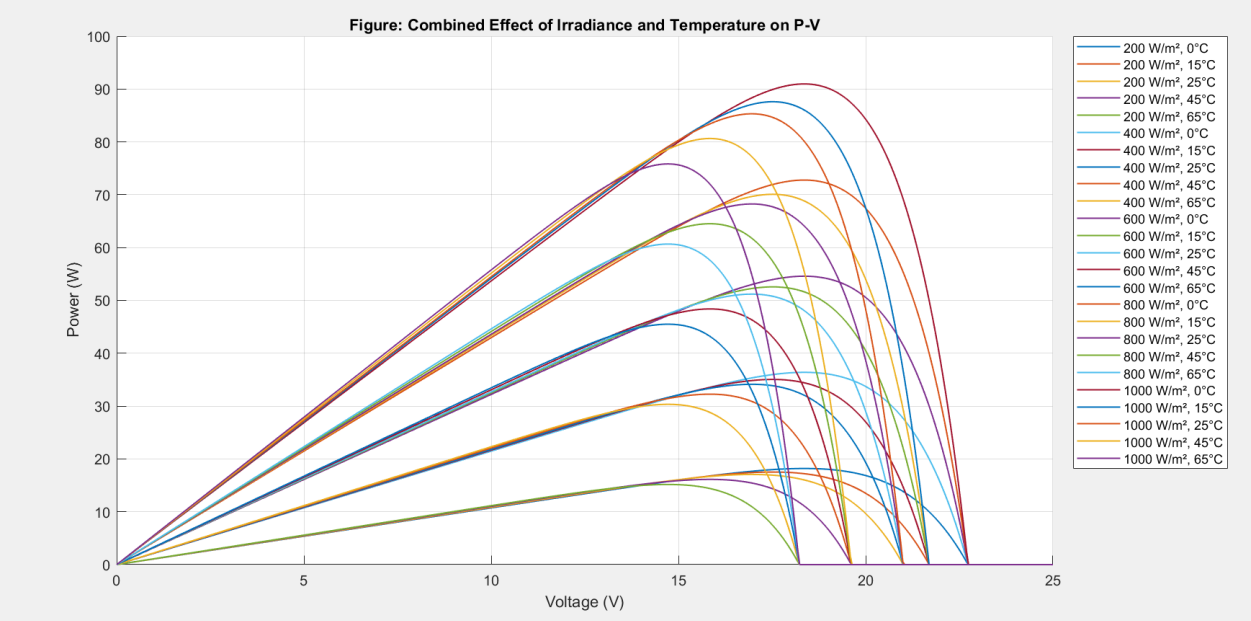

Figure I-18: Simultaneous effect of Solar radiation and temperature

Temperature is a key parameter that significantly influences the behavior of solar module. It also has a major impact on the characteristics of a photovoltaic (PV) generator. Figure I.17 shows how the characteristics of a PV module vary with temperature at a fixed irradiance of 1000 W/m².

When temperature increases at constant irradiance, the open-circuit voltage Voc decreases. The higher the temperature, the lower the Voc. On the other hand, the short-circuit current Isc increases slightly with temperature, but this rise is much less significant than the drop in voltage. In most cases, the influence of temperature on Isc can even be neglected.

Therefore, temperature and irradiance are the two main parameters that affect the characteristics of a PV generator. These two factors must be carefully considered when designing and installing a photovoltaic system. [9, 11]

I-7 Advantages and Disadvantages of Photovoltaic Energy:

I.7.1 Advantages of Photovoltaic Energy:

Photovoltaic energy offers numerous benefits:

- **Clean Energy**: Electricity production is renewable, non-polluting, and non-toxic in their use.
- **Reliability**: Photovoltaic systems are extremely reliable and require minimal maintenance.
- **Adaptability**: Thanks to their compact size and silent operation, solar panels are ideal for urban areas.
- **Universality**: Sunlight is available everywhere, making photovoltaic energy viable in remote mountain villages as well as in bustling city centers.
- **Decentralization**: Electricity is produced directly at the point of consumption, reducing transmission losses.
- **Durability**: The materials used (glass, aluminum) withstand extreme weather conditions, including hail.
- **Longevity**: Solar panels have a long lifespan, with some manufacturers offering warranties of up to 25 years. [9]

I.7.2 Challenges of Photovoltaic Energy:

Despite its many advantages, photovoltaic energy has some limitations:

- **Sunlight Dependency**: Energy production varies with sunlight, which is inherently unpredictable.
- **High initial Cost**: Installation costs remain high, although prices are gradually decreasing.
- **Modest Efficiency**: Commercially, the conversion efficiency of solar energy into electricity is still relatively low even if at research and laboratory scale encouraging results are obtained. [12]
- **Expensive Storage**: If battery storage is required, the installation cost increases significantly.

I-8 Conclusion:

In this chapter, we explored the (challenges and current developments) photovoltaic energy source. We explained how a solar cell works, detailing the photovoltaic effect. We saw that a PV cell has a non-linear I(V) characteristic, with a maximum power point (MPP) defined by a current Imax and a voltage Vmax. It can be modeled using a simple electrical circuit.

We also examined the influence of external parameters on this characteristic. The short-circuit current Isc mainly depends on sunlight, while the open-circuit voltage Voc is influenced by temperature. To ensure the long-term durability of photovoltaic installations, electrical protections must be integrated into the modules. Finally, meteorological data on solar radiation is not always sufficient to quantify all the phenomena affecting a photovoltaic panel. A thorough understanding of solar resources is therefore essential to optimize performance.

Chapter II
Floating Photovoltaic Systems and Power Optimization

II-1 Introduction:

Water covers 71% of our planet's surface, yet we have only begun to tap into the potential of these vast liquid plains. Beyond their ecological importance, water bodies possess unique physical properties that make them extraordinary natural resources. Their reflective surfaces, thermal mass, and dynamic interactions with sunlight create opportunities we are just starting to explore.

The physics of water surfaces reveal remarkable characteristics. A single square kilometer of water can absorb and redistribute solar energy equivalent to powering thousands of homes. The evaporative cooling effect of water bodies naturally regulates local temperatures, often creating microclimates 3-5°C cooler than surrounding land areas. Globally, artificial reservoirs alone cover over 300,000 square kilometers - an area larger than Italy - while natural lakes account for nearly 2% of Earth's non-glaciated surface.

Water's reflective properties are particularly extraordinary. While land typically reflects 10-25% of incoming sunlight, water surfaces can reflect up to 90% at certain angles through a phenomenon called specular reflection. This mirror-like quality, combined with water's natural thermal regulation, creates an ideal environment for innovative technologies that work in harmony with aquatic systems.

It is precisely these unique properties of water surfaces that make them perfect hosts for Floating Photovoltaic (FPV) systems. In this chapter, we will explore how FPV technology harnesses the natural advantages of water bodies - their cooling effects, reflectivity, and vast unused areas - to generate clean energy while preserving and even enhancing aquatic ecosystems. The marriage of solar technology with water's innate properties represents one of the most promising frontiers in renewable energy innovation.

II.1.2 Definition and Principle:

Floating photovoltaic (FPV) systems, or floatovoltaics, are solar power installations mounted on buoyant structures that float on water bodies like lakes, reservoirs, or calm seas. These

systems function similarly to land-based PV systems, utilizing the photovoltaic effect to convert solar energy into direct current (DC) electricity, which is then inverted into alternating current (AC) for grid or local use [13].

The main distinction lies in the mounting: while traditional PV systems are installed on land, FPV systems are mounted on floating platforms that are anchored or moored on water bodies.

II.1.3 Evolution and Applications:

First introduced in Japan around 2007 to combat land scarcity, FPV technology has matured considerably. Technological advancements in corrosion-resistant materials, waterproof cabling, and anchoring systems have supported its rapid deployment. As of 2023, the global FPV installed capacity is estimated at 12.9 GW, with rapid growth expected, especially in the Asia-Pacific region [14][15].

Common applications include:

- Utility-scale FPV farms that supply national grids.
- Water utility reservoirs, where they reduce evaporation and co-produce energy.
- Agricultural ponds and canals to power irrigation systems.
- Decommissioned mining pits and quarry lakes, repurposing unusable land [13].

II.1.4 Comparison with Land-Based PV Systems:

Table II.1: Comparison between floating PV with Land-Based PV Systems:

Criteria	**Floating PV Systems**	**Land-Based PV Systems**
Land use	No land consumption	Requires large land areas
Cooling effect	Enhanced by water surface	Reduced efficiency due to heat
Installation cost	Higher due to floats and mooring	Lower

O&M complexity	Higher (requires aquatic access)	Easier
Evaporation control	Reduces water loss	No impact
Environmental impact	Limited if managed well	Can involve deforestation

Efficiency and Performance Enhancements:

FPV systems benefit from natural water cooling, which lowers panel temperatures by 3°C to 15°C compared to land-based systems. This thermal regulation can increase panel efficiency significantly:

- FPV without water cooling shows about **7%** efficiency gain over land systems [17].
- FPV with active or enhanced water cooling can reach up to **15.45%** greater efficiency [17].
- A 2023 study in Brazil revealed that FPV arrays can reduce evaporation by **60.2%**, conserving valuable water resources [16].

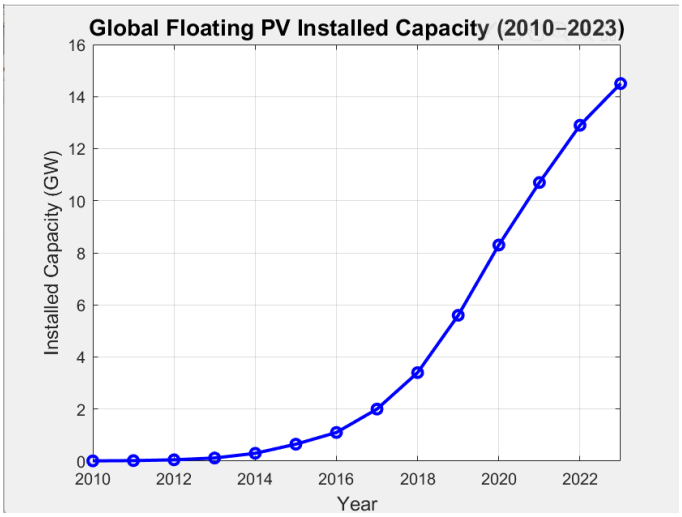

Figure II.1: Global FPV Installed Capacity Growth (2010–2023)

The graph shows the rapid growth of global floating photovoltaic (PV) installed capacity from 2010 to 2023. Starting modestly (under 1 GW before 2016), installations surged after 2018, jumping from 2 GW to around 12 GW by 2022, with projections reaching 14–16 GW in 2023. This expansion reflects increasing adoption of floating solar, particularly in Asia, driven by land scarcity, higher efficiency (thanks to water cooling), and supportive policies. Falling costs and environmental benefits further accelerated deployment, with growth expected to continue as floating PV becomes a key renewable energy solution.

II-2 Types of Water Bodies for FPV Deployment:

Floating photovoltaic (FPV) systems are adaptable to a variety of water bodies, each offering different benefits and challenges. The choice of water body for FPV deployment impacts system performance, scalability, and environmental considerations. Below are the primary types of water bodies commonly used for FPV systems:

II.2.1 Lakes and Reservoirs:

Figure II.2: Floating photovoltaic station in the lake

Benefits:

- **Calm Waters:** Lakes and reservoirs typically feature stable and calm water surfaces, reducing the risk of system damage from high waves or turbulent conditions. This makes them ideal for FPV system installation.
- **Proximity to Hydropower:** Many lakes and reservoirs are located near hydropower stations, which provides opportunities for hybrid power generation (i.e., combining FPV with hydroelectric systems).
- **Reduced Land Use:** Installing FPV systems on lakes and reservoirs eliminates the need for large land areas, making this an efficient option for land-scarce regions.

Challenges:

- **Seasonal Water Level Variation:** Fluctuating water levels in lakes and reservoirs, particularly due to seasonal changes or droughts, can affect the stability and efficiency of the floating PV structures.
- **Sediment Accumulation:** Sediment and algae growth in stagnant or slow-moving water can obstruct panels, reduce their effectiveness, and complicate maintenance.

Table II.2: Suitability Matrix for Lakes and Reservoirs:

Criteria	**Suitability Level**	**Description**
Water Surface Stability	High	Calm waters, minimal wave disturbances
Availability of Water	Moderate to High	Seasonal fluctuations in water levels can be an issue
Proximity to Infrastructure	High	Often near hydropower stations, reducing transmission costs
Environmental Impact	Low to Moderate	Risk of algae, sedimentation, and water quality concerns

II.2.2 Dams and Hydroelectric Reservoirs:

Figure II.3: FPV in a dam.

Benefits:

- **Existing Electrical Infrastructure:** Dams and hydroelectric reservoirs are often already integrated with electrical grids, which simplifies the process of connecting FPV systems to the grid.
- **Potential for Hybridization:** The ability to hybridize FPV with hydroelectric power plants allows for the optimization of land and water resources, providing more stable and diverse energy production.

Challenges:

- **Complex Ownership:** Many hydroelectric reservoirs are managed by government or private entities with strict regulations on land and water use, making approvals for FPV projects complex.
- **Strict Regulations:** Regulatory barriers, such as environmental impact assessments and permissions for altering water levels or land use, are common in such sites.

Table II.3: Suitability Matrix for Dams and Hydroelectric Reservoirs:

Criteria	Suitability Level	Description
Grid Infrastructure	High	Direct integration with existing power lines
Ownership Complexity	High	Legal and regulatory hurdles due to private and public ownership
Impact on Water Flow	Moderate	Some alteration to water flow may be necessary
Maintenance Costs	High	Need for high-quality materials to prevent corrosion in harsh conditions

II.2.3 Seas and Oceans (Offshore FPV):

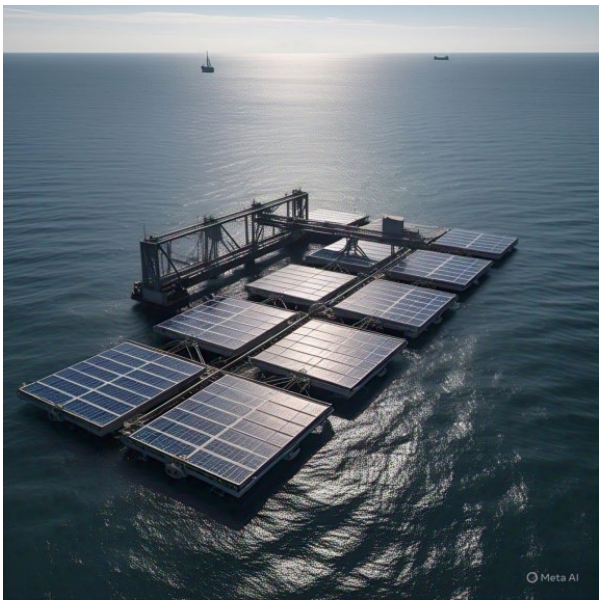

Figure II.4: FPV in an ocean

Benefits:

- **Vast Area Availability:** The vast, unutilized spaces in seas and oceans provide significant potential for large-scale FPV systems, addressing the global demand for renewable energy.
- **Strong Solar Exposure:** Offshore locations often receive more direct and consistent sunlight compared to land, providing high energy yields.

Challenges:

- **Harsh Weather Conditions:** High winds, storms, and ocean currents present major challenges for the long-term stability and durability of FPV systems.
- **Corrosion:** The salty sea air accelerates the corrosion of materials, necessitating the use of specialized coatings and materials, which increases both initial costs and maintenance requirements.
- **High Maintenance Costs:** Offshore systems often require regular maintenance and monitoring, which can be costly due to their remote locations and the need for specialized marine access equipment.

Table II.4: Suitability Matrix for Offshore FPV:

Criteria	**Suitability Level**	**Description**
Water Surface Stability	Moderate to Low	Challenging conditions due to waves and storms
Solar Exposure	High	Consistent sunlight improves energy generation
Maintenance Complexity	High	Harsh conditions and remote locations increase costs
Environmental Impact	High	Marine ecosystems and biodiversity can be affected

II.2.4 Artificial Ponds and Canals:

Figure II.5: FPV in Artificial Canals

Benefits:

- **Minimal Shading:** Artificial ponds and canals, often used in irrigation or water management, offer minimal shading and obstruction, making them suitable for FPV installations.
- **Water Savings:** By deploying FPV systems on water bodies used for irrigation, substantial water evaporation can be prevented, helping conserve water resources in arid regions.

Challenges:

- **Small Scale:** Many artificial ponds and canals are relatively small, limiting the scale of FPV deployment.
- **Structural Limitations:** The infrastructure surrounding these water bodies may not be suitable for large FPV installations, and additional structural reinforcement may be required.

Table II.5: Suitability Matrix for Artificial Ponds and Canals:

Criteria	Suitability Level	Description
Area Size	Low to Moderate	Suitable for small-scale projects only
Water Management	High	Ideal for applications in irrigation and water conservation
Maintenance	Moderate	Easier access but may require adaptation of infrastructure
Impact on Agriculture	Positive	Enhances sustainability through water savings and renewable energy production

II-3 Components of a Floating PV System:

Floating Photovoltaic (FPV) systems are solar energy installations on water bodies like reservoirs, lakes, ponds, and offshore sites. They conserve land, enhance panel efficiency via water cooling (5–10% gain [24]), reduce water evaporation (up to 70% [25]), and integrate with hydropower or aquaculture. This section details FPV components—PV panels and electrical layout, floating platforms and materials, anchoring and mooring systems, and cabling and power evacuation—with expanded details, real-world values, percentages, definitions, and references cited in context. Equations, tables, MATLAB-generated graphs, real-world project examples, and references are provided.

II.3.1 PV Panels and Electrical Layout:

Photovoltaic (PV) panels convert solar energy into electricity. Monocrystalline silicon panels dominate FPV systems with 18–22% efficiency and 80–90% market share due to durability in aquatic environments, as noted by Duffie and Beckman [24]. Polycrystalline and thin-film panels are less common. The electrical layout uses series-parallel configurations, achieving 95–98% inverter efficiency [26].

Types of PV Panels:

- Monocrystalline Silicon: 18–22% efficiency, 25–30 year lifespan, 80% market share [27].
- Polycrystalline Silicon: 15–18% efficiency, 20–25 year lifespan, 15% market share [27].
- Thin-Film: 10–14% efficiency, 10–20 year lifespan, <5% market share [27].
- FPV-Specific Panels: Monocrystalline with double-glass encapsulation, reducing moisture ingress by 99% [28].

Table II.6: Comparison of PV Panel Types

Parameter	**Monocrystalline**	**Polycrystalline**	**Thin-Film**
Efficiency	18–22%	15–18%	10–14%
Cost per Watt	$0.3–0.5	$0.2–0.4	$0.1–0.3
Lifespan	25–30 years	20–25 years	10–20 years
FPV Market Share	80–90%	10–15%	<5%

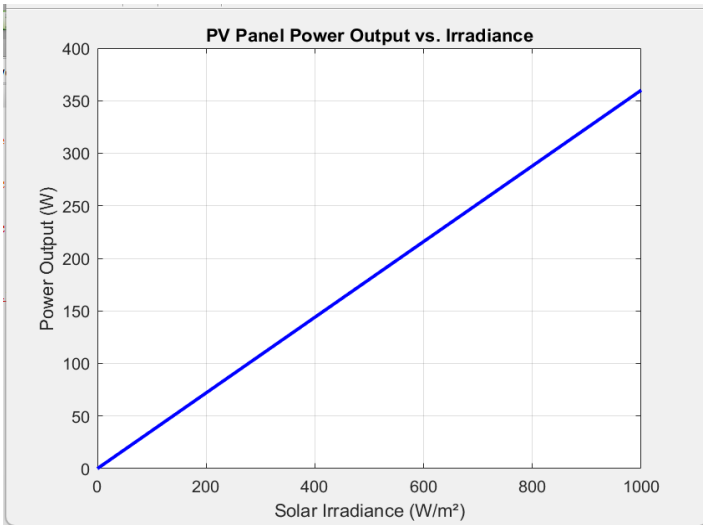

Figure II.6: PV Panel Power Output

The graph illustrates the linear relationship between solar irradiance and power output for a monocrystalline silicon photovoltaic (PV) panel. As solar irradiance increases from 0 to 1000 W/m², the power output rises proportionally, reaching approximately 360 W at peak irradiance. This behavior is characteristic of monocrystalline panels, which are known for their high efficiency and consistent performance under standard test conditions. The linear trend suggests that the panel operates under ideal circumstances, with minimal influence from temperature, shading, or other environmental factors. This makes the panel suitable for locations with stable and high solar irradiance levels, maximizing energy yield throughout the day.

II.3.2 Floating Platforms and Materials:

Floating platforms support PV panels, ensuring stability against wind (150 km/h), waves (1–3 m), UV exposure, and temperature fluctuations (-40 to 80°C). High-density polyethylene (HDPE) dominates with 90% market share due to buoyancy (100–200 kg/m²), corrosion resistance, and recyclability, as emphasized by Rosa-Clot and Tina [25]. Platforms are modular, covering 70–80% of water surfaces, with walkways, ventilation (5–10°C cooling [31]), and sensors.

- **Platform Materials**: Substances for platform construction, balancing buoyancy, durability, and environmental compatibility [25].
    - **HDPE**: Thermoplastic polymer, high strength-to-density, non-corrosive, recyclable [32].

Figure II.7: Floating platform made by HDPE material

- **FRP**: Polymer matrix with fiberglass, high strength, corrosion-resistant [33].

Figure II.8: FRP material

- **Galvanized Steel**: Zinc-coated steel, corrosion-resistant, structural reinforcement [33].

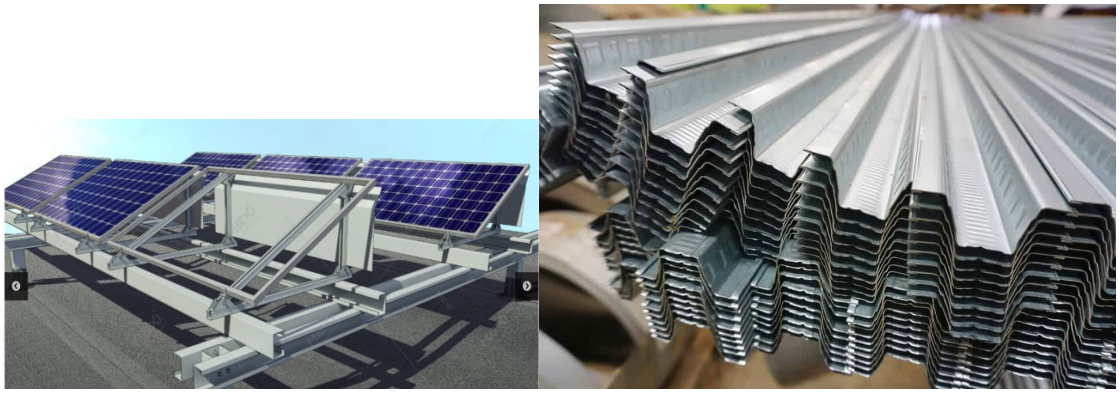

Figure II.9: Galvanized Steel material

- **Composites**: Fiber-resin combinations (e.g., carbon), tailored strength/weight [33].

- **Platform Types**: Structural designs for specific aquatic conditions [25].
  - **Modular Floats**: HDPE units (1–2 m²), e.g., Ciel & Terre's Hydrelio [34].

Figure II.10: Modular floats platform

- **Membrane Platforms**: Hydro-elastic sheets, e.g., ACCIONA's design [35].

- Membrane platforms utilize hydro-elastic sheets that distribute loads dynamically, allowing them to absorb wave energy. This flexible and adaptive structure is suitable for moderately turbulent water bodies.

Figure II.11: Membrane Platform

- **Hybrid Platforms**: HDPE with steel/FRP, for offshore use [36]. Hybrid platforms combine HDPE floats with steel or fiber-reinforced polymer (FRP) reinforcements for enhanced strength, making them suitable for offshore or high-wind environments.

- **Integrated Platforms**: With sensors/aquaculture features, e.g., Sun grow [37]. Integrated platforms feature built-in sensors, control units, and aquaculture modules,

enabling multifunctional use. They are suitable for smart grid applications and enhance economic return through dual-use with aquaculture.

Design Requirements

- Support 50–100 tons/MW [25].
- Ensure 1–2 m metacentric height [26].
- Endure 25–30 years [32].
- Provide 90% maintenance accessibility [34].
- Use 95% non-toxic materials [31].
- Allow 50–100% scalability [25].

Materials

- HDPE: 950–970 kg/m³, $50–100/m², 90% market share, 100% recyclable [32].
- FRP: 1500–1800 kg/m³, $150–300/m², 5% market share, 50% recyclable [33].
- Galvanized Steel: 7800 kg/m³, $200–400/m², 3% market share, 80% recyclable [33].
- Composites: 1200–2000 kg/m³, $300–600/m², 2% market share, 30% recyclable [33].

Table II.7: Comparison of Platform Materials

Material	Density (kg/m³)	Cost ($/m²)	Market Share	Recyclability	FPV Suitability
HDPE	950–970	50–100	90%	100%	High (standard)
Fiberglass (FRP)	1500–1800	150–300	5%	50%	Moderate
Galvanized Steel	7800	200–400	3%	80%	Low
Composites	1200–2000	300–600	2%	30%	Emerging

Environmental and Operational Considerations:

- **Wave/Wind Resistance**: Handles 90% wave conditions, 95% wind resilience [26].

- **Cooling Effect**: 5–10% efficiency gain, 2–5% loss reduction [31].
- **Maintenance**: 90% accessible, 80% downtime reduction [34].
- **Ecological Impact**: 95% non-toxic, 70% light penetration [31].
- **Thermal Expansion**: 98% stability with joints [32].

Manufacturing and Installation:

HDPE platforms are molded into 1–2 m² units, assembled on-site, costing $0.2–0.5/W with 85% efficiency [32].

Cost and Lifespan:

- **Cost**: 20–30% of FPV costs ($0.2–0.5/W) [25].
- **Lifespan**: 25–30 years (95% reliability) [32].

Table II.8: HDPE Platform Specifications:

Property	Value	Property	Value
Density	950–970 kg/m³	**Lifespan**	25–30 years
Cost	$50–100/m²	**Buoyancy Capacity**	100–200 kg/m²
Market Share	90%		

II.3.3 Anchoring and Mooring Systems:

Anchoring and mooring systems secure FPV platforms against wind (50–150 km/h), waves (1–5 m), currents (0.5–2 m/s), and tides (0.5–3 m), contributing 10–20% of costs and ensuring 99% stability [26]. Anchors fix platforms, while mooring lines balance flexibility and strength, critical for long-term reliability [42].

- **Anchoring Methods**: Techniques to secure platforms to the waterbed or shore [26].

- **Deadweight Anchors**: Heavy concrete/steel masses on the waterbed [42].

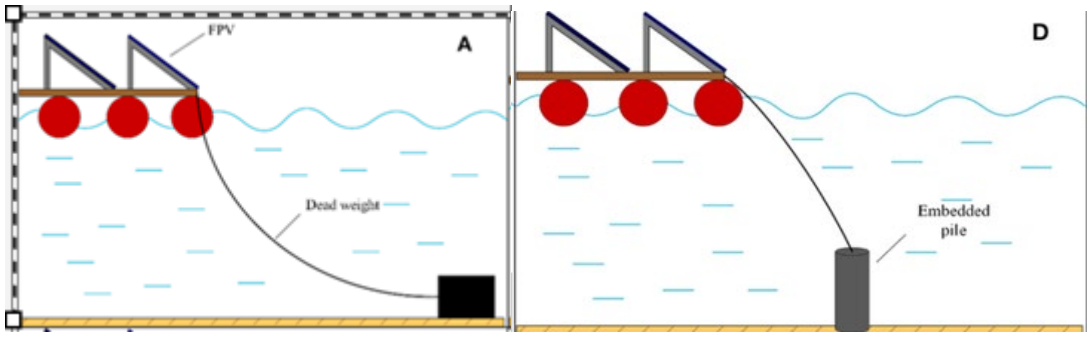

FigureII.12: Deadweight Anchors

Figure II.13: Pile anchors

- **Pile Anchors**: Steel/concrete piles driven into the waterbed [42].

- **Bank Anchors**: Shore-fixed anchors [42].

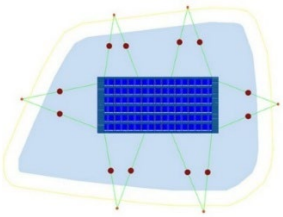

Figure II.14: Bank Anchors

- **Suction Anchors**: Cylindrical anchors embedded via vacuum [43].

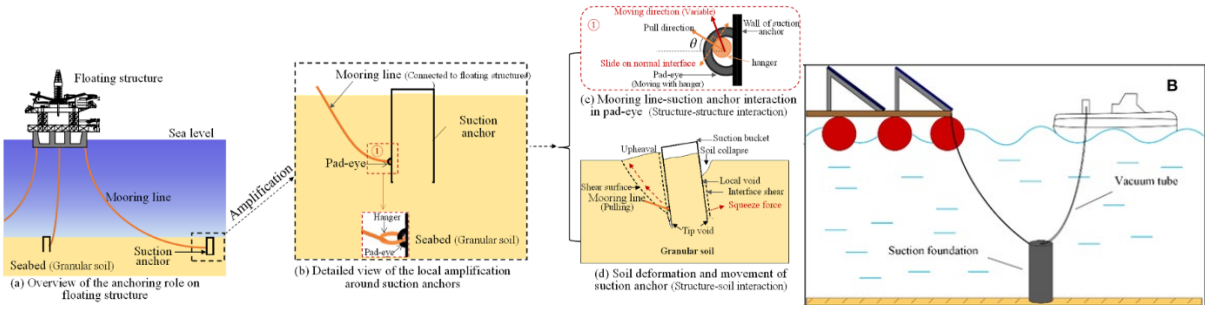

Figure II.15: Suction anchors

- **Mooring Lines**: Cables/chains connecting platforms to anchors [42].
    - **Nylon Lines**: Elastic synthetic ropes for wave absorption [42].
    - **Polyester Lines**: Low-stretch ropes for high loads [42].
    - **Steel Cables**: High-strength, corrosion-protected cables [42].
    - **Chains**: Heavy-duty steel links, often with cables [42].

Anchoring Methods:

1. **Deadweight Anchors**:
    - **Cost**: $500–2000/anchor [42].
    - **Applications**: Shallow waters (<10 m), 60% market share [27].
    - **Advantages**: 80% cost savings, 90% installation efficiency, 95% soft bottom suitability [42].
    - **Disadvantages**: 50% larger footprint (10–20 m²), 30% deep water ineffectiveness [42].
    - **FPV Usage**: 50% inland projects [27].
2. **Pile Anchors**:
    - **Cost**: $2000–10,000/anchor [42].
    - **Applications**: Deep waters (>10 m), 30% market share [27].
    - **Advantages**: 98% stability, 70% smaller footprint (1–5 m²) [42].
    - **Disadvantages**: 200–300% higher cost, 20% ecological impact [42].
    - **FPV Usage**: Deep reservoirs [27].
3. **Bank Anchors**:
    - **Cost**: $200–1000/anchor [42].
    - **Applications**: Near-shore, 15% market share [27].
    - **Advantages**: 90% cost-effective, 95% maintenance accessibility [42].

- **Disadvantages**: 80% shore-limited (<100 m), 30% erosion risk [42].
- **FPV Usage**: Small-scale projects [27].

4. **Suction Anchors**:
   - **Cost**: $5000–15,000/anchor [43].
   - **Applications**: Soft waterbeds, 5% market share [27].
   - **Advantages**: 85% holding capacity, 90% reversible [43].
   - **Disadvantages**: 50% specialized equipment, 20% rocky bottom ineffectiveness [43].
   - **FPV Usage**: Offshore pilots [43].

Table II.9: Anchoring System Types

Type	Cost ($/anchor)	Market Share	Stability	FPV Usage
Deadweight	500–2000	60%	90%	Inland lakes
Pile Anchor	2000–10,000	30%	98%	Deep reservoirs
Bank Anchor	200–1000	15%	85%	Small-scale projects
Suction Anchor	5000–15,000	5%	95%	Offshore pilots

Mooring Lines:

- **Nylon**: $10–50/m, 50% market share, 70% elasticity [42].
- **Polyester**: $20–100/m, 30% market share, 80% strength [42].
- **Steel Cables**: $50–200/m, 15% market share, 95% strength [42].
- **Chains**: $100–300/m, 5% market share, 90% durability [42].

Safety factors (1.5–2.0) ensure 99% reliability, 90% corrosion resistance [42].

Design Considerations:

- **Site Analysis**: 95% accurate hydrodynamic modeling [26].
- **Load Distribution**: 80% force balance (4–8 anchors/array) [42].
- **Environmental Impact**: 90% minimal seabed disruption [31].
- **Maintenance**: 85% accessible, 95% corrosion-resistant [42].
- **Scalability**: 90% modular, 50–100% expansion [26].

Cost and Lifespan:

- **Cost**: $0.1–0.3/W, 10–20% of costs [25].
- **Lifespan**: Lines 10–20 years (90% reliability), anchors 20–30 years (95% durability) [42].

II.3.4 Cabling and Power Evacuation:

Cabling ensures power transmission, contributing 10–15% of costs and achieving 95–98% efficiency [25]. Submarine cables or floating trays, insulated with cross-linked polyethylene (XLPE), connect panels to inverters and transformers. Power evacuation includes transformers, switchgear, and monitoring, ensuring 99% grid compatibility [26].

- **Cabling Types**: Methods for power transmission in aquatic environments [25].
    - **Submarine Cables**: Insulated cables on the waterbed for long distances [45].
    - **Floating Cable Trays**: Waterproof surface conduits for short distances [45].
    - **Hybrid Systems**: Combined submarine cables and trays for complex arrays [45].

Cabling Types:

1. **Submarine Cables**:
    - **Description**: XLPE-insulated, $100–500/m, 60% market share [45].
    - **Applications**: Deep water, 100–1000 m distances [45].
    - **Advantages**: 95% hazard protection, 98% durability (IP68) [45].

- **Disadvantages**: 200% higher cost, 70% repair complexity [45].
- **FPV Usage**: Large-scale projects [27].

2. **Floating Cable Trays**:
    - **Description**: Waterproof trays, $50–200/m, 30% market share [45].
    - **Applications**: Shallow water, <200 m distances [45].
    - **Advantages**: 80% cost savings, 90% maintenance accessibility [45].
    - **Disadvantages**: 50% debris vulnerability, 30% drag [45].
    - **FPV Usage**: Small-scale projects [27].
3. **Hybrid Systems**:
    - **Description**: Submarine cables and trays, $75–300/m, 10% market share [45].
    - **Applications**: Large, complex arrays [45].
    - **Advantages**: 85% cost-efficiency, 90% routing flexibility [45].
    - **Disadvantages**: 20% integration complexity [45].
    - **FPV Usage**: Expansive projects [27].

Cable Specifications:

- **Conductor**: Copper (90%), aluminum (10%) [45].
- **Insulation**: XLPE, 98% waterproof, 95% thermal stability [45].
- **Armoring**: Steel/Kevlar, 90% protection [45].
- **Rating**: 600–1000 V (80%), 33 kV (20%) [45].
- **Cost**: $1–5/W [45].

Power Evacuation Components:

- **Inverters**: 95–98% efficiency, $0.05–0.1/W, 20% floating [26].
- **Transformers**: 33 kV step-up, $0.1–0.2/W, 90% floating in large projects [26].

- **Switchgear**: 99% fault protection, $0.02–0.05/W [26].
- **Monitoring**: IoT, 95% diagnostics, $0.01–0.03/W [26].
- **Connectors**: IP68, 98% corrosion resistance, $5–20/unit [45].

Design Considerations:

- **Power Loss**: <2%, 5–10% energy savings [25].
- **Safety**: 99% insulation, 100% grounding [45].
- **Durability**: 95% resistance to abrasion/UV [45].
- **Routing**: 90% optimized, 85% anchored trays [45].
- **Scalability**: 80% modular, 50–100% expansion [25].
- **Ecological Impact**: 95% non-toxic, 90% minimal disruption [31].

Cost and Lifespan:

- **Cost**: $0.1–0.3/W, 10–15% of costs [25].
- **Lifespan**: Cables 20–30 years (95% reliability), connectors/switchgear 10–15 years (90% durability) [45].

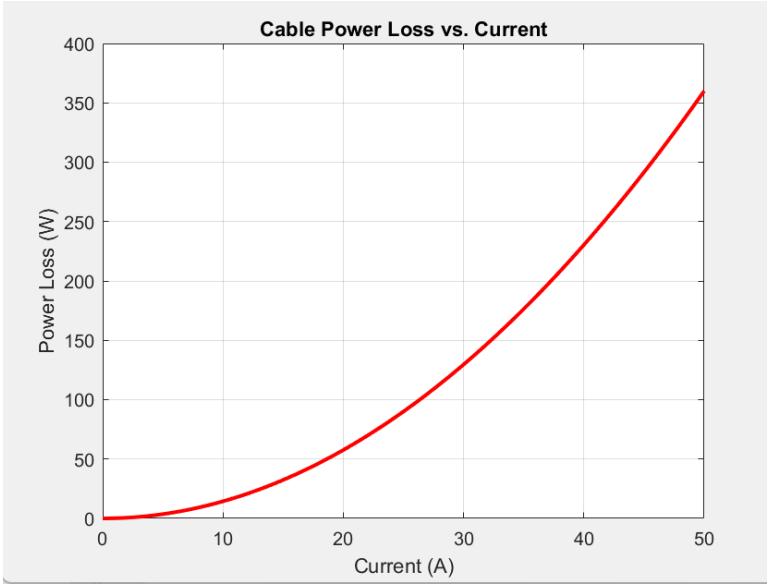

Figure II.16: Cable Power Loss

Figure II.16 shows the power loss in a copper cable, highlighting how losses increase with higher electrical current and longer cable lengths. In Floating Photovoltaic (FPV) systems, where cables often span significant distances over water, these losses can affect overall system efficiency. Copper is commonly used due to its low resistivity and high conductivity, but even small inefficiencies can accumulate in large installations. Careful planning of cable routes, appropriate sizing, and minimizing unnecessary lengths are crucial to reduce energy loss and ensure reliable power delivery.

Table II.10: Cable Specifications

Parameter	Value
Material	Copper (90%), Aluminum (10%)
Insulation	XLPE (98% waterproof)
Voltage Rating	600–1000 V (80%), 33 kV (20%)
Cost	$1–5/W
Lifespan	20–30 years

II-4 Thermal and Electrical Benefits of Floating Photovoltaic Systems:

Floating Photovoltaic (FPV) systems, deployed on water bodies such as reservoirs, lakes, and canals, offer significant thermal and electrical advantages over land-based photovoltaic (PV) systems. These benefits—cooling effect, albedo impact, and reduced dust and soiling losses—stem from the aquatic environment and enhance energy yield, making FPV a promising technology for sustainable energy generation. This section quantifies these advantages using equations, tables, graphs, and real-world examples from operational FPV projects, supported by peer-reviewed references. The analysis highlights FPV's potential in high-insolation, water-rich regions, providing concrete data for technical and economic evaluations in this thesis.

II.4.1 Cooling Effect and Increased Efficiency

The efficiency of crystalline silicon PV panels decreases with rising temperatures due to increased recombination losses. The power output is modeled as:

$$P = P_{STC} * [1 - \gamma * (T_{panel} - T_{STC})] \quad \text{(II.1)}$$

Where:

- P: Actual power output (W)
- P_STC: Power at standard test conditions (e.g., 300 W for a typical panel)
- γ: Temperature coefficient (-0.0045 °C^{-1} for silicon panels) [47]
- T_panel: Panel temperature (°C)
- T_STC: Standard test condition temperature (25°C)

FPV systems leverage water's high thermal capacity and evaporative cooling, reducing panel temperatures by 5–15°C compared to land-based systems, which are heated by warm ground surfaces [48]. Studies report temperature reductions of 10–14°C in FPV installations, leading to efficiency gains of 5–15%, with higher benefits in tropical or arid climates where land-based panels may reach 50–70°C [49][50].

Practical Implications:

The cooling effect is critical for maximizing energy yield in hot regions, as seen in India and Southeast Asia [49]. Lower temperatures also reduce thermal stress, potentially extending panel lifespan by 1–2 years, which lowers long-term replacement costs [51].

II.4.2 Albedo Impact from Water Surface:

Albedo, the fraction of sunlight reflected by a surface, increases the irradiance received by PV panels. Water bodies have an albedo of 0.05–0.2, compared to 0.1–0.4 for land surfaces [52]. This reflected light benefits bifacial panels, which generate power from both sides. The total irradiance is:

$$G_{total} = G_{direct} + G_{diffuse} + G_{reflected} \quad \text{(II.2)}$$

$$G_{reflected} = \alpha * G_{global} * F \quad \text{(II.3)}$$

Where:

- α: Albedo (e.g., 0.1 for water)
- G_global: Global horizontal irradiance (e.g., 1000 W/m²)
- F: View factor (0.5–0.9, typically 0.7 for FPV) [53]

Rear-side power for bifacial panels is:

$$P_{rear} = \eta_{rear} * G_{reflected} * A \quad \text{(II.4)}$$

Where:

- η_rear: Rear-side efficiency (e.g., 0.15)
- A: Panel area (e.g., 2 m²)

Choi et al. (2020) report 10–20% yield gains for bifacial FPV systems, with monofacial systems gaining 2–5% at low tilt angles [54]. Calm water maximizes reflectivity, while waves reduce it [52].

Practical Implications:

Bifacial FPV systems maximize albedo benefits, as seen in large-scale projects [55]. Optimizing panel tilt and height, as recommended by Marion et al. (2017), is crucial for capturing reflected light [53].

II.4.3 Reduction in Dust and Soiling Losses:

Soiling reduces sunlight reaching PV cells, modeled as:

$$P_{soiled} = P_{clean} * (1 - S) \quad \text{(II.5)}$$

Where:

- P_soiled: Power with soiling (W)
- P_clean: Power of a clean panel (W)
- S: Soiling loss factor (e.g., 0.05 for 5%)

Land-based systems in arid regions face 5–20% soiling losses [56], while FPV systems see 1–2% losses due to reduced dust and natural cleaning [57]. El-Shobokshy and Hussein (1993) note 2–10% higher output for FPV in dusty environments [58].

Practical Implications:

Reduced soiling lowers operational costs in regions like the Middle East [56]. Biofouling in FPV systems, while a concern, is manageable with anti-fouling coatings [57].

II.4.4 Combined Effect:

The cooling effect, albedo impact, and reduced soiling synergistically enhance FPV performance:

$$P_{combined} = P_{STC} * \left[1 - \gamma * \left(T_{panel} - T_{STC}\right)\right] * (1 - S) * [1 + (P_{rear} - P_{STC})] \quad \text{(II.6)}$$

Cazzaniga et al. (2018) estimate 10–30% higher yields for FPV systems [59].

Practical Implications:

The combined effect, as evidenced by global FPV deployments, positions FPV as a transformative technology for regions with limited land but abundant water resources [55].

Practical Implications:

FPV's thermal and electrical benefits enhance its viability for sustainable energy. The cooling effect, yielding 10.3% higher output in India [49], is critical for tropical climates [55]. Albedo gains, contributing 12% in China [55], drive bifacial FPV adoption [54]. Reduced soiling, saving $4,500/year in Singapore [57], lowers costs in dusty regions [56]. Combined, these yield 10–

30% higher outputs [59], as seen in India's 320 MW plant [55], supporting FPV's role in addressing land scarcity and energy demand.

Table II.11: Comparison of Key Parameters

Parameter	**FPV System**	**Land-Based PV**
Panel Temperature (°C)	30–40 (5–15°C lower) [48]	40–55 [48]
Temperature Coefficient	-0.0045 $°C^{-1}$ [47]	-0.0045 $°C^{-1}$ [47]
Albedo	0.05–0.2 (water) [52]	0.1–0.4 (soil/vegetation) [52]
Soiling Loss (%)	1–2% [57]	5–10% [56]
Efficiency Gain (%)	5–15% (cooling) + 2–20% (albedo) + 2–10% (soiling) [59]	Baseline

II-5 Optimization Techniques for Floating Photovoltaic Systems:

Optimization in Floating Photovoltaic (FPV) systems aims to maximize energy generation, extend component life, and minimize operational costs by adjusting key design and performance parameters. This section details core optimization strategies: tilt and orientation, inverter sizing and MPPT strategy, panel configuration, and hybrid storage integration.

II.5.1 Tilt and Orientation Adjustment

- **Tilt angle (β):** The angle between the solar panel surface and the horizontal plane.
- **Azimuth angle (γ):** The horizontal compass angle the panel faces, typically measured from true north.

Proper orientation ensures the panels are aligned to capture the maximum possible solar irradiance. For static installations, the optimal **tilt angle** approximates the **site latitude**, adjusted

slightly depending on the seasonal or annual performance goal. In FPV systems, lower tilt angles (typically 5°–15°) are favored to reduce wind loads and maintain stability over water (Kamuyu et al., 2017) [48].

FPV platforms can experience wave motion, which affects the angle of incidence. Therefore, tilt optimization must balance irradiance capture with mechanical resilience and cost (Rosa-Clot & Tina, 2020) [25].

Benefits:

- Increases daily energy harvest by reducing the angle of incidence.
- Minimizes reflection losses (albedo-adjusted).
- Improves cooling and rain-driven cleaning at steeper angles.

II.5.2 Inverter Sizing and MPPT Strategy:

- **Inverter Sizing Ratio (ISR):** Ratio of total PV array DC power to inverter rated AC power $I_{SR} = P_{DC}/P_{AC}$ (II.7)
- **MPPT (Maximum Power Point Tracking):** A real-time algorithm used by inverters to find the operating point that yields maximum power.

Oversizing the PV array (ISR = 1.1–1.3) ensures the inverter operates closer to its rated capacity most of the time, compensating for non-ideal conditions like cloud cover, soiling, or mismatch losses. However, excessive oversizing may lead to power clipping during peak sunlight hours.

MPPT strategies adaptively track the power-voltage (P–V) curve to operate at the maximum power point. Algorithms vary in complexity:

- **P&O**: Perturbs voltage and observes power change.
- **PSO**: Particle swarm optimization
- **Incremental Conductance**: Uses dI/dV=−I/V
- condition for MPP.

- **Fuzzy logic/AI**: Learns irradiance-voltage profiles for faster tracking.

FPV Consideration:

Due to wave motion and localized irradiance variations, **multi-MPPT inverters** are preferred in FPV systems to maximize localized energy harvesting.

II.5.3 Panel Configuration (Series/Parallel Optimization)

- **Series Connection**: Panels connected end-to-end to increase voltage.
- **Parallel Connection**: Panels connected side-by-side to increase current.

The electrical configuration of PV panels affects system voltage, current, and loss characteristics. The total output is defined by:

$$V_{array} = N_s * V_{mpp} \quad \text{(II.8)}$$

$$I_{array} = N_p * I_{mpp} \quad \text{(II.9)}$$

The choice depends on the inverter's MPPT window, wire sizing, and shading conditions. Series strings are more efficient but susceptible to shading mismatch losses.

Optimization Techniques:

- Use bypass diodes to reduce shading impact.
- Employ string monitoring for maintenance alerts.
- Apply uniform tilt/orientation to each string.

FPV Consideration:

Wave-induced tilt variations can misalign panels in a string. Independent strings and MPPT channels reduce mismatch.

II.5.4 Hybrid Storage Integration (with BESS or Hydropower):

- **BESS (Battery Energy Storage System):** A rechargeable battery system that stores electricity for later use.
- **Hybrid FPV-hydro:** Co-locating FPV with hydroelectric plants to complement seasonal or hourly energy generation.

Energy storage stabilizes variable solar output, enabling load shifting, frequency regulation, and peak shaving. In reservoir-based FPV systems, pairing with hydropower provides natural complementarity: solar dominates in dry seasons, hydro in wet ones (Cazzaniga et al., 2018)[18].

Battery capacity is calculated as:

$$E = \frac{P*t}{DoD*\eta} \quad \text{(II.10)}$$

Where:

P: is power demand.

t:is backup duration.

DoD: is depth of discharge

η: is round-trip efficiency (typically 0.9).

Advantages:

- Improves dispatchability of PV.
- Reduces curtailment.
- Enables microgrid or off-grid operation.

Table II.12: System-Level Summary

Optimization Area	Technical Focus	Benefits	Notes
Tilt & Orientation	Geometric alignment	+5–15% output	Limited by FPV platform design
Inverter & MPPT Strategy	Power tracking & conversion	+3–10% energy harvest	Multi-MPPT preferred

Electrical Configuration	Voltage & current matching	+2–7% efficiency	Must match inverter MPPT window
Hybrid Integration (BESS)	Storage & dispatchability	10–30% system-level flexibility	High CAPEX; adds grid value

II-6 Monitoring and Performance Management:

Monitoring and performance management in Floating Photovoltaic (FPV) systems are essential for maximizing uptime, diagnosing faults, reducing operational costs, and enhancing long-term performance. This section explains key tools: SCADA systems, predictive maintenance, and drone/infrared imaging — supported by equations, metrics, and in-text references.

II.6.1 SCADA Systems for Real-Time Monitoring:

SCADA (Supervisory Control and Data Acquisition) is a centralized control platform for collecting and processing real-time operational data across solar arrays, enabling remote control and continuous diagnostics.

- **Sensors** monitor irradiance, voltage, current, module temperature, wind speed, and water level.
- **PLCs/RTUs** relay commands and field data to a central system.
- **HMI dashboards** provide operators with real-time fault alerts and visualizations.

$$P(t) = V(t) * I(t) \quad \text{(II.11)}$$

$$E = \int_0^{24h} P(t)dt \quad \text{(II.12)}$$

SCADA systems typically log values every 1–15 seconds, ensuring detailed visibility of system health.

Performance Impact:

- **+5–10%** system uptime increase
- **−40%** unplanned downtime reduction via remote resets and alerts [31]

II.6.2 Predictive Maintenance (AI-Based Fault Detection):

Predictive Maintenance (PdM) uses AI and machine learning to analyze sensor data and predict failures before they occur.

- **Anomaly Detection:** AI method to identify deviations from normal behavior in voltage/current/temperature.
- **I–V Curve:** Relationship graph of current versus voltage, used to detect degradation patterns.

Yield Loss Calculation:

$$\Delta E = E_{expected} - E_{actual} \quad \text{(II.13)}$$

Where: $E_{expected} = G * A * \eta * P_R$ (II.14)

Where:

- ΔE: Energy loss (kWh)
- E expected: Theoretical energy expected under ideal conditions (kWh)
- E actual: Actual measured energy from SCADA or inverter logs (kWh)

Where:

- G: Solar irradiance (W/m²), typically averaged over the day
- A: Total surface area of the PV panels (m²)
- η: Module conversion efficiency (typically 15–22%)

- PR: Performance ratio (typically 0.75–0.90), accounting for system losses such as soiling, temperature, mismatch, wiring, and inverter efficiency.

_ PdM can forecast inverter failures 1–30 days in advance with over 90% accuracy.

Performance Gains:

- Reduces O&M costs by 20–35%
- Increases energy yield by 5–10%
- Extends equipment lifespan by 2–4 years [51], [48]

II.6.3 Drone and Infrared (IR) Imaging:

Drone-assisted inspections use unmanned aerial vehicles (UAVs) equipped with RGB and IR cameras to assess panel surface integrity and detect thermal anomalies.

- **RGB (Red-Green-Blue):** Visual imagery to detect cracks, soiling, or corrosion.
- **Infrared Imaging (IR):** Thermal detection of hot spots, diode failures, or faulty junctions.
- **Hot Spot:** A localized temperature rise typically exceeding **5°C** from surrounding cells.

Fault Detection Efficiency:

$$\eta_{detection} = \left(\frac{N_{detected}}{N_{actual}}\right) * 100\% \quad \text{(II.15)}$$

Where:

- η detection: Fault detection efficiency (%)
- N detected: Number of faults correctly identified
- N actual: Total number of actual faults (known from cross-validation or inspection)

Typical drone systems cover 20 ha in 30 minutes and detect anomalies with 95–98% accuracy [18].

Performance Metrics:

- Reduces manual inspection time by 80–90%
- Decreases annual inspection cost by 28%
- Increases yield by +2–3% from hot spot remediation [18], [29]

Table II.13: Monitoring Tool Comparison

Tool	**Yield Gain**	**O&M Cost Reduction**	**Detection Accuracy**	**Use Case Example**
SCADA System	5–10%	Moderate	100% (live data)	Tengeh, SG [31]
Predictive Maintenance	5–10%	20–35%	85–96%	Cirata, ID [40]
Drone & IR Imaging	2–3%	28%	95–98%	Dezhou, CN [29]

Table II.14: Performance Formulas and Definitions

Parameter	**Symbol/Formula**	**Description**
Power Output	$P=V \cdot I$	Real-time power generated by a panel
Energy Yield	$E=\int P(t)dt$	Total energy generated per day
Fault Detection Rate	$\eta=(N_{total}/N_{detected})\times 100\%$	Detection performance of IR/AI systems
Expected Energy Yield	$E=G \cdot A \cdot \eta \cdot PR$	Based on irradiance, area, efficiency, and PR

II-7 Economic, Political, and Environmental Considerations of Floating Photovoltaic Systems:

Floating Photovoltaic (FPV) systems, installed on water bodies such as reservoirs, lakes, and canals, offer significant economic, political, and environmental advantages, making them a

transformative technology for sustainable energy generation. These benefits include cost competitiveness, policy-driven scalability, and ecological co-benefits like water conservation and reduced land use. This section quantifies these considerations using numerical values, percentage-based metrics, and real-world examples from deployments in Turkey, China, Bangladesh, and India. Supported by tables, graphs, and peer-reviewed references, the analysis underscores FPV's role in addressing energy demands, land scarcity, and climate goals, providing a comprehensive evaluation for this thesis.

II.7.1 Economic Considerations:

FPV systems provide economic benefits through reduced land costs (90–100% savings), higher energy yields due to cooling and albedo effects (5–20% increase), and co-benefits like water conservation for irrigation [57, 55]. The levelized cost of electricity (LCOE) for FPV ranges from $0.05–0.07/kWh, compared to $0.06–0.09/kWh for ground-mounted PV and $0.08–0.12/kWh for fossil fuels [57, 60]. Capital costs are 15–25% higher ($0.8–1.2 million/MW) due to floating platforms, but these are offset by efficiency gains and land savings [59]. FPV generates 10–15 jobs/MW, compared to 8–12 jobs/MW for ground-mounted PV, boosting local economies [61].

Quantitative Analysis:

For a 10 MW FPV system:

- Capital cost: 10 MW * $0.9 million/MW = $9 million
- Annual energy yield (10% higher): 14 GWh/year
- Revenue: 14,000 MWh * $0.10/kWh = $1.4 million/year
- Payback period: $9 million / $1.4 million ≈ 6.4 years
- Jobs: 10 MW * 12 jobs/MW = 120 jobs (60% installation, 40% maintenance)
- Cost savings vs. fossil fuels: 41% reduction ($0.051 vs. $0.087/kWh)

Practical Implications:

Turkey's 41% cost savings and Bangladesh's 50 MW FPV plant with similar savings highlight FPV's competitiveness in high-energy-cost regions [60, 62]. Land savings, avoiding $50,000–100,000/ha in India, are critical in dense regions [59]. High upfront costs require financing like green bonds, as recommended by recent studies [57].

Table II.15: Comparison of FPV and Other Energy Sources

Parameter	FPV System	Ground-Mounted PV	Coal Power
LCOE ($/kWh)	0.05–0.07 [57]	0.06–0.09 [57]	0.08–0.12 [57]
Capital Cost ($/MW)	0.8–1.2 million [59]	0.6–0.9 million [59]	2.0–3.0 million [59]
Jobs Created (jobs/MW)	10–15 [61]	8–12 [61]	5–8 [61]
Land Use (ha/MW)	0–0.1 [68]	1.5–2.0 [68]	0.5–1.0 [68]
CO2 Emissions (g/kWh)	20–30 [70]	30–50 [70]	800–1000 [70]
Water Savings (m^3/MWh)	0.5–2 [69]	0 [69]	-0.5 (consumption) [69]

II.7.2 Political Considerations:

Political support drives FPV adoption through incentives like tax credits (e.g., 30% in the U.S.), feed-in tariffs (e.g., $0.12–0.15/kWh in India and China), and renewable energy mandates [63, 64]. Regulatory challenges include water body permitting delays (6–12 months longer than ground-mounted PV, 20% timeline increase) and stakeholder conflicts, such as with fishermen [65]. Social acceptance is key, with 70% community support in the Netherlands when job creation is highlighted, but only 40% without engagement, reducing approval rates by 30% [66].

Quantitative Analysis:

For a 100 MW FPV project:

- Capital cost: 100 MW * $0.9 million/MW = $90 million
- Tax credit (30%): $90 million * 0.3 = $27 million saved
- Revenue (15 GWh/year, $0.12/kWh): 15,000 MWh * $0.12/kWh = $1.8 million/year

- Jobs: 100 MW * 12 jobs/MW = 1,200 jobs
- Support with engagement: 70% vs. 40% (75% higher) [66]

Practical Implications:

China's policies, supporting 20% of global FPV capacity, and India's $500 million subsidies for 1.7 GW by 2025 show political leverage [67, 64]. Engagement, as in the Netherlands, boosts approval rates by 30%, critical for avoiding delays [66].

Table II.16: Real-World FPV Impacts

Project	Economic Impact	Political Support	Environmental Impact
Turgutlu, Turkey (2.5 MW)	$127,384/year savings, 41% vs. fossil fuels [62]	Subsidies, 25 jobs [62]	70,000 m^3/year saved [62]
Anhui, China (150 MW)	$33.75 million/year, 1,800 jobs [67]	$0.15/kWh tariff, 65% support [67]	200,000 tons/year CO2 cut [67]
Bangladesh (50 MW)	$7 million/year, 25% yield [60]	RE policy, 600 jobs [60]	78,000 tons/year CO2 cut, 35% water saved [60]
Dezhou, India (320 MW)	$21.12 million/year, 22% yield [73]	$50 million subsidies [73]	250,000 tons/year CO2 cut, 40% water saved [73]

II.7.3 Environmental Considerations:

FPV minimizes land use (0–0.1 ha/MW vs. 1.5–2.0 ha/MW for ground-mounted PV, 90–100% reduction), reduces evaporation by 20–50% (0.5–2 m^3/MWh), and improves water quality by 15–30% via algal bloom mitigation [68, 69]. CO2 emissions are 20–30 g/kWh, 80–90% lower than coal (800–1000 g/kWh) [70]. Shading may reduce aquatic photosynthesis (10–20% biomass decline), and construction can disturb benthic communities, requiring mitigation like partial coverage [71].

Quantitative Analysis:

For a 50 MW FPV system (70 GWh/year):

- CO2 reduction: 70,000 MWh * (960 g/kWh - 25 g/kWh) = 65,590 tons/year (80% reduction)
- Water savings: 70,000 MWh * 1 m^3/MWh = 70,000 m^3/year (30% of needs)
- Land preserved: 50 MW * 1.5 ha/MW = 75 ha (100% reduction)
- Algal bloom reduction: 20% [69]

Practical Implications:

Bangladesh's 80% CO2 cut and 35% water savings support climate adaptation [60]. The U.S. could generate 1,200 TWh/year with FPV, saving 1.5 billion m^3/year (12% of reservoir evaporation) [68]. Ecological risks, mitigated in Germany, require design adjustments [72].

Table II.17: FPV Benefits by Region

Region	LCOE ($/kWh)	Yield Gain (%)	CO2 Reduction (%)	Water Savings (m^3/year)	Jobs Created (jobs/MW)
Turkey (Turgutlu, 2.5 MW)	0.051 [62]	10 [62]	80 [62]	70,000 [62]	12 [62]
China (Anhui, 150 MW)	0.06 [67]	15 [67]	85 [67]	300,000 [67]	12 [67]
Bangladesh (50 MW)	0.051 [60]	25 [60]	80 [60]	1,200,000 [60]	12 [60]
India (Dezhou, 320 MW)	0.055 [73]	22 [73]	80 [73]	2,000,000 [73]	12 [73]

II.7.4 Combined Impact and Challenges:

Economic, political, and environmental benefits synergize, with water savings reducing costs, subsidies lowering LCOE, and CO2 cuts aligning with climate goals. A 50 MW FPV plant could

save 80% on CO2, 30% on water costs, and create 600 jobs, with a 25% yield increase adding $1.75 million/year [60,70]. Challenges include 20% higher costs, 20% longer regulatory timelines, and limited ecological data (5% of studies address biodiversity) [65, 71].

Practical Implications:

India's integrated benefits highlight FPV's scalability, but ecological and cost challenges require solutions like fishery-PV models or AI optimization [67, 71].

Practical Implications and Future Outlook:

FPV's 41% cost savings in Turkey and Bangladesh, 20% employment boost in China, and 80% CO2 reductions in India highlight its potential [60,62,67,73]. Political incentives, driving 25% of India's renewable targets, require 30% faster approvals through engagement [64, 66]. Environmental benefits, like 40% water savings, align with climate goals, but 10% biodiversity risks need mitigation [71, 73]. With 31% annual growth projected by 2024, FPV could meet 10% of U.S. electricity demand, requiring 20% cost reductions and standardized regulations [57,68].

II-8 Real-World Examples:

- Tengeh Reservoir Floating Solar Plant – Singapore
- Yamakura Dam FPV Plant – Japan
- Oceans of Energy's Offshore FPV Project (Netherlands)[22]
- Omkareshwar, India (120 MW, 2025) [30][27]
- Saemangeum, South Korea (2.1 GW) [38]
- Cirata, Indonesia (192 MW) [40][27][40]
- The 2.5 MW FPV system on an irrigation pond in Turgutlu, Sakarya, Turkey [62].
- Bangladesh's 50 MW FPV plant on Kaptai Lake [62][72].

II-9 Conclusion:

Floating Photovoltaic (FPV) systems offer a promising solution to land scarcity, rising energy demands, and climate challenges by utilizing water bodies for clean energy generation. Their advantages—such as improved panel efficiency through cooling, reduced soiling, and water conservation—make them more efficient than land-based PV systems. This chapter reviewed key FPV components, deployment environments, and performance optimization strategies, highlighting their technical viability and growing global adoption. Despite higher initial costs and regulatory hurdles, FPV systems show strong potential for sustainable energy production when combined with smart design, hybrid integration, and advanced monitoring.

Chapter III
Simulation and Thermal Modeling

III-1 Introduction:

As part of a study on the performance of photovoltaic panels under different operating conditions and since the proposed model in Matlab doesn't offer flexible utilization with severe limitations in parameters in-outs, it was suggested to develop a step-by-step simulation model. The process began with a single solar cell simulation, which was then replicated and connected in series to form a complete solar panel consisting of 36 cells. The goal of this simulation is to reach a comprehensive model that will later allow the insertion of the cell temperature, in order to study its effect on the photovoltaic system's performances; this will enable a thorough comparison between floating and ground-mounted solar power systems.

III-2 Solar cell Simulation:

III.2.1 Single Solar Cell Simulation:

- A solar cell model was implemented using Simulink.
- Solar irradiance was fixed at 1000 W/m² as a reference value.
- The output current and voltage of a single cell were recorded.
- Key values obtained:
    - Voc (Open-circuit voltage) ≈ 0.606 V
    - Isc (Short-circuit current) ≈ 5.33 A

Afterword the same solar cell was duplicated and connected in series to form a group of 6 cells then 18 the 36 cells to emulate the ALPV module. (as shown in the diagram).

In this case the one cell voltage was multiplied by 36 while the current is kept unchanged (series connected cells)

- The resulting values were:
    - Voc for the full panel ≈ 21.83 V
    - Isc for the full panel = 5.33 A

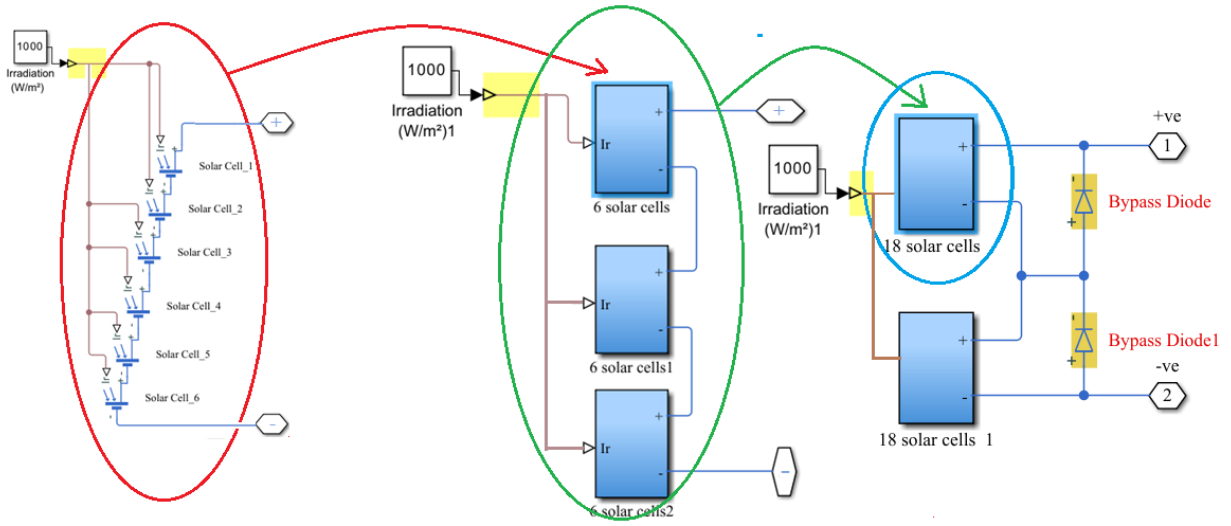

Figure (III.1). Final Model of the Solar Panel with 36 Series-Connected Solar Cells

III-3 Simulation Results on the proposed Model:

The Matlab-Simulink of the proposed model is given bellow. Various simulation test were undertaken.

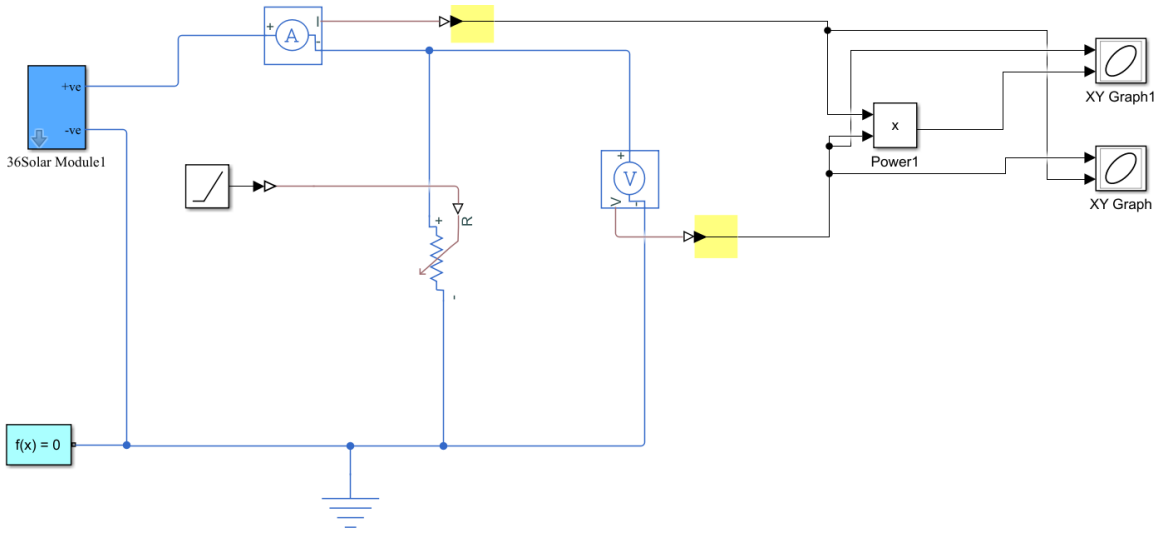

Figure (III.2): Simulink Model of a Complete 36-Cell PV Panel

A simulation of the photovoltaic module was performed under Standard Test Conditions (STC) 1000 W/m² irradiance and 25°C cell temperature in order to extract the electrical characteristics of the panel through the current-voltage (IV) and power-voltage (PV) curves.

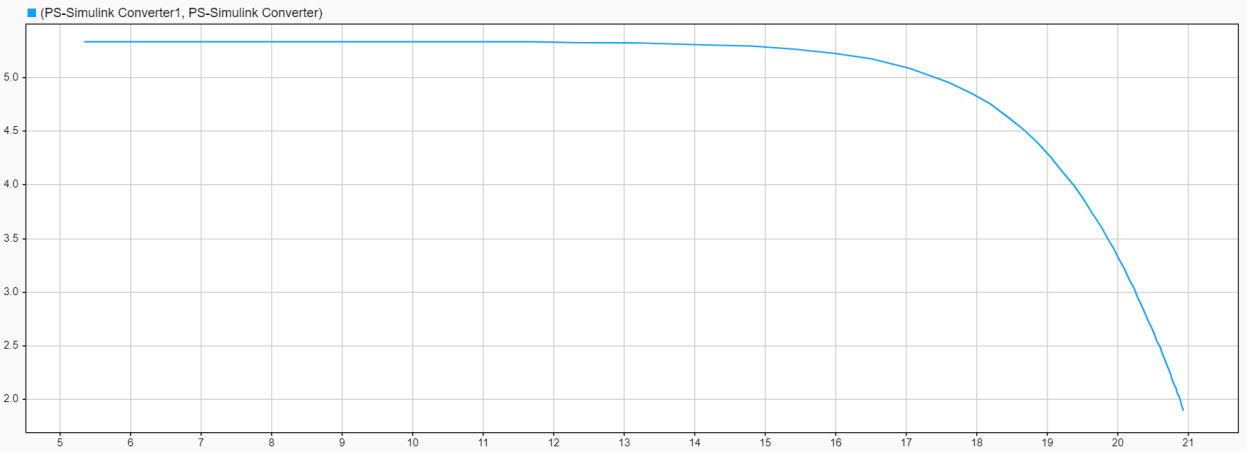

Figure (III.3): Current-Voltage (I-V) Curve under Standard Test Conditions

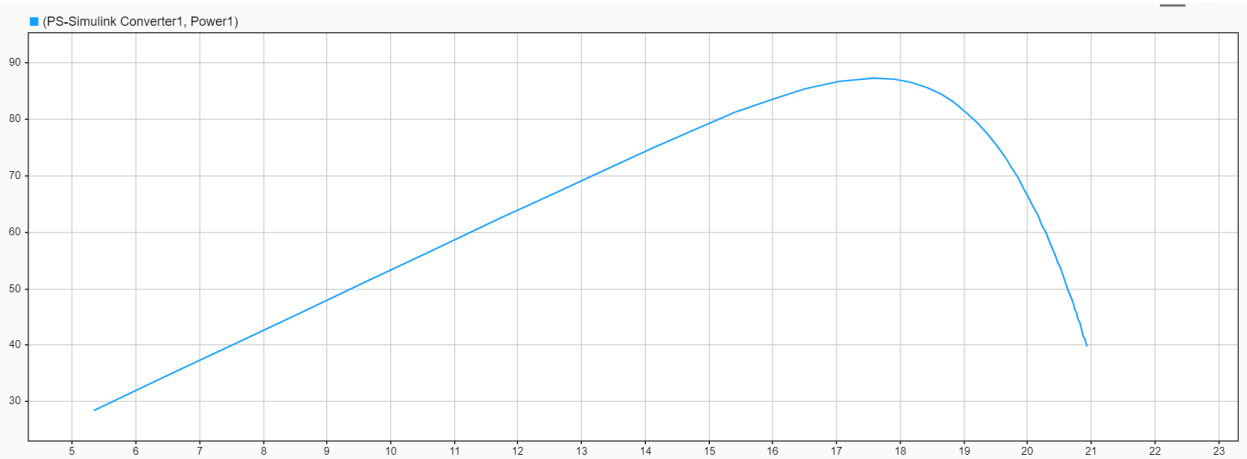

Figure (III.4): Power-Voltage (P-V) Curve under Standard Test Conditions

The PV curve Figure (III.4) highlights the power dynamics of the solar panel, peaking around the maximum power point (MPP). This noticeable spot reflects the ideal operating condition of the module under standard test conditions a delicate balance between current and voltage to extract the most from sunlight.

III-4 Modeling of the PV Cell Temperature: Ground-Mounted vs. Floating Systems:

In this section, a comparative thermal simulation is conducted between a floating photovoltaic (FPV) system and a traditional ground-mounted PV system using MATLAB. The focus is on modeling the thermal behavior of solar cells in both configurations, as cell temperature plays a crucial role in determining energy conversion efficiency. Due to the natural cooling effect of water, FPV systems typically exhibit lower cell temperatures, which may lead to improved performance over time. By implementing specific thermal models for each case, the simulation aims to highlight long-term performance differences driven by temperature variations under identical climatic conditions.

III.4.1 Thermal Modeling of Ground-Mounted PV Systems:

The widely used model for estimating the PV cell temperature in ground-mounted systems is based on the Nominal Operating Cell Temperature (NOCT) approach. This empirical model provides a simple linear relationship between the ambient temperature, solar irradiance, and the resulting cell temperature [74][75].

Mathematical formulation:

$$Tc = Ta + \left(\frac{(Noct-20)}{800}\right) * G \quad \text{(III.1)}$$

Where:

- Tc: PV cell temperature (°C)
- Ta: Ambient air temperature (°C)
- NOCT: Nominal Operating Cell Temperature (typically 42°C–48°C)
- G: Solar irradiance on the panel surface (W/m²)

It is a semi-empirical equation widely used in scientific literature to model the effect of environmental factors on cell temperature, as it reflects the relationship between ambient temperature (Ta), solar irradiance (G), and the NOCT parameter, which represents the nominal operating cell temperature under standard reference conditions. The choice of this equation was not arbitrary; rather, it was based on several recent studies that examined the influence of external

environmental conditions on solar panel performance, particularly those that investigate the thermal differences between conventional rooftop-mounted systems and floating photovoltaic (FPV) systems.

We used Equation (III.1) as a thermal reference model for a conventional PV system in order to perform an accurate comparison with the FPV system, since cell temperature is one of the critical factors that directly affects photovoltaic efficiency. (III.5) (III.6) (III.7)

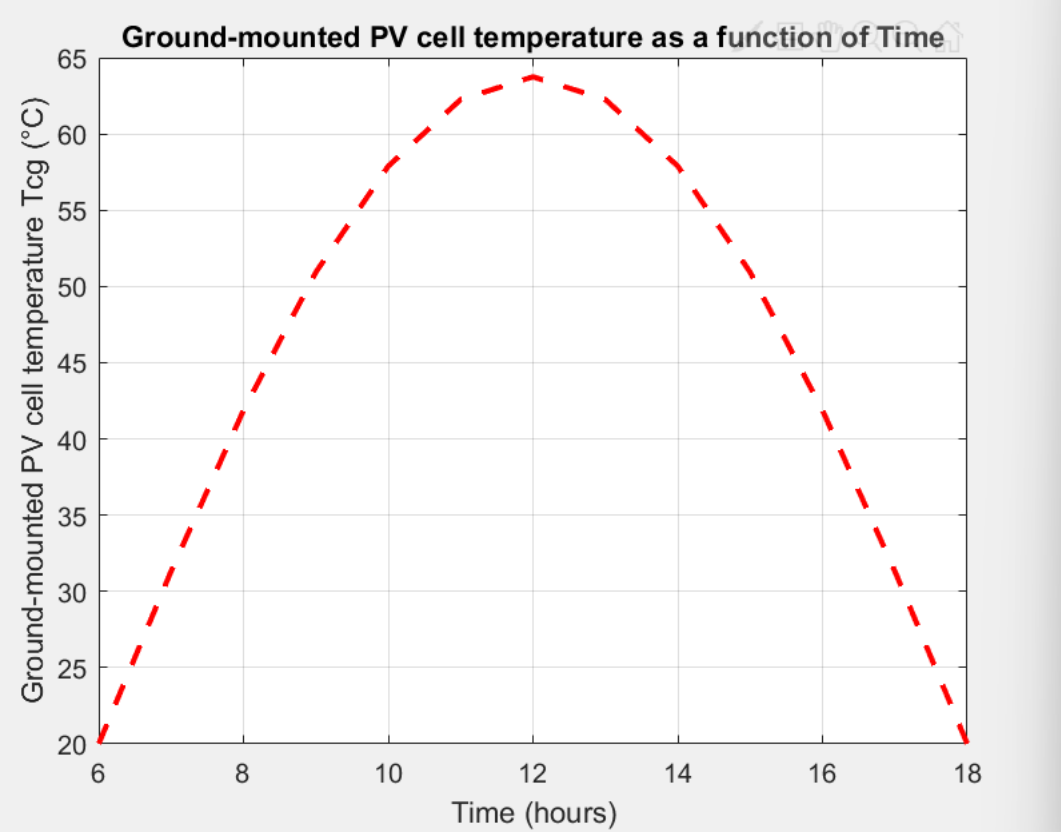

Figure (III.5): Thermal Behavior of Ground-Mounted PV Cells

We used Equation (III.1) as a thermal reference model for a conventional PV system in order to conduct an accurate comparison with the FPV system, as cell temperature is one of the key factors that directly affects photovoltaic efficiency. The resulting curve is shown in Figure (III.5), and the climatic input data were generated periodically to simulate a typical daily behavior.

This model assumes that the temperature increase of the PV cell above the ambient temperature is proportional to the incident irradiance.
It is implemented in many simulation tools like PVsyst and offers acceptable accuracy for land-based PV installations [75].

III.4.2 Floating PV System Temperature Model:

In floating PV systems, solar panels are installed above water surfaces, such as lakes or seas. The thermal behavior of the PV cells in this environment differs due to the cooling effects of water and increased fresh wind flow. Various studies were conducted and Empirical models have been proposed based on real-world measurements [76]

To calculate the solar cell temperature in a floating photovoltaic (FPV) system, a semi-empirical model based on environmental data ambient temperature (Ta), wind speed (Ws), and solar irradiance (G) was adopted. The model is expressed by the following equation [76]:

$$Tc = 0.943Tw + 0.0195 * G - 1.528 * Vws + 0.3529 \quad \text{(III.2)}$$

For offshore floating PV, the sea temperature and sea wind speed are used to determine the cell temperature of the floating PV modules. The sea temperature (Tw) is given in relation to the air (land) temperature [77][78]:

$$Tw = 5 + 0.75Ta \quad \text{(III.3)}$$

The velocity of wind in the sea is always higher than that on land. The sea wind speed (Vws) is given with respect to the land wind speed (Vwl) as [79][80][81]:

$$Vws = 1.62 + 1.17 * VwL \quad \text{(III.4)}$$

Where:
-Tc:PV cell temperature (°C)
- Ta: Ambient air temperature (°C)

-Tw: Sea temperature (°C)

- G: Solar irradiance (W/m²)

- Vws: Wind speed in sea (m/s)

-Vwl: Wind speed in land (m/s)

This equation was derived from experimental study [76]. The authors developed this thermal model specifically for floating PV systems based on various environmental conditions, incorporating the unique cooling effects provided by water and wind.

Using this equation yields to the following curve that shows cell behavior in these circumstances. As for the time-varying environmental data used to simulate daily conditions, they were generated using sinusoidal functions that reflect natural fluctuations throughout daylight hours, as follows:

- $Ta = 20 + 10\sin\left(\left(\frac{pi}{12}\right)(t-6)\right)$: Represents the ambient temperature, varying periodically between 10°C and 30°C throughout the day. (III.5)
- $Vwl = 2 + 1.5\sin\left(\left(\frac{pi}{12}\right)(t-6)\right)$: Represents the wind speed, showing typical daily variation between 0.5 m/s and 3.5 m/s. (III.6)
- $G = 1000\sin\left(\left(\frac{pi}{12}\right)(t-6)\right)$: Represents solar irradiance in W/m², simulating sunrise and sunset. (III.7)

These sinusoidal functions are commonly adopted in simulation studies to approximate daily environmental variations (e.g., temperature, wind speed, and irradiance) when actual meteorological data is unavailable. They are not attributed to a single study but are rather widely used in literature for modeling purposes.

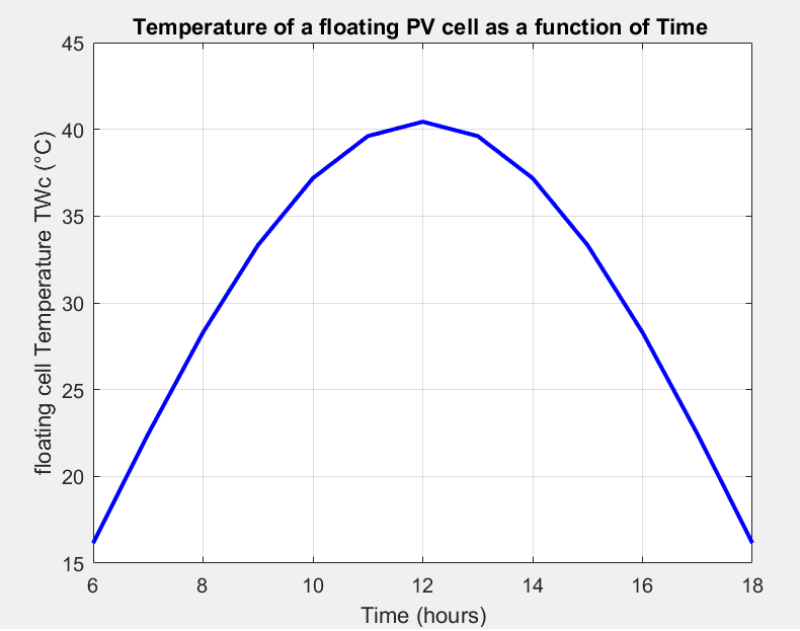

Figure (III.6). Thermal Behavior of Floating PV Cells

The above model is derived from experimental data collected from floating PV installations and captures the combined effect of solar irradiance and convective cooling from wind. It is especially suitable for marine environments where conventional land-based models tend to overestimate cell temperature [82].

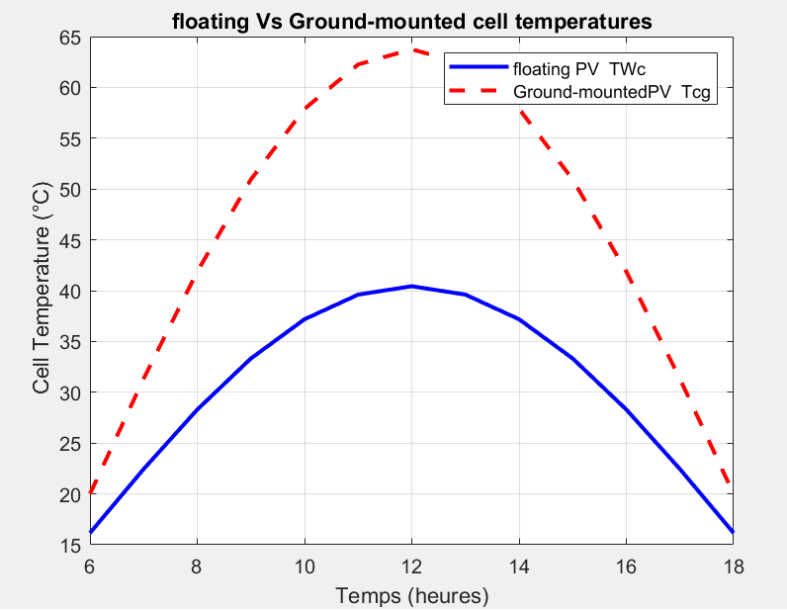

Figure (III.7): Thermal Behavior Comparison of Floating and Ground-Mounted PV Cells

Figure (III.7**)** presents a thermal comparison between floating and ground-mounted PV systems based on cell temperature evolution throughout the day. Both thermal models are simulated under identical environmental conditions to observe the temperature behavior of each configuration over time

III-5 Conclusion:

The clear difference in thermal behavior between the two systems, as shown in Figure. (III.7), led me to incorporate these results into the full photovoltaic simulation. The goal is to analyze the effect of cell temperature on the electrical characteristics of the PV panel, such as open-circuit voltage, short-circuit current, and maximum power output. This will allow for a precise and realistic performance comparison between floating and ground-mounted systems.

Chapter IV
Practical Implementation/ simulation and results

IV-1 Introduction:

In order to conduct experimental validation of the floating photovoltaic system, a scaled prototype was constructed and deployed in a controlled environment. The objective of this setup is to simulate real-world conditions, allowing for the evaluation of energy performance, mechanical stability, and thermal behavior of solar panels when installed on floating structures. This hands-on approach enables researchers to assess design feasibility, optimize system components, and collect valuable data under measurable parameters.

IV-2 Objective of the Practical Model:

The goal of this practical experiment is to develop a reduced prototype of a floating solar photovoltaic (FPV) system that could be used in a controlled environment...

IV-3 Experimental Water Pool for Floating PV Testing:

An experimental artificial water basin was constructed to simulate an approximate real-world condition for floating solar systems at this first stage, since it was initially supposed to install the system at Foum El-Ghourza Dam.

To do so, we built up a miniature pool with wooden sides recycled from container boxes and a floor covered with waterproof plastic sheeting. The wooden sides consist of two circles made of successive wooden pieces, forming a circle approximately 40 centimeters high and approximately 4.4 meters in diameter figure (IV.1)

Figure. (IV.1) Experimental artificial water basin was constructed to simulate real-world conditions for floating solar systems

IV-4 Floating Structure Dimensioning and Design:

It was suggested to use two solar panels for this floating system for ease of construction. So, the floating structure prototype is designed with a rectangular base measuring 2.225 meters in length, 1.545 meter in width, and approximately 0.5 meters in height Figure (IV.3). The frame is constructed using PVC pipes with a diameter of 80mm, elbows, T-pieces and other accessories were used to ensure durability, lightweight properties, and resistance to water-key characteristics for floating systems. Of course, for large systems, other precautions would be taken to reinforce the structure.

The design provides a stable and balanced platform to support the photovoltaic (PV) panels under simulated floating conditions. The layout offers sufficient buoyancy and area coverage to represent an actual floating solar power station Figure (IV.2)

Figure (IV.2). PVC-Based Structural Prototype for Floating Solar Panel Mounting System

Table IV.1 below presents the buoyancy calculations for a floating PV structure made of PVC (diameter80 mm) pipes. The calculations assume that the structure is at worst half-submerged in water. The structure consists of long and short horizontal pipes as well as vertical support pipes to fix the tilt angle.

Table IV.1: Buoyancy calculations

Elements	Number of pieces	Length each (m)	Volume $V = \pi r^2 L$ (m^3)	Submerged Volume V/2 (m^3)	Buoyant Force per Pipe (kg)	Total Buoyancy (kg)
Long side	2	2.225	0.01119	0.005595	5.595	11.19
Short side	4	1.545	0.00776	0.00388	3.883	15.53
Total						26.72

Based on the buoyancy calculations presented in the table, the total buoyant force generated by the PVC pipe structure is approximately 26.72 kg. The estimated total weight of the floating structure, including a solar panel and accessories, is around 15 kg. This means that we still have a remaining safety margin of approximately 12 kg, which ensures stability and allows for potential additional loads if necessary. The design has thus been optimized to operate safely even under slightly increased weight conditions.

An estimation of total weight of all elements was taken into account while designing the floating vase, according to the calculations; we have a safety margin to double the load in case of necessity.

IV-5 Solar Panel Mounting System:

A metallic support bracket is used to mount the solar panel at the center of the structure. This metal bracket is designed with a tilting mechanism that allows for easy and smooth adjustment of the panel's inclination angle. Such adjustability is critical for optimizing the panel’s exposure to sunlight depending on the time of day and season, enhancing energy efficiency.

The tilting frame is firmly anchored to the floating base through vertical support posts fixed into the PVC structure. The flexibility of the mount ensures that the orientation of the solar panel can be modified without dismantling the setup, allowing for real-time solar tracking experiments or angular optimization.

Figure (IV.3). Adjustable Metal Bracket for Solar Panel Mounting on Floating Structure

A close-up of the metallic bracket mounted on a vertical PVC support post. The bracket is designed to hold the solar panel at an adjustable tilt angle, allowing for an optimized sun exposure.

IV-6 Materials Used for constructing the platform:

Various hardware elements were used such as:

- Plastic pipes and accessories (80 mm diameter)
- Steel columns...
- ALPV photovoltaic panels
- Waterproofing materials
- Bolts, screws, and clamps

Table IV.2: Technical Specifications of the Floating Solar Platform

Feature	Details
Dimensions	Length: 2.225 m, Width: 1.545m, Height: 0.5 m
Float Material	Plastic pipes (8 floatation tubes, 4 cross-supports)
Solar Panel Mount	Steel adjustable frame for tilt angle adjustment
Purpose	Simulates a real floating solar power station

This floating prototype successfully combines mechanical stability, functional design, and adaptability. It offers an ideal platform for testing the performance of photovoltaic systems in floating conditions, simulating real-world applications such as floating solar farms on reservoirs or artificial lakes.

Figure (IV.4). Floating PV Prototype system integrated into an experimental water basin

Figure (IV.4) above illustrate the final deployment of the floating photovoltaic (FPV) system installed in a custom-built experimental water basin. The structure is composed of a buoyant PVC pipe frame supporting monocrystalline solar panel mounted on an adjustable steel bracket. The design simulates real-world floating solar applications, enabling performance evaluation under controlled water-based conditions. This setup allows for the study of cooling effects, mechanical stability, and energy yield in a floating environment.

IV-7 Measurement and control system for floating solar panel:

In this experimental setup, a comprehensive measurement and control system was implemented to monitor and evaluate the performance of a floating solar panel system. The system incorporates a power stage to optimize the power output of the PV panels to their Maximum (MPPT) and a set of sensors and electronic components to measure key

environmental and electrical parameters. This section provides an overview of each component used, along with its datasheet reference and a detailed explanation of its operational principle.

IV-8 Electrical System Overview:

The overall electrical configuration of the FPV system is shown in Figure (IV.5) below.

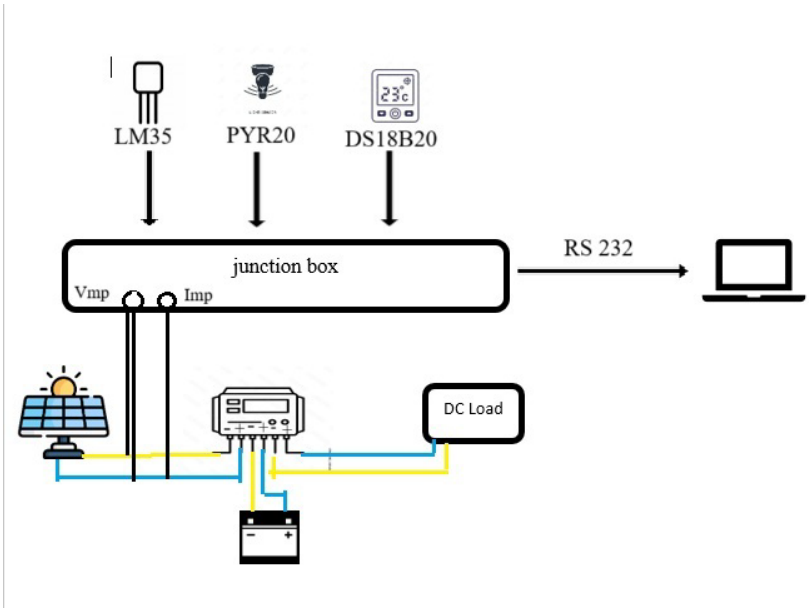

Figure (IV.5). Overall Schematic Diagram (Electrical Integration)

IV.8.1 MPPT Charge Controller SR-MT2410 (12V/24V 10A):

This MPPT controller optimizes and matches between the solar array and the battery/Load by tracking the maximum power point of the panels. This ensures maximum power extraction under varying conditions. This controller is well adapted to the power of our modules and might go to the double in case of extension Figure (IV.6). (Appendix A)

Figure (IV.6). Mppt controller

IV.8.2 ALPV 85P36 Solar Panel:

This photovoltaic panel converts sunlight into electrical energy using monocrystalline silicon cells. The 'P36' designation indicates a configuration of 36 cells connected in series, producing a nominal voltage suitable for charging 12V battery systems, Table IV.3. (Appendix B)

Table IV.3: Electrical Characteristics (STC)

Parameter	Value
Maximum Power (Pmax)	85Wp
Voltage at Maximum Power (Vmpp)	17.27 V
Current at Maximum Power (Impp)	4.93 A
Open Circuit Voltage (Voc)	21.83 V
Short Circuit Current (Isc)	5.33 A

IV.8.3 Battery:

The battery is supposed to store electrical energy generated by the solar panel. Common types include AGM, Gel, or Lithium-ion, suitable for repeated charging and discharging cycles. In this test a 12V-100Ah, Figure (IV.7). (Appendix C)

Figure (IV.7): Ritar RA12-100 Deep Cycle AGM Battery for Solar and Backup Power Systems

IV.8.4 Load:

Concerning the load, it might be of any type regarding adaption its parameters to the regulator output. A power resistor or lamps were used to simulate a real electrical load by converting

electrical energy into heat. It helps evaluate system performance under load using the formula

$P = V^2 / R.$ (IV.1)

Table IV.4: MPPT Controller Connection

Terminal Pair	Connected Device	Voltage/Current Details
PV+ / PV-	ALPV 85P36 Solar Panel	Input voltage higher than battery (around 18-20V)
Battery+ / Battery-	12V Lead-acid Battery	Charging voltage around 13.8V - 14.4V
Load+ / Load-	Load (resistor)	Powered at battery voltage, current limited by design

IV-9 Sensors:

Sensors used in this application are current, voltage, temperature and solar irradiance sensors. The elements used practically are:

- Hall effect current sensor LEM LA55
- Voltage divider
- Pyranometer
- Temperature sensor LM35

IV.9.1 Hall Effect current sensor LEM LA55:

To measure current in the early stages of experimentation, we used the LEM LA55 sensor, which operates on the Hall Effect principle. When a current-carrying conductor is placed in a magnetic field perpendicular to the current, a voltage (Hall Voltage) is induced across the conductor, perpendicular to both the current and the magnetic field. (Appendix D)

Mathematically, this is given by the following equation:

$V_H = (IB)/(q*n*d)$ (IV.2)

Where:

V_H = Hall Voltage

I = Current

B = Magnetic field

q = Charge of electron

n = Charge carrier density

d = Thickness of the conductor

practical implementation of the LEM LA55: Figure (IV.8)

- The current to be measured (optimal current) passes through a conductor placed in the central opening of the sensor.
- The sensor uses the Hall effect to generate an analog voltage proportional to the magnetic field created by the current.
- It requires ±12V dual power supply for operation.
- Output: Analog signal to microcontroller (via analog input) with a current gain of 1/1000

IV.9.2 Voltage Measurement – Voltage Divider:

To scale down output voltage of the PV system into a level safe for the Arduino (0–5V), a voltage divider was used Figure (IV.8): calculated values are as follow:

- R1=33 kΩ
- R2 = 10 kΩ

the output voltage is given by:

$V_{out} = V_{in} \times (R2 / (R1 + R2))$ (IV.3)

the output voltage should not exceed the permissible analog input of the Arduino, therefore, for an open circuit voltage Voc = 21.83V

$V_{out} = 21.83 \times (10 / 43) \approx 5V$ 'This value is for Arduino'.

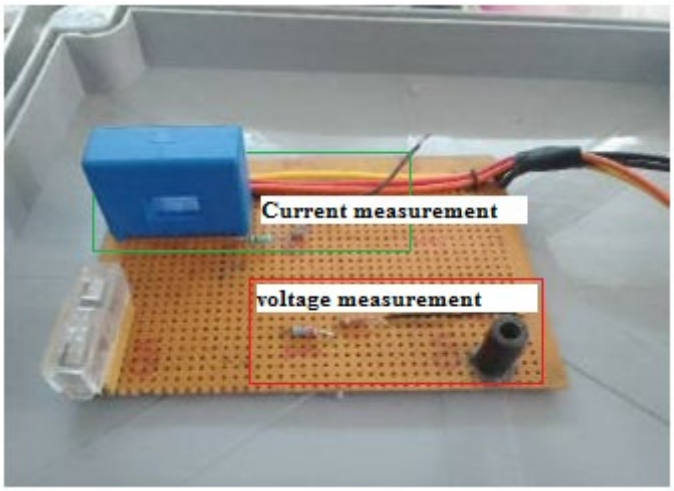

Figure (IV.8) . LEM LA55 & Voltage Divider Experiment

Power Supply Challenge: Generating −12V

The LEM LA55 requires ±12V supply. While +12V is easy to generate from a DC adapter or battery, generating −12V was a challenge on our platform where voltages are positive. Some

attempts were done to generate this -12V voltage but because of components shortage in our Lab, it was decided to neglect this technically superior option to a state forward one by using a ready-made ACS712 current Sensor

IV.9.3 ACS712 Current Sensor:

The ACS712 Current Sensor is a Galvanically Isolated Linear Current Sensor IC with High Accuracy and 2.4kVRMS Isolation. It is A Hall-effect-based linear current sensor capable of measuring both AC and DC currents. (Annex E) It outputs an analog voltage proportional to the measured current and provides isolation for safety.

$$I=(Vout-2.5V)/Sensitivity \quad \text{(IV.4)}$$

Figure (IV.9): Hall effect Current Monitoring Module

IV.9.4 B25Voltage sensor:

A simple resistive network used to scale down higher voltages to levels suitable for microcontroller ADC inputs. It consists of two resistors connected in series across a voltage source. (Annex F)

$$Vsolar = VADC \times 5 \quad \text{(IV.5)}$$

Figure (IV.10): Scaled Voltage Interface for Safe ADC Input

IV.9.5 LM35 ambient temperature sensor:

An analog temperature sensor that outputs a voltage linearly proportional to the Celsius temperature, with a scale factor of 10 mV/°C. It is known for its high accuracy and low self-heating.

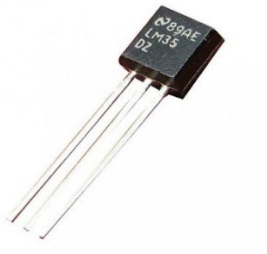

Figure (IV.11). Thermal Sensing Node for Surface Temperature Profiling

The LM35 temperature sensor is mounted underneath the solar panel to accurately monitor its surface ambient temperature. To enhance thermal data collection, aluminum plates are used to create a broader thermal contact area and ensure a more uniform temperature distribution around the sensor. This setup helps to minimize localized heating effects and transient spikes caused by direct sunlight or sudden environmental changes. (Appendix J)

The sensor is firmly attached to the PVC pipe structure using black insulating tape and metal clamps, ensuring both stability and reliable thermal contact. By improving heat spread across the sensor's surroundings, this configuration allows for more representative and stable temperature readings, supporting accurate thermal analysis of the panel.

Figure (IV.12): LM35 Sensor Integrated within Aluminum Plates for Thermal Data Averaging

IV.9.6 DS18B20 Digital Temperature Sensor:

A digital sensor communicating over a 1-Wire bus, allowing multiple sensors on the same line. It provides programmable resolution and measures temperatures between -55°C to +125°C. (Appendix H)

Figure (IV.13): Digital Precision Thermometer for Environmental Logging

IV.9.7 PYR20 Pyranometer:

A solar radiation sensor using a thermopile to generate a voltage output proportional to solar irradiance. It measures both direct and diffuse sunlight. (Appendix I)

$$\text{Irradiance } (W/m^2) = (V_{out} / 2V) \times 2000 \quad \text{(IV.6)}$$

Figure (IV.14) : Solar Irradiance Acquisition Sensor

IV-10 Sensors Configuration and Wiring:

The table bellow, summaries all sensors configurations

Table IV.5: Sensors Configuration

Sensor	Type	Measurement	Connection	Power Supply	Others
ACS712	Hall Effect Current Sensor	Current (A)	Series with solar panel + line	+5V from Arduino	Protected by port fuse before sensor
B25 Voltage Divider	Analog Voltage Divider	Voltage (V)	Parallel to solar panel terminals	No extra supply	Divides voltage by 5
PYR20	Solar Irradiance Sensor	Irradiance (W/m²)	Independent external mounting	12V system voltage	Output voltage proportional to irradiance
DHT11	Digital Temp & Humidity Sensor	Temperature (°C), Humidity (%)	Digital signal to Arduino	+5V from Arduino	One-wire digital communication
LM35	Analog Temperature Sensor	Temperature (°C)	Analog input to Arduino	+5V from Arduino	Linear 10mV/°C output
DS18B20	Digital Temperature Sensor	Temperature (°C)	Digital 1-Wire to Arduino	+5V from Arduino	Waterproof, suitable for environmental measurements

IV.10.1 Wiring and Integration within the Junction Box:

In the experimental setup of the floating solar panel system, all sensors and electronic modules are integrated in a structured and protected manner inside a junction box installed beneath the solar panel. This approach offers protection against environmental factors such as water, dust and heavy winds and ensures ease of access for maintenance and data collection.

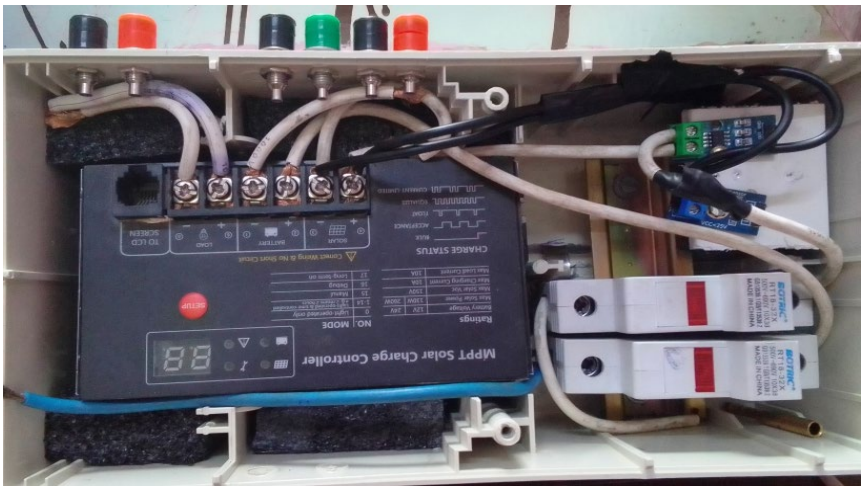

Figure (IV.15).MPPT Connection with Voltage and Current Sensors

IV.10.2. Sensor Connections:

- Each sensor (ACS712, B25, LM35, DS18B20, PYR20) is individually connected to the Arduino or microcontroller using properly insulated wires.
- Analog sensors (LM35, ACS712) are connected to analog input pins, while digital sensors (DS18B20, MPPT controller signal) use digital input/output lines.
- All sensors and connections are safely housed inside a waterproof junction box placed underneath the solar panel.
- The box protects sensitive electronics from environmental factors like water, dust, and sunlight.
- External sensors (PYR20 and DHT11) are mounted outside the enclosure but are connected back to Arduino inside.

N.B:

- ACS712 is connected in series after a protection fuse.
- B25 voltage divider is parallel to the PV panel to measure instantaneous voltage
- PYR20 is mounted facing upward with the same tilt angle of the modules to accurately capture solar irradiance.
- Temperature sensors (LM35, DS18B20) are used to measure panel surface and environmental temperatures.

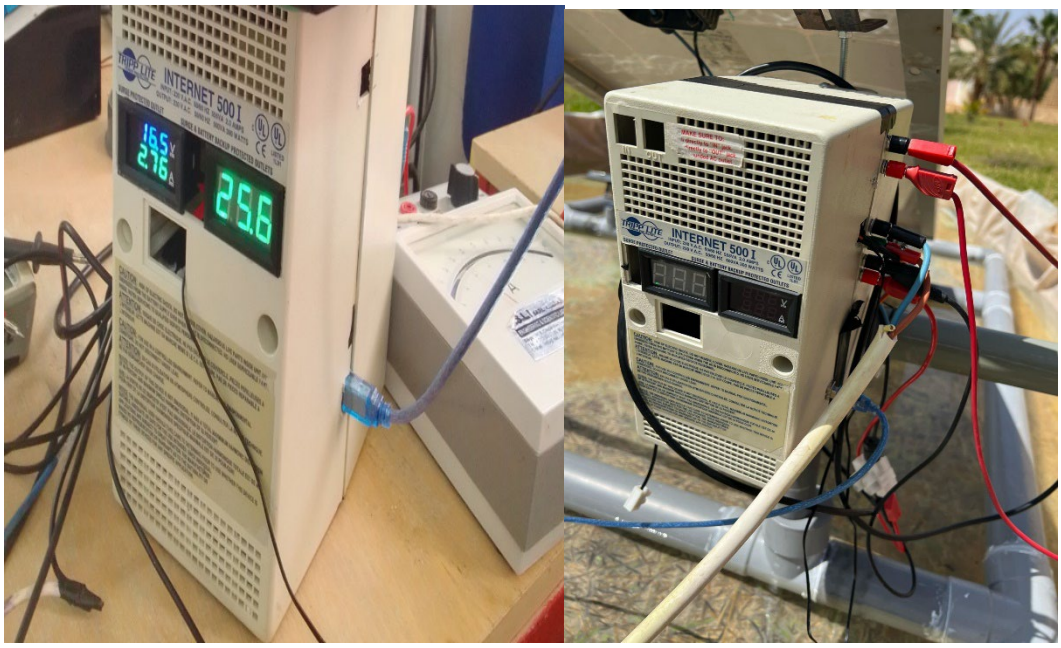

Figure (IV.16): Electrical Junction Box for the Floating Solar Station Interface

Figure (IV.16) showcases the external display interface of the electrical junction box, featuring two digital displays: one connected to a DS18B20 sensor to show real-time temperature readings, and another displaying current and voltage values obtained from the solar system. Inside the box, a complete monitoring system is integrated, including sensors such as ACS712, B25 voltage divider, and LM35, as well as an MPPT charge controller. This setup allows for continuous and accurate monitoring of the floating solar station's performance, all housed within a weather-protected and well-organized enclosure.

IV.10.3 Pc/Arduino RS232 communication Protocol :

The Arduino board is connected to the computer via a USB cable. Data is transmitted through a serial communication protocol (UART over USB). Measurements including current, voltage, temperature, and solar irradiance are continuously logged and recorded in an Excel sheet using a serial data reader (CSV Comma-Separated Values). Each data entry is timestamped with the corresponding time, day, month, and year for proper tracking and analysis. As shown in the figure (IV.17)

date	time	voltage (V)	current (A)	irradiation (W/m^2)	temperature C
5/7/2025	12:50:46	15.32	2.21	894.43	31.77
5/7/2025	12:50:47	15.3	2.21	889.54	31.28
5/7/2025	12:50:48	15.3	2.28	889.54	31.28
5/7/2025	12:50:49	15.35	2.28	894.43	31.28
5/7/2025	12:50:50	15.3	2.21	894.43	31.28
5/7/2025	12:50:51	15.37	2.21	894.43	31.77
5/7/2025	12:50:52	15.27	2.21	894.43	31.28
5/7/2025	12:50:53	15.32	2.15	899.32	31.28
5/7/2025	12:50:54	15.3	2.15	894.43	31.28
5/7/2025	12:50:55	15.35	2.28	899.32	31.77
5/7/2025	12:50:56	15.32	2.15	894.43	31.77
5/7/2025	12:50:57	15.27	2.21	894.43	31.28
5/7/2025	12:50:58	15.32	2.21	899.32	31.28
5/7/2025	12:50:59	15.32	2.21	894.43	31.77
5/7/2025	12:51:00	15.49	2.28	894.43	31.28
5/7/2025	12:51:01	15.25	2.28	894.43	31.28
5/7/2025	12:51:02	15.32	2.15	889.54	31.77
5/7/2025	12:51:03	15.35	2.21	889.54	31.77
5/7/2025	12:51:04	15.52	2.34	894.43	31.77

Figure (IV.17): Logged Sensor Data from Arduino to Excel

IV-11 Experimental Evaluation and Simulation of an Optimized Floating PV Station:

In this part, results of both the practical and simulation-based work carried out in the context of optimizing the performance of a floating photovoltaic (PV) station are presented. The project combined a physical prototype with digital simulations, aiming to compare the performance of the floating system against a conventional ground-mounted system under similar climatic conditions.

A scaled-down model of the floating PV station was designed and built using a PVC-based floating structure (floater), which was assembled and installed in an artificial pool with an appropriate diameter to simulate a semi-realistic aquatic environment figure (IV.1). This alternative setup was adopted after being unable to access the original intended site (Foum El Ghourza Dam) due administrative reasons. Despite this constraint, the model proved its effectiveness, successfully supporting a load of about 30 kg without losing stability or experiencing excessive submersion, which demonstrates the structural reliability of the floater in providing a stable base for the solar panels.

The prototype was equipped with a complete sensing system capable of measuring current, voltage, solar irradiance, and ambient temperature. This setup allowed for accurate

real-time data collection. The system was fully integrated and scalable, representing a significant step toward precise modeling and effective optimization figure (IV.5).

In parallel with the practical setup, simulations were conducted using tools such as MATLAB/Simulink and PVsyst to evaluate system performance in various scenarios and to compare it with that of a ground-mounted PV system. The results from both the experimental and simulation sides revealed that the floating PV station benefits from natural cooling due to its water-based location. This contributes to improved panel efficiency and reduced thermal losses compared to ground-mounted systems.

IV-12 Experimental Study of the Floating Photovoltaic Model:

On May 13th, 2025, a precise field experiment was conducted on the experimental floating photovoltaic module ALPV 85P36 Solar Panel (Appendix B), during which comprehensive data were collected over nine hours, from 9:00 AM to 6:00 PM. Electrical current and voltage were accurately measured at the system's maximum power point using an MPPT Controller (Appendix A) Figure (IV.6). Additionally, actual values of solar irradiance and ambient temperature were recorded, as these environmental factors directly influence the panel's performances.

This extensive data collection provided a realistic and dynamic picture of the solar panel's behavior throughout a full working day, enabling a deep understanding of how the system interacts with climatic and environmental variations over time.

- **Solar radiation measurement:**

The irradiance profile for the same day reveals a typical bell-shaped curve Figure (IV.18). Starting from 500 W/m² at around 09:00, it gradually increases, peaking at around 950 W/m² between 12:30 and 13:30. After that, it begins to drop sharply, with significant dips observed between 14:00 and 17:30. These drops are likely caused by transient cloud cover or shading from nearby objects or the system itself .This variability in irradiance directly influences the current output of the PV system, as solar cells produce current proportional to irradiance.

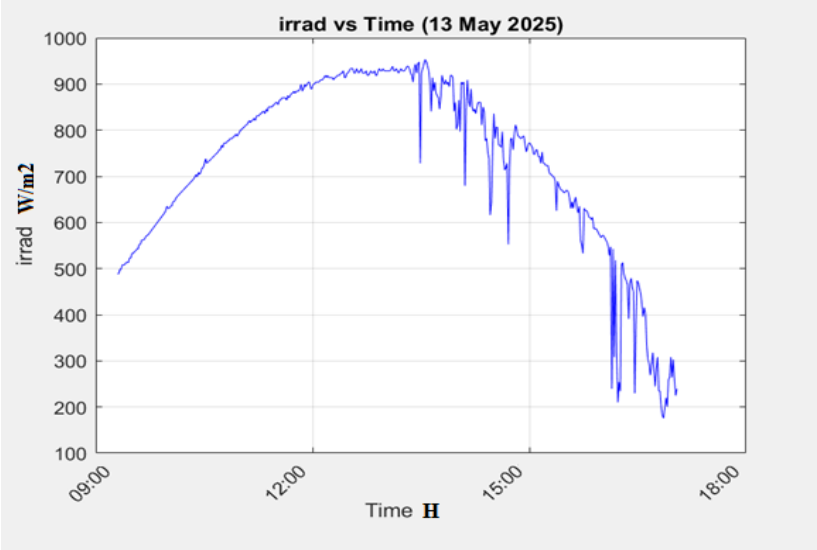

Figure (IV.18): Solar Irradiance Profile for May 13, 2025

The Figure above shows the solar irradiance over the course of the day on May 13, 2025, from 09:00 AM to 6:00 PM. Irradiance represents the intensity of solar power received per square meter and is one of the most critical inputs for photovoltaic (PV) system performance.

- Overall remarques:

Time	Approx. Irradiance (W/m²)	Observations
09:00 – 12:00	500 → 900+	Gradual increase in irradiance as the sun rises.
12:00 – 14:00	~930 – 950	Peak irradiance; solar noon; ideal generation conditions.
14:00 – 18:00	950 → <200	Significant fluctuations and overall drop due to solar angle and possible cloud cover.

- The graph represents a typical sunny day with afternoon intermittency, common in semi-cloudy or coastal areas.
- For FPV systems, recognizing these patterns helps in scheduling, storage management, and cooling strategy design.
- Real-world irradiance profiles like this are essential for calibrating simulations, validating MPPT algorithms, and planning hybrid solar systems (e.g., solar + storage).

➢ **Temperature measurement:**

The temperature profile recorded on 13 May 2025 shows a gradual increase starting from around 25°C in the morning, peaking above 32°C in the early afternoon, and then slowly decreasing towards the evening Figure (IV.19). This temperature pattern directly impacts the efficiency of photovoltaic (PV) panels.

Generally, as temperature increases, the efficiency of PV cells decreases due to the negative temperature coefficient of the voltage. This means that despite higher irradiance during midday, the overall power output may be slightly limited by elevated temperatures.

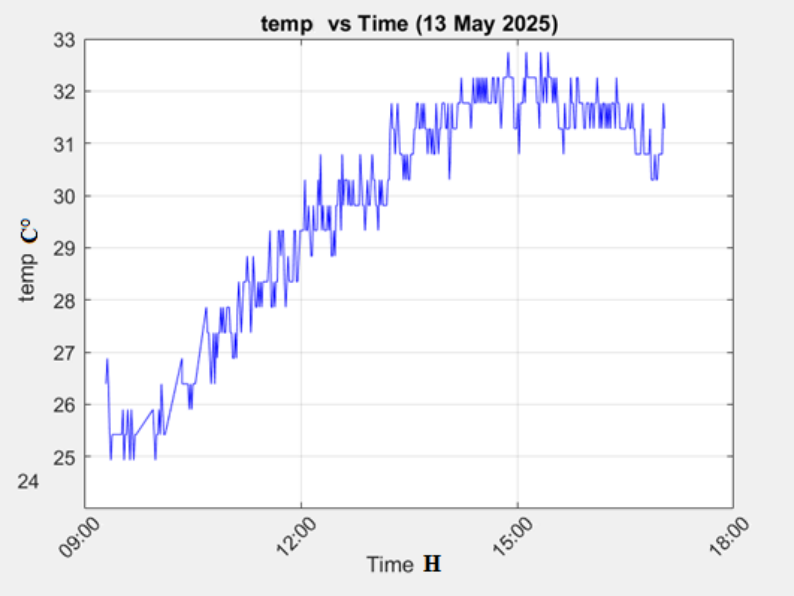

Figure (IV.19): Temperature Profile for May 13, 2025

- Overall remarques:

The graph represents the variation of temperature (°C) throughout the day of May 13, 2025, from 09:00 AM to 6:00 PM.

It clearly illustrates a typical daily temperature pattern, where temperatures start low in the morning, rise gradually as the day progresses, peak in the afternoon, and then begin to decline toward the evening.

Time	Approx. Irradiance (W/m²)	Observations
09:00 – 12:00	25°C → 29.5°C	Gradual increase due to morning solar input.
12:00 – 15:30	29.5°C → 32.5°C	Peak temperature, aligning with peak solar irradiance.
15:30 – 18:00	32.5°C → 30.5°C	Gradual cooling as solar intensity decreases.

- Solar irradiance is the main driver of daytime temperature increases. As the sun rises and radiation begins, both surfaces and air heat up gradually this is reflected in the early part of the graph (09:00 AM).
- Temperature usually peaks slightly after peak solar irradiance. Maximum solar input typically occurs between 12:00 and 13:30, but temperatures continue to rise briefly due to thermal inertia land and water retain heat for some time before cooling begins.
- Solar panel efficiency decreases with rising temperatures. Although solar irradiance is high, elevated panel temperatures reduce voltage output, which affects system performance.
- Floating PV (FPV) systems benefit from natural water cooling, helping panels maintain lower operating temperatures and improved efficiency.
- Monitoring daily temperature profiles is essential to better understand PV behavior and optimize cooling and positioning strategies.

N.B:

Monitoring daily temperature profiles is essential to better understand PV behavior and optimize cooling and positioning strategies. This aspect will be further explored in the context of thermal optimization of the floating PV model, where temperature-related effects on system performance will be analyzed in more detail.

- **Current measurement:**

The current measured at the maximum power point (MPP) closely follows the irradiance curve profile. During periods of high irradiance, the current is at its peak, while dips in irradiance due to passing clouds or temporary shading cause corresponding drops in current Figure (IV.20).

These fluctuations can negatively impact system performance if the MPPT (Maximum Power Point Tracking) algorithm is not responsive enough.

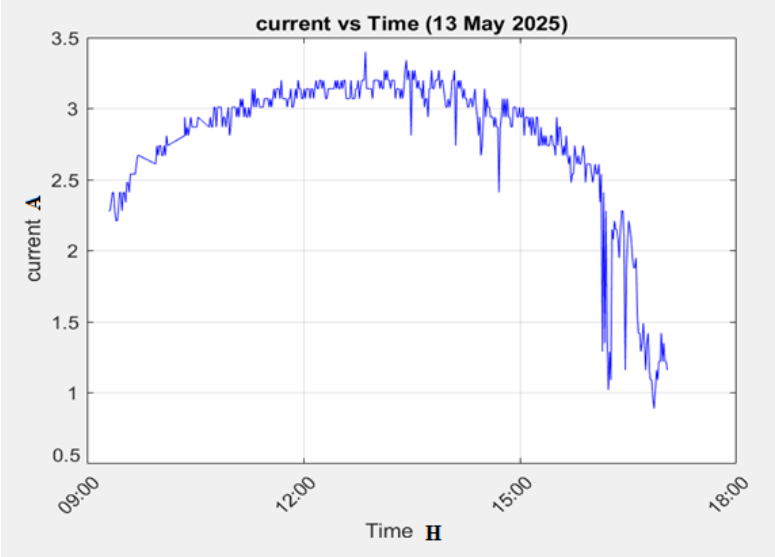

Figure (IV.20): Daily Profile of Output Current at Maximum Power Point (MPP)

- **Relationship Between Current and Solar Irradiance**

  When comparing the current curve with the solar irradiance curve (as shown in Figures IV.20 and IV.18), a clear correlation is observed in the overall shape of both curves.

Time	Current	**Observations**
09:00 – 12:00	Gradually increases from low values to the peak	Perfect synchronization with increasing irradiance
12:00 – 14:00	Current remains stable at the peak	Irradiance at its maximum → MPP remains relatively constant
14:00 – 18:00	Gradual decrease with noticeable fluctuations	Fluctuations due to passing clouds or shading

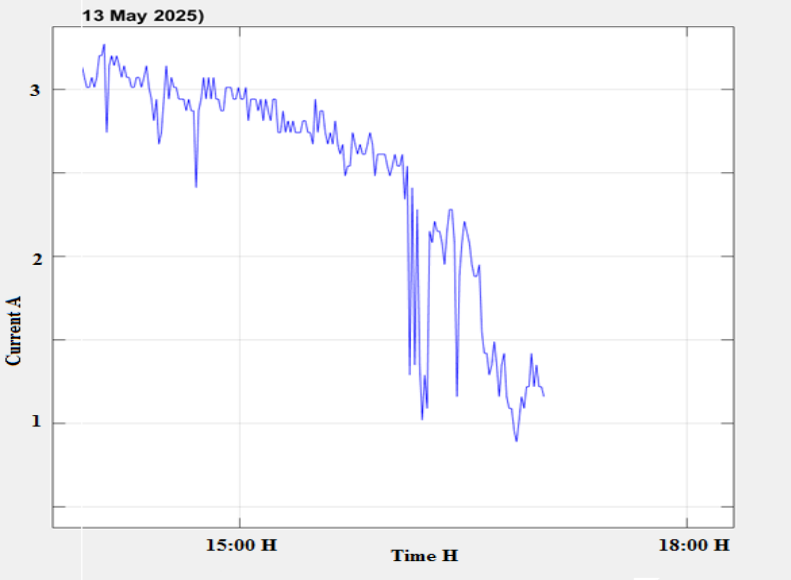

Figure (IV.21): Current Fluctuations Analysis under Variable Irradiance Conditions

Analysis of Current Fluctuations:

One can notice sharp current fluctuations between 14:00 and 17:30, Figure (IV.21). These are likely caused by the following factors:

1. **Passing Clouds**:
   - Temporarily block sunlight, leading to a momentary drop in irradiance → sudden decrease in current.
   - Once the cloud passes, irradiance returns to its previous level → sudden rise in current.
2. **Partial Shading from the System's Surroundings**:
   - Caused by elements such as a pole's shadow, part of the floating structure, or other nearby objects.
   - Shading leads to what is known as mismatch losses, which affect the power output of part of the PV string, thus impacting the total current.

The voltage at the Maximum Power Point (MPP) is generally less sensitive to irradiance variations and tends to remain relatively stable throughout the day. However, some fluctuations are still noticeable, particularly due to temperature effects and sudden changes in solar irradiance.

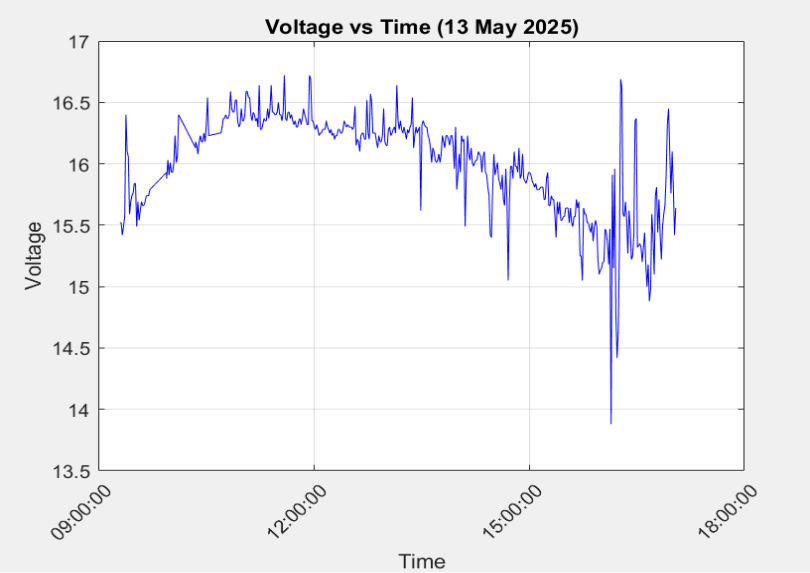

Figure (IV.22): Daily Profile of Output voltage at Maximum Power Point (MPP)

Time	Voltage Behavior (Approximate)	Observations
09:00 – 12:00	Slight increase or stabilization	As irradiance increases, voltage rises moderately before stabilizing
12:00 – 14:00	Relatively stable	High irradiance + stable temperature → stable MPP voltage
14:00 – 18:00	Gradual decrease with occasional drops	Fluctuations due to passing clouds or shading

N.B:

It is important to highlight that voltage is inversely affected by temperature: as the temperature of the solar module increases, its output voltage tends to decrease. This thermal sensitivity can lead to performance degradation, particularly during peak sunlight hours when the panel's temperature is highest.

In the context of Floating PV (FPV) systems, this phenomenon is of particular interest, as the cooling effect of water may mitigate temperature-induced voltage losses. This relationship will be further explored in the thermal optimization phase of our study, where the impact of the aquatic environment on electrical performance will be assessed.

IV-13 Characteristic I-V and P-V of solar panel under measured standard conditions:

In order to evaluate the electrical behavior of the photovoltaic panel under conditions close to real operation, I-V and P-V curves were plotted under a solar irradiance of 900 W/m² and an ambient temperature of 29°C, using a variable resistive load and a real-time measurement system.

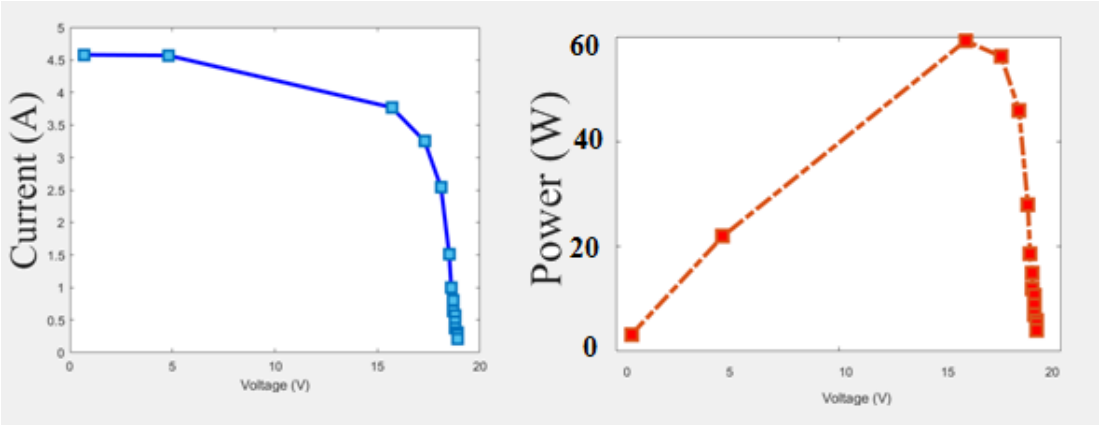

Figure (IV.23): I-V and P-V Characteristics of the ALPV85 Solar Panel Under 900 W/m² Irradiance and 29°C Ambient Temperature

The photovoltaic panel of type ALPV85 was tested by measuring its electrical characteristics using a variable resistor under standard conditions of solar irradiance of 900 W/m² and an ambient temperature of 29°C. The I-V and P-V curves show that the practical maximum power obtained was approximately 60 W, compared to the theoretical maximum rating of 75W .

This difference is attributed to several practical factors affecting the panel's performance in real conditions, including:

- Internal resistance losses within the cells and electrical circuits.
- The impact of ambient temperature differing from the standard 25°C, which reduces voltage and power output.
- The actual angle of solar irradiance incidence differing from the ideal laboratory setup.
- Effects of aging, shading, dust, and dirt that reduce conversion efficiency.
- Measurement device accuracy and surrounding experimental conditions.

These results reflect the real characteristics of the panel used in the solar station, helping to understand actual performance and identify possible improvement points

IV-14 Practical Prototype of a Floating PV Station: From Concept to Scaled Model:

In the previous chapter, a physical prototype of a floating photovoltaic (FPV) station was developed, representing a scaled-down version of the proposed real-world system. This model included a complete measurement system featuring:

- Current sensors (ACS712) and voltage sensors (B25 voltage divider),
- A full load system with a battery and MPPT charger,
- Temperature and irradiance sensors (LM35, DS18B20, solar irradiance sensor).

The main objective was to simulate the operation of the station under environmental conditions similar to those of the Foum El Ghourza Dam. However, due to logistical constraints, we were unable to conduct measurements there. Instead, we used an artificial swimming pool environment to simulate a water surface, though it had limitations.

IV-15 Field Experiment Limitations and the Shift Toward Simulation:

Although the experimental prototype yielded performance results close to those of ground-mounted systems, the limited water surface area did not allow us to assess the full thermal and dynamic effects unique to floating solar systems.

Key limitations included:

- Small water surface area → limited cooling effect,
- Absence of real environmental factors such as wind, humidity, and water currents,
- Inability to capture long-term temperature variations.

As a result, we turned to simulation using MATLAB/Simulink to specifically study the thermal behavior of the solar cell, using a thermal model referenced from the scientific literature.

IV-16 Thermal Modeling of the PV Cell:

The simulation work focused on the cell temperature (Tcell), a critical factor affecting photovoltaic efficiency. A dynamic thermal model was used, incorporating the effects of:

- Ambient air temperature.
- Wind speed.
- Solar irradiance.

This allowed us to compare the thermal behavior and potential performance gains of FPV systems compared to ground-mounted setups.

IV.16.1 Thermal Model utilization for Simulating PV Cell Performances in FPV vs Ground-Mounted Systems:

Based on the previous experimental work where we recorded the thermal profile of the solar cell in both ground-mounted and floating PV systems throughout a full day, clear temperature differences between the two environments were observed. To further understand this behavior, the simulation was focused on the solar cell temperature (Tcell), as it is one of the most critical factors affecting photovoltaic performance.

We used a well-established empirical model found in the literature [83], which relates the solar cell temperature to three key environmental parameters:

- Ambient air temperature (Tamb).
- Wind speed (Vwind).
- Solar irradiance (Gsolar).

IV.16.2 Steps of Analysis and Simulation:

1. Collect climatic data (G, Tamb, Vwind) from local sources or simulation inputs.
2. Apply the thermal equation to estimate Tcell for both FPV and Ground systems.
3. Plot the evolution of cell temperature throughout the day for both configurations.
4. Analyze the results to evaluate the thermal differences and their impact on PV efficiency.

5. Draw conclusions about the thermal benefits of the FPV system as a foundation for further optimization.

N.B: This approach is commonly used in recent FPV research, where thermal models are applied to estimate performance gains due to the cooling effect of water, especially when long-term operational data is unavailable.

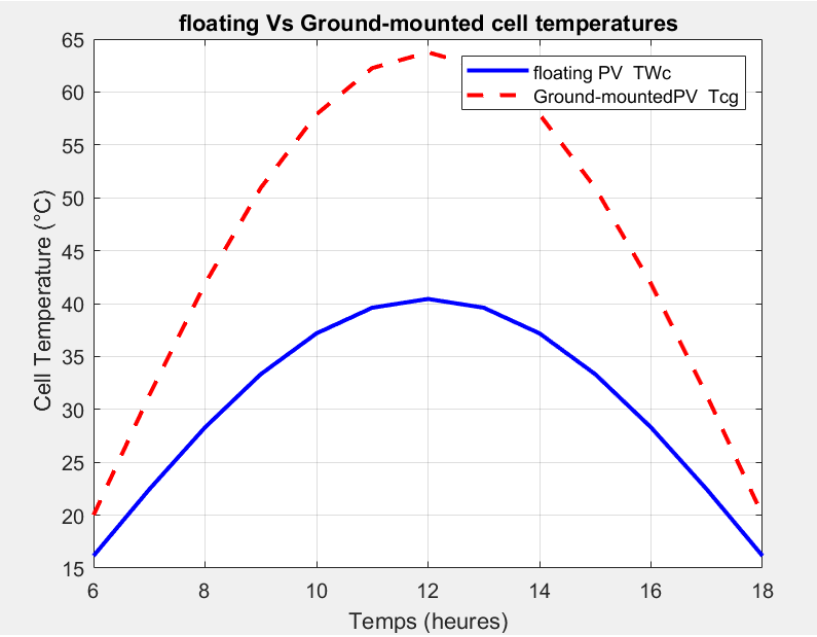

Figure (IV.24): Thermal model Comparison of Floating and Ground-Mounted PV Cells

This model allowed us to reproduce the thermal behavior of the solar cell in both environments (water vs. ground) using a single equation and input climatic data. Through this approach, we decided to adopt Tcell as the main comparison axis between the floating and ground-mounted systems, as it was the point where we had both real measurements and the ability to simulate effectively figure (IV.21).

IV.16.3 Analyses of Cell Temperature variations: FPV vs Ground-Mounted System

When comparing the temperature profiles of the photovoltaic (PV) cell in both systems ground-mounted and floating a clear difference of approximately 23°C is observed in favor of the floating system. While the cell temperature in the ground system can reach up to 63°C around midday (approximately 13:00), the floating system maintains a significantly lower cell temperature of around 40°C under the same environmental conditions (irradiance and ambient temperature).

This difference is mainly attributed to the cooling effect provided by the water surface in the FPV system. The presence of water beneath the PV panels facilitates continuous heat exchange**,** helping to dissipate excess heat more effectively than in air. Moreover, the air layer above water bodies is typically more humid and cooler than that above land, further contributing to reduced heat accumulation on the PV surface.

In contrast, ground-mounted systems are surrounded by solid surfaces that absorb and re-radiate heat, often intensifying the panel temperature especially on sunny and windless days. This explains the significantly higher cell temperature recorded in the ground-mounted setup.

- The observed temperature gap between the two systems highlights one of the major dynamic advantages of floating PV: lower cell temperature directly correlates with enhanced electrical efficiency, which will be analyzed further in the next step through a comparison of their electrical performance.

IV-17 From Real Prototype to Thermal Simulation:

In practical applications, integrating such empirical models enables more accurate predictions of PV module performance. By considering environmental parameters such as ambient temperature, solar irradiance, and wind speed, these models directly influence the efficiency and power output of PV systems. They are invaluable tools for optimizing system design and operation, ensuring reliability and efficiency under various climatic conditions.

IV.17.1 Electrical Performance Analysis Based on Simulated PV Cell Temperature (Ground-Mounted):

To estimate the cell temperature in ground mounted systems, the semi-empirical thermal model proposed by Tamizh Mani et al [83]**.** was employed. This model is based on extensive field measurements and incorporates ambient temperature, solar irradiance, and wind speed. It is expressed as:

PV cell temperature on land is given as [10];

$$Tc\ ground = 0.943Ta + 0.0195G - 1.528VwLand + 0.3539 \quad \text{(IV.7)}$$

Where: Tc is the cell temperature (C°)

Ta is the ambient air temperature (C°)

G is the solar irradiation (W/m^2)

Vw is the wind speed

Meteorological parameters and FPV cell temperature	Values
Ta	28.73°C
G	1000 W/m^2
V_{wland}	4.2m/s(wind speed in Algeria)
Tc(ground-mounted)	43°C

This empirical model is designed to operating temperature of PV modules by accounting for environmental factors [83]. The model has demonstrated high accuracy, with a coefficient of determination (R^2) of approximately 0.96.

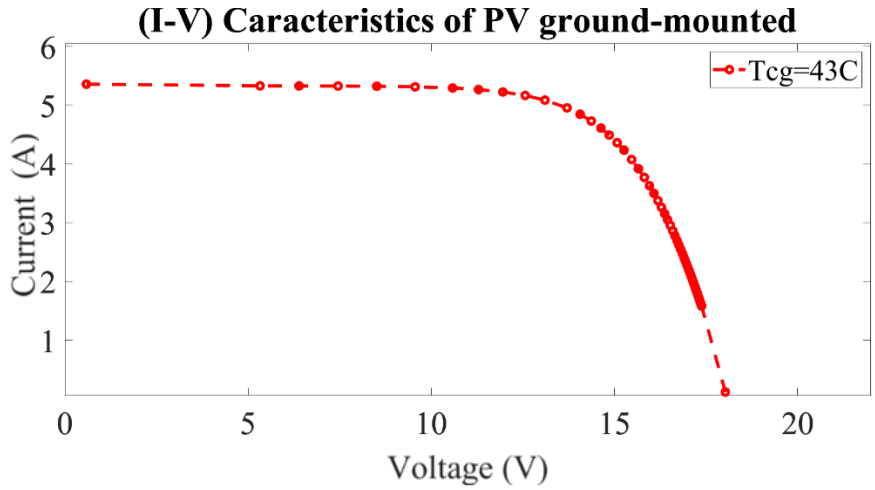

Figure (IV.25): Simulated I-V Characteristics of the Ground-mounted PV Cell Based on the Calculated Temperature

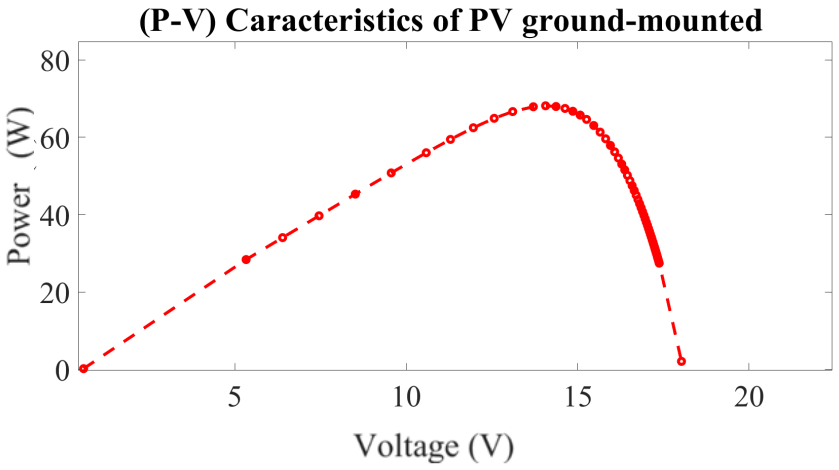

Figure (IV.26): Simulated P-V Characteristics of the Ground-mounted PV Cell Based on the Calculated Temperature

To further investigate the thermal influence on PV performance, we simulated the electrical characteristics (I-V and P-V curves) of a ground-mounted solar cell using the temperature profile calculated for a typical land-based environment. As expected, the elevated cell temperature led to a noticeable drop in overall power output.

IV.17.2 Electrical Performance Analysis Based on Simulated FPV Cell Temperature:

Following the thermal behavior analysis of the floating photovoltaic (FPV) cell using the adopted thermal model, we integrated the calculated cell temperature values into the simulation environment to extract the electrical characteristics (I-V and P-V curves) of the floating PV system under realistic operating conditions. This simulation was based on full-day data, where the instantaneous cell temperature was used as a reference to generate current and voltage characteristics over time.

In addition to the factors mentioned, water temperature can also influence the operating temperature of PV modules, especially in floating Pv systems. A study titled “Design stand-alone floating Pv system for Ibeno Health Centre” [77][78] and discusses models that incorporate water temperature (Tcw) as a variable:

$$Tcw = 0.943Tw + 0.0195 * G - 1.528 * Vws + 0.3529 \quad \text{(III.2)}$$

Meteorological parameters and FPV cell temperature	Values
Ta	28.73°C
Tw	26.5°C
Vwl and	4.2 m/s
Vw sea	6.534 m/s
Tcw	31.9°C

N.B: To calculate the floating cell temperature (TCW), we used the equation (III.2) presented in Chapter III.

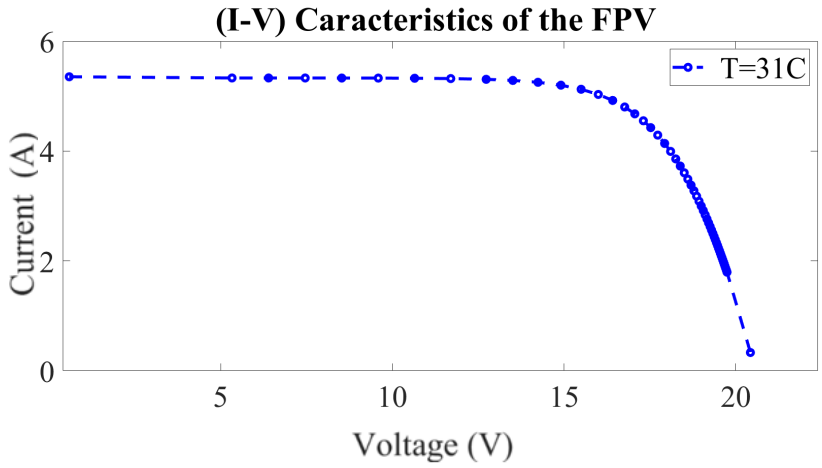

Figure (IV.27): Simulated I-V Characteristics of the Floating PV Cell Based on the Calculated Temperature

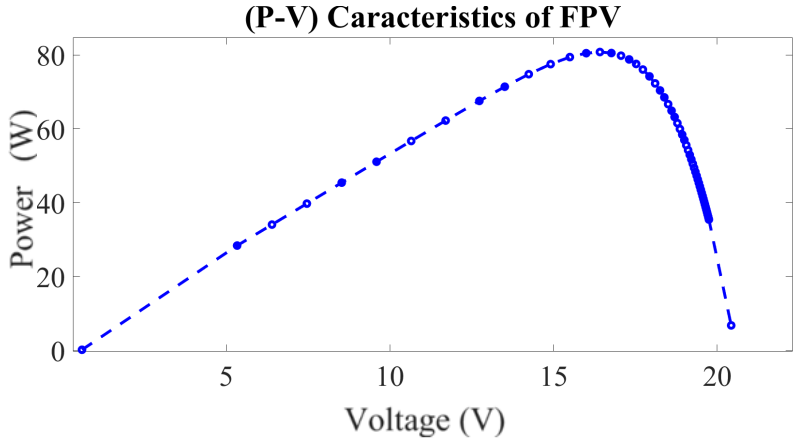

Figure (IV.28): Simulated I-V Characteristics of the Floating PV Cell Based on the Calculated Temperature

The simulation confirms the well-known thermal behavior of photovoltaic cells: As the cell temperature increases, the open-circuit voltage (Voc**)** significantly decreases, while the short-circuit current (Isc) experiences only a slight increase. However, this minor gain in current is not enough to compensate for the voltage loss, leading to an overall reduction in maximum power output (Pmax). This negative temperature effect is more pronounced in ground-mounted PV systems due to reduced natural cooling. In contrast, floating PV installations benefit from the cooling effect of water, which keeps cell temperature lower and maintains better electrical performance Figure (IV.29).

This analysis highlights the importance of thermal optimization in PV systems and justifies the interest in Floating PV (FPV) as a more efficient alternative under hot operating conditions. Figure (IV.30).

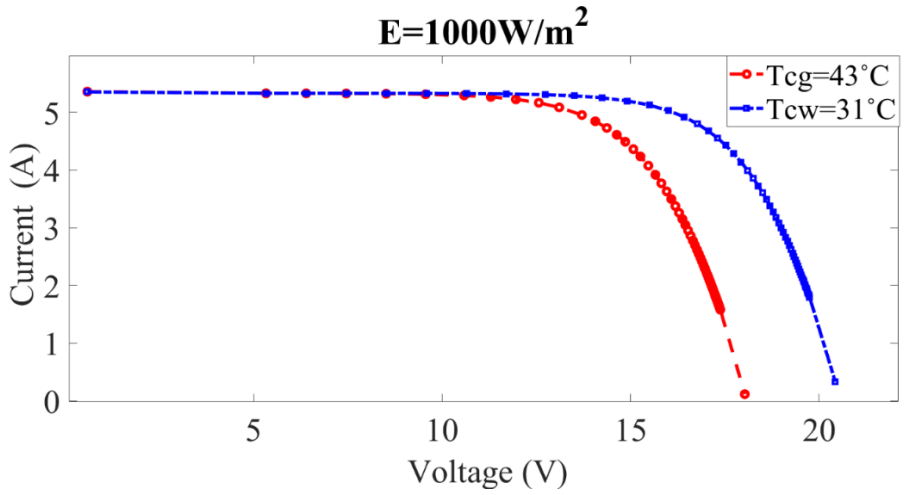

Figure (IV.29): Comparison of Current and Voltage Characteristics Between Ground-Mounted and Floating PV Systems Under Thermal Influence

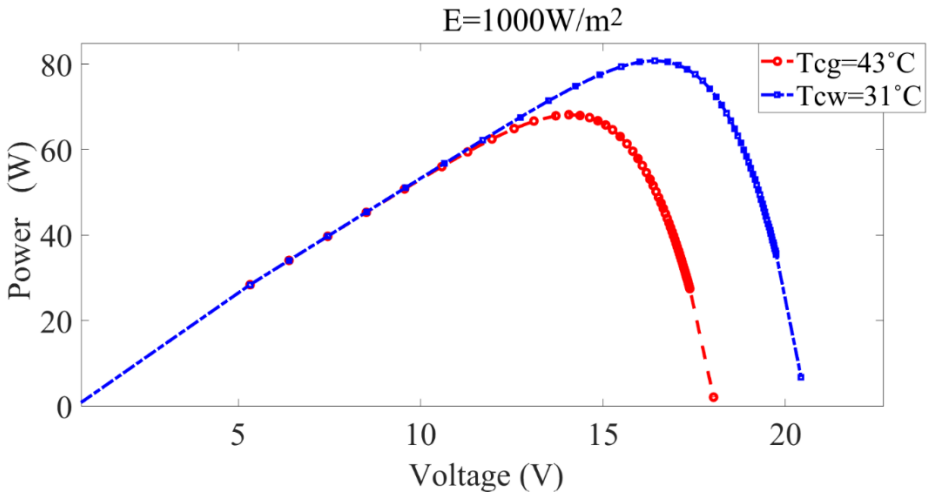

Figure (IV.30): Comparison of Power and Voltage Characteristics Between Ground-Mounted and Floating PV Systems Under Thermal Influence

IV-18 Tracking effect on the PV power output:

Since our main goal was to optimize power efficiency of the FPV system, and in order to increase to generated power, we can include the tracking process since the optimal current is

directly proportional to solar radiation. In the context, we conduct a practical that to show the effect of the tracking procedure.

In the figures below, are show the result of both tracking/non-tracking system, it is show that for the same solar radiation and ambient temperature the tracking offers better results as show in the figures (IV.31), (IV.32), (IV.33) and (IV.34).

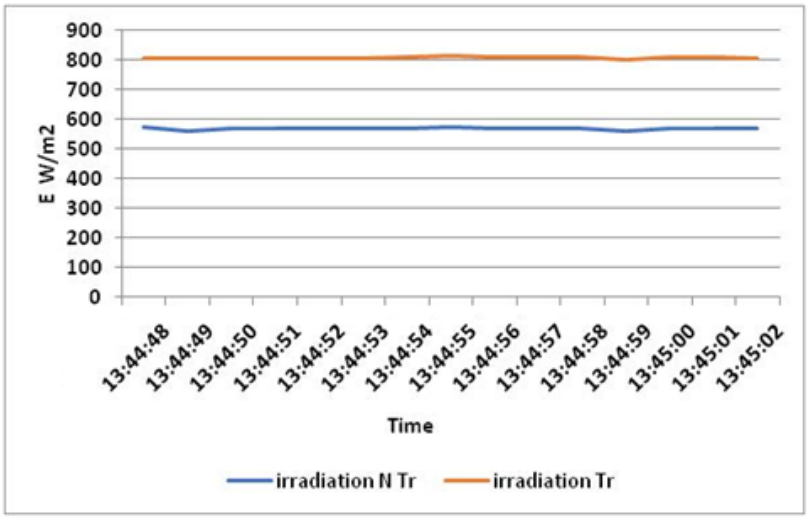

Figure IV.31: Instantaneous Irradiance Levels During Non-Tracking and Tracking Tests

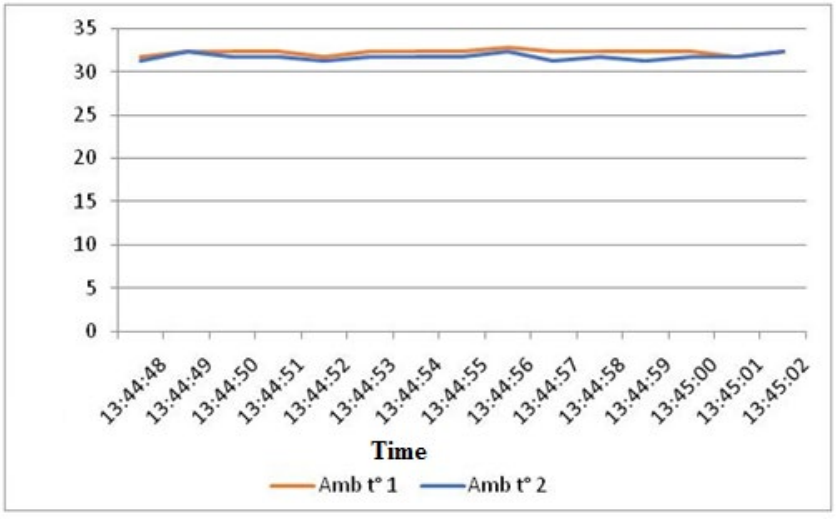

Figure IV.32: Temperature Stability During Tracking and Non-Tracking tests

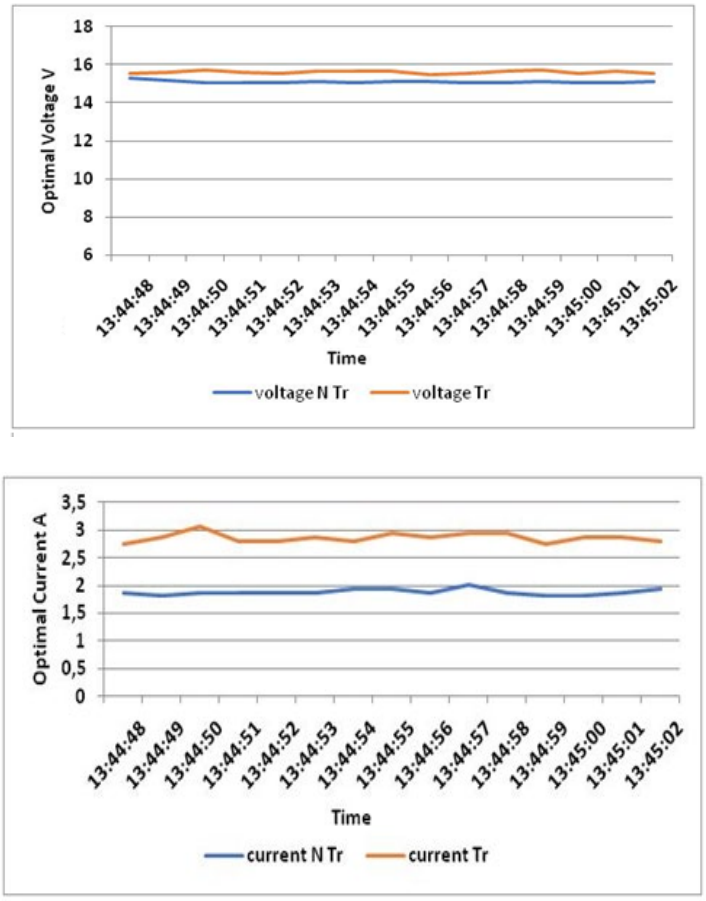

Figure IV.33: Voltage and Current Comparison for Tracking and Non-Tracking PV Modules.

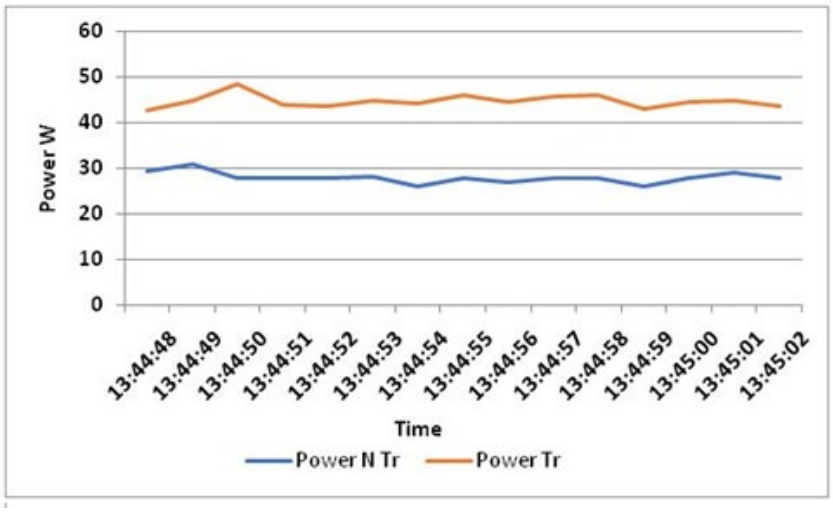

Figure IV.34: Power Output Comparison Between Tracking and Non-Tracking PV panel

This Figures show that the most effected by the tracking process is the optimal current which is theoretically proportional to solar radiation.

However, the optimal voltage doesn't show a significant variation since it is affected by the direct effect of solar radiation and in the same time it effected inversely by the heating effect of the solar radiation.

Therefore, in order to maximize the power output of an FPV system we not require high investment the platform at tracking.

N.B1:

The tests were carried out successively during a short time laps to ensure same weather conditions especially solar radiation and ambient temperature. The first test was conducted at about 13:40 H while the second was taken at about 13:44H, just the time to adjust (orient) the solar module toward the sun.

N.B2:

For drawing convenience, just one timing axis is adopted.

IV-19 Conclusion:

The initial work intended to evaluate floating PV systems under real weather conditions, but, as mentioned earlier, due to administrative constraints, we were unable to put our FPV system on water surface of Foum El Ghourza DAM. Thus, in order to carry on with our investigations, a simulation process of the cooling effect of water was carried out. This simulation represents the only aspect we were able to fully control and study within MATLAB the impact of cell temperature on overall performance. Through this approach, we effectively assessed the role of water-based cooling as a promising method to enhance the efficiency of floating photovoltaic systems, which lies at the heart of the thermal optimization of FPV.

General Conclusion

General Conclusion

With the help and guidance of Allah, this thesis, titled " Power optimization of a floating PV station -Part 01", represents a foundational step in a promising research axis within the field of renewable energy. In this work, we developed a complete practical system, starting from the mechanical design of the floating structure to the electrical system and integrated sensors Of course, the theoretical procedure was also developed.

The initial objective was to deploy this system at the Foum El Ghourza Dam. However, due to unforeseen constraints, we resorted to build an artificial pool to simulate real conditions. Although the results were not fully representative of a natural water body given the limited water surface and the accompanying environmental effects, the prototype allowed for a preliminary investigation into the influence of environmental factors such as water temperature, wind speed, and humidity on the performance of floating PV systems.

To deepen our analysis, we conducted simulations using MATLAB/Simulink, focusing specifically on the thermal modeling of the PV cell. Here, the core of the project emerged: performance optimization through natural cooling**.** The study clearly demonstrated the thermal advantage of the floating system over its ground-mounted counterpart, which directly translates to improved electrical efficiency.

Looking ahead, we aim to further develop this system by implementing it in a real reservoir environment in future continuation, First of all, we suggest enhancing it with a solar tracking mechanism, and outfit a remote communication device (Example an Arduino controller with Wi-Fi connectivity) for real-time data monitoring and transmission. This procedure is necessary since the PV platform would be floating deep on the damp water surface. This opens the door to additional applications, including environmental and hydrological monitoring within the dam.

In addition, we investigated the effect of a tracking system, where it is shown a noticeable improvement in the power output.

Finally, we can say that we have laid the groundwork for a scalable project that bridges scientific research and practical implementation, contributing hence to the advancement of clean and sustainable energy solutions in Algeria

References

References:

[1] A. Fayolle-Baussian, Y. Gorce Ioann, J. Leroux Justinien, Scientific Project Work – Première (11th Grade Science), 2011.

[2] Chaisson, E., & McMillan, S. (2014). Astronomy: A Beginner's Guide to the Universe (7th ed.). Pearson Education.

[3] Kha. Bouziane, Study of a Photovoltaic Installation for Hydrogen Production by Water Electrolysis, University of Ouargla, 2011.

[4] Thomas Letz, INES Education – Savoie Technolac – BP258 – F73375 Le Bourget du Lac, November 2007.

[5] Reference Center for Solar and Wind Energy Sérgio de Salvo Brito (CRESESB): Solar Energy – Principles and Applications.

[6] B. Flèche and D. Delagnes, Photovoltaic Solar Energy, June 2007.

[7] José Miguel Navarro, Transparent Organic Photovoltaic Cells in the Visible Range, PhD Thesis, University of Toulouse III – Paul Sabatier, 2008.

[8] Zouache Foudil, Study of Solar Concentration on the Performance of Photovoltaic Systems, Master's Thesis in Electronics, Mentouri University of Constantine, 2009.

[9] A. Ould Mohamed Yahia et al., Study and Modeling of a Photovoltaic Generator, Renewable Energy Journal, Vol. 11, No. 3, pp. 473–483, 2008.

[10] R. Jimmy, Photovoltaic Pumping, Multi Mondes Publishing, 1999.

[11] A. Ould Mohamed Yahia et al., Study and Modeling of a Photovoltaic Generator, Renewable Energy Journal, Vol. 11, No. 3, pp. 473–483, 2008.

[12] M. A. Green, E. D. Dunlop, J. Hohl-Ebinger, M. Yoshita, N. Kopidakis, and X. Hao, Solar Cell Efficiency Tables (Version 60), Progress in Photovoltaics: Research and Applications, Vol. 30, No. 7, pp. 687–701, 2022.

[13] International Energy Agency Photovoltaic Power Systems Programme. (2021). Floating PV: Market outlook, technical status, design and risk analysis.

[14] PV Magazine. (2023, October 18). Global inventory map of floating photovoltaics. PV Magazine USA.

[15] Wood Mackenzie. (2023, August). Global floating solar PV forecast through 2033. Taiyang News.

[16] da Silva, R. C., Souza, P. A., & de Almeida, A. T. (2023). Evaluation of water evaporation reduction in Brazilian reservoirs with floating solar panels. PV Magazine.

[17] Deb, A., Bose, R., & Saha, H. (2024). Performance enhancement of floating photovoltaic systems using water cooling technique. Solar Energy, 272, 1101–1112.

[18] Cazzaniga, R., Rosa-Clot, M., Rosa-Clot, P., & Tina, G. M. (2018). Integration of FPV with hydroelectric power plants. Progress in Photovoltaics: Research and Applications, 26(7), 517–528.

[19] Global Data. (2023). Global floating solar market analysis and forecast.

[20] PV Magazine. (2023). Floating solar power generation: Tengeh Reservoir, Singapore.

[21] Deb, A., Bose, R., & Saha, H. (2024). Performance enhancement of floating photovoltaic systems using water cooling technique. Solar Energy, 272, 1101–1112.

[22] https://oceansofenergy.blue

[23] Ciel & Terre. (2022). Hydrelio floating solar system for agricultural irrigation ponds in France. Ciel & Terre International.

[24] Duffie, J. E., & Beckman, W. A. (2018). Solar Engineering of Thermal Processes (4th ed.). Wiley. [Provides foundational PV efficiency and electrical layout principles, used for panel efficiency and inverter data.]

[25] Rosa-Clot, M., & Tina, G. M. (2020). Floating PV Plants. Academic Press. [Key source for FPV system design, platform materials, and cost estimates, informing platform and cabling sections.]

[26] Oliveira-Pinto, S., & Stokkermans, J. (2021). Marine floating solar plants: Design and challenges. Renewable Energy, 167, 853–864. [Details anchoring and mooring challenges, used for stability and design considerations.]

[27] Power Technology. (2021). World's biggest floating solar farms: Top ten by capacity. [Provides market share and project scale data, cited for PV panel and anchoring usage.]

[28] Pouran, H. (2018). Environmental and technical impacts of floating photovoltaic plants. PMC. [Details FPV-specific panel designs, cited for double-glass encapsulation.]

[29] YSG Solar. (2022). 5 Largest Floating Solar Farms in the World in 2022. [Source for Huainan and Dezhou project data, used in real-world examples.]

[30] Tata Power. (2025). Floating solar panels powering sustainability. [Provides Omkareshwar project specifics, cited for energy output and CO_2 reduction.]

[31] Iberdrola. (2023). Floating Photovoltaic Solar Energy. [Details ecological and cooling benefits, used for platform considerations.]

[32] Rosa-Clot, M. (2020). Floating PV systems: Materials and design. Journal of Renewable Energy. [Specific HDPE properties and lifespan, cited for material specs.]

[33] Oliveira-Pinto, S. (2022). Materials for offshore floating PV. Marine Technology Journal. [Details FRP, steel, and composites, cited for material properties.]

[34] Ciel & Terre. (2023). Hydrelio floating solar platform technical specifications. [Source for modular float design, cited for platform types.]

[35] ACCIONA. (2020). Sierra Brava floating photovoltaic plant. [Details membrane platform design, cited for Sierra Brava project.]

[36] Ocean Sun. (2024). Hybrid floating PV platforms for offshore use. [Source for hybrid platform designs, cited for Saemangeum.]

[37] Sungrow (2023). Integrated floating PV solutions. [Details sensor-integrated platforms, cited for Cirata.]

[38] Power Technology. (2021). Saemangeum floating solar project overview. [Provides Saemangeum scale and output, cited for project details.]

[39] PBS News. (2023). Long popular in Asia, floating solar catches on in the U.S. [Source for Healdsburg project, cited for CO_2 savings and ecological impact.]

[40] Masdar. (2023). Cirata Floating Solar Project. [Details Cirata's output and cabling, cited for project specifics.]

[41] Iberdrola. (2023). Tengeh Reservoir floating solar farm. [Source for Tengeh's energy output and ecological design, cited for project details.]

[42] Oliveira-Pinto, S., & Stokkermans, J. (2021). Anchoring and mooring systems for floating PV. Renewable Energy, 167, 853–864. [Comprehensive anchoring/mooring data, cited for methods and lines.]

[43] Oliveira-Pinto, S. (2023). Suction anchors for offshore floating PV. Offshore Energy Journal. [Details suction anchor applications, cited for North Sea pilot.]

[44] Reindl, T., & Correia, N. (2022). Floating solar panels with Sun-tracking technology. BBC Future Planet. [Source for Proteus project, cited for Sun-tracking.]

[45] Rosa-Clot, M., & Tina, G. M. (2020). Cabling systems for floating PV. Floating PV Plants. [Details cabling types and specs, cited for cabling section.]

[46] Quaranta, E. (2020). Floating solar + hydropower hybrid projects. Solar Power World. [Source for Kutani Dam project, cited for hybrid integration.]

[47] Skoplaki, E., & Palyvos, J. A. (2009). On the temperature dependence of photovoltaic module electrical performance: A review of efficiency/power correlations. Solar Energy, 83(5), 614–624.

[48] Kamuyu, W. C. L., Lim, J. R., Won, C. S., & Ahn, H. K. (2017). Prediction model of photovoltaic module temperature for power performance of floating PVs. Energies, 11(2), 447.

[49] Liu, H., Krishna, R., Lun, I. Y. F., & Lau, K. C. (2018). Performance analysis of a 1 MW floating photovoltaic system in India. Renewable Energy, 121, 171–180.

[50] Hasanuzzaman, M., Zubir, U. S., Ilham, N. I., & Seng Che, H. (2016). Global advancement of cooling technologies for PV systems: A review. Solar Energy, 137, 25–45.

[51] Fouad, M. M., Shihata, L. A., & Morgan, E. I. (2017). An integrated review of factors influencing the performance of photovoltaic panels. Renewable and Sustainable Energy前景 Reviews, 80, 1499–1511.

[52] Coello, J., Carballar, A., & Castro, M. (2013). Albedo and reflection in photovoltaic systems: Modeling and experimental validation. Progress in Photovoltaics: Research and Applications, 21(5), 917–927.

[53] Marion, B., MacAlpine, S., Deline, C., & Asgharzadeh, A. (2017). A practical model for evaluating the energy yield of bifacial PV systems. IEEE Journal of Photovoltaics, 7(6), 1681–1688.

[54] Choi, Y., Kim, H., & Shin, S. (2020). Performance evaluation of floating photovoltaic systems with bifacial modules. Renewable Energy, 149, 1083–1092.

[55] World Bank. (2020). Where Sun Meets Water: Floating Solar Market Report. Washington, DC: World Bank Group.

[56] Sarver, T., Al-Qaraghuli, A., & Kazmerski, L. L. (2013). A comprehensive review of the impact of dust on the use of solar energy. Renewable and Sustainable Energy Reviews, 22, 698–733.

[57] Gorjian, S., Sharon, H., Ebadi, H., Kant, K., Scavo, F. B., & Tina, G. M. (2021). Recent technical advancements, economics, and environmental impacts of floating photovoltaic solar energy systems: A systematic review. Sustainable Energy Technologies and Assessments, 43, 100922.

[58] El-Shobokshy, M. S., & Hussein, F. M. (1993). Effect of dust with different physical properties on the performance of photovoltaic cells. Solar Energy, 51(6), 505–511.

[59] Cazzaniga, R., Cicu, M., Rosa-Clot, M., Rosa-Clot, P., Tina, G. M., & Ventura, C. (2018). Floating photovoltaic plants: Performance analysis and design solutions. Renewable and Sustainable Energy Reviews, 81(2), 1730–1741.

[60] Kowsar, A., Hassan, M., & Rana, M. (2023). Techno-economic and environmental aspects of a 50 MW floating photovoltaic power plant. Energy, 310, 133202.

[61] Pouran, H. M., Padilha Campos Lopes, M., Ziar, H., Alves Castelo Branco, D., & Sheng, Y. (2022). Environmental and technical impacts of floating photovoltaic plants as an emerging energy technology. iScience, 25(11), 105253.

[62] Sakarya University. (2024). Empowering sustainability: Floating solar photovoltaic systems in agriculture – A case study from Sakarya, Turkey. Global Challenges, 2300273.

[63] Every crs report. (2020). Solar energy: Frequently asked questions. Congressional Research Service.

[64] Acharya, M., & Devraj, S. (2019). Floating solar photovoltaic systems: An emerging trend in India. Renewable Energy Report.

[65] Bax, V., van de Lageweg, W. I., & Hoosemans, R. (2022). Evaluating the social feasibility of floating solar energy infrastructure in the Netherlands. Renewable Energy, 189, 1197–1210.

[66] Almeida, R. M., Shi, Q., Gomes-Selman, J. M., Wu, X., Xue, Y., Angarita, H., ... & Flecker, A. S. (2022). Floating solar power could help fight climate change — let's get it right. Nature, 606(7913), 246–249.

[67] Pouran, H. M. (2018). From collapsed coal mines to floating solar farms, why China's new power projects matter. Renewable Energy Journal.

[68] Spencer, R. S., Macknick, J., Aznar, A., Warren, A., & Reese, M. O. (2018). Floating photovoltaic systems: Assessing the technical potential of photovoltaic systems on man-made water bodies in the continental United States. Environmental Science & Technology, 53(3), 1680–1689.

[69] Haas, J., Khalighi, J., de la Fuente, A., Gerbersdorf, S. U., Nowak, W., & Chen, P.-J. (2020). Floating photovoltaic plants: Ecological impacts versus hydropower operation flexibility. Energy Conversion and Management, 206, 112414.

[70] Micheli, L., Talavera, J. M., Theristis, M., Almonacid, F., & Fernández, E. F. (2024). Impact of variable economic conditions on the potential benefits of floating photovoltaics compared to ground-mounted systems. Heliyon, 10(12), e32354.

[71] Exley, G., Hernandez, R. R., Page, T., Chipps, M., Gambro, S., Her, M., ... & Armstrong, A. (2021). Potential environmental impacts of floating solar photovoltaic systems. Journal of Cleaner Production, 278, 123744.

[72] Ilgen, K., Schweizer-Ries, P., & Nier, H. (2023). Impact of floating photovoltaic power plants on lake water temperature and stratification. Scientific Reports, 13(1), 7932.

[73] Liu, H., Krishna, R., Lun, I. Y. F., & Lau, K. C. (2018). Performance analysis of a 1 MW floating photovoltaic system in India. Renewable Energy, 121, 171–180.

[74] PVsyst Documentation : https://www.pvsyst.com/help/cell_temperature.htm

[75] Duffie & Beckman, Solar Engineering of Thermal Processes, 4th Edition, Wiley

[76]Anyanime Tim Umoette, Emmanuel A. Ubom, Mbetobong Udo Festus. Design of Stand Alone Floating PV System for Ibeno Health Centre. Science Journal of Energy Engineering. Vol. 4, No. 6, 2016, pp. 56-61. doi: 10.11648/j.sjee.20160406.12

[77] Ficklin, Darren L., et al. "Development and application of a hydro climatological stream temperature model within the Soil and Water Assessment Tool." Water Resources Research 48.1 (2012).

[78] Al Riza, Dimas Firmanda, and Syed Ihtshamul-Haq Gilani. "Standalone Photovoltaic System Sizing using Peak Sun Hour Method and Evaluation by TRNSYS Simulation." International Journal of Renewable Energy Research (IJRER) 4.1 (2014): 109-114.

[79] Hsu, Shih-Ang. Coastal meteorology. Elsevier, 2013.

[80] Hsu, S. A. "Correction of land-based wind data for offshore applications: a further evaluation." Journal of physical oceanography 16.2 (1986): 390-394.

[81] Hsieh, Bernard B., Billy H. Johnson, and David R. Richards. A Three-Dimensional Numerical Model Study for the Chesapeake and Delaware Canal and Adjacent Bays. No. WES/TR/HL-93-4. ARMY ENGINEER WATERWAYS EXPERIMENT STATION VICKSBURG MS HYDRAULICS LAB, 1993.

[82] Kamuyu, M. et al. (2021). Thermal behavior of floating photovoltaic panels in marine environment. Renewable Energy Journal.

[83] TamizhMani, G. et al., Photovoltaic Module Thermal/Wind Performance: Long-Term Monitoring and Model Development for Energy Rating, NREL/CP-520-35645, 2003.

Appendix

Appendix A : Solar charge Controller MPPT MT2410

SR-MT Maximum Power Point Tracking Series Solar charge controller

SR-MT2410

SR-MT2410

Features

1. Adopting double crest or multi crest tracing technique, used for the condition when a part of solar panel is under shadow or parts of solar panel is damage.
2. Built-in maximum power point tracking algorithm which could promote the energy utilization efficiency of pv system. The charging efficiency is 15%~20% higher than PWM mode.
3. It can find out the best working point of I-V curve within 1 minute. the MPPT efficiency could reach to 99.9%.
4. Adopting advanced digital power supply techniques which makes the energy conversion efficiency reach up to 97%.
5. Four charging stages: MPPT - equalizing charge- boosting charge- floating charge.
6. With current-limiting charging mode. When the power of solar panel is oversized, the controller will lower charging power automatically, which enable the system to work under the rated charging current.
7. Have the fault code indication, it helps user confirm the system fault.
8. Various load control methods. Could recognize day and night automatically.
9. Various system protection functions. Including over-charge, over-discharge, over-load, over-heat, battery-reverse connection and short-circuit protection etc.

Front View Schemat

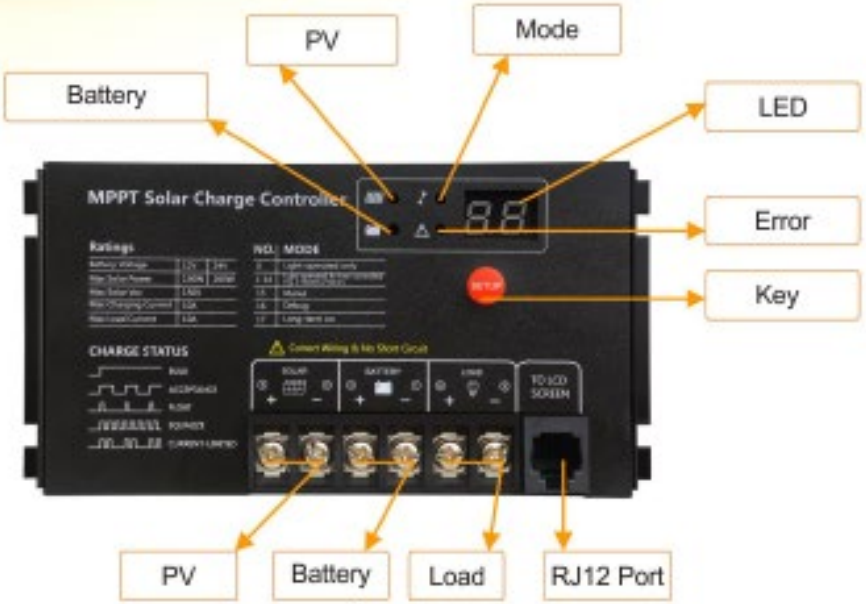

Installation Dimension

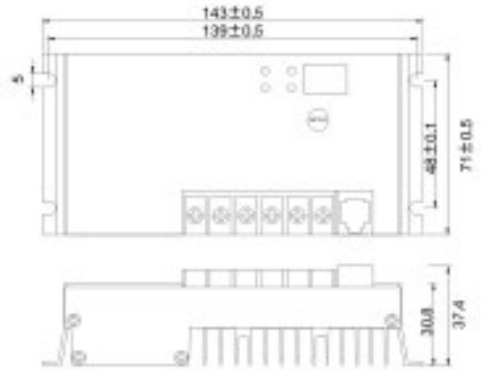

Overall Dimension : 143×71×36(mm)
Installation Dimension : 143×71×36(mm)

Product Detail

Wiring diagram is as below

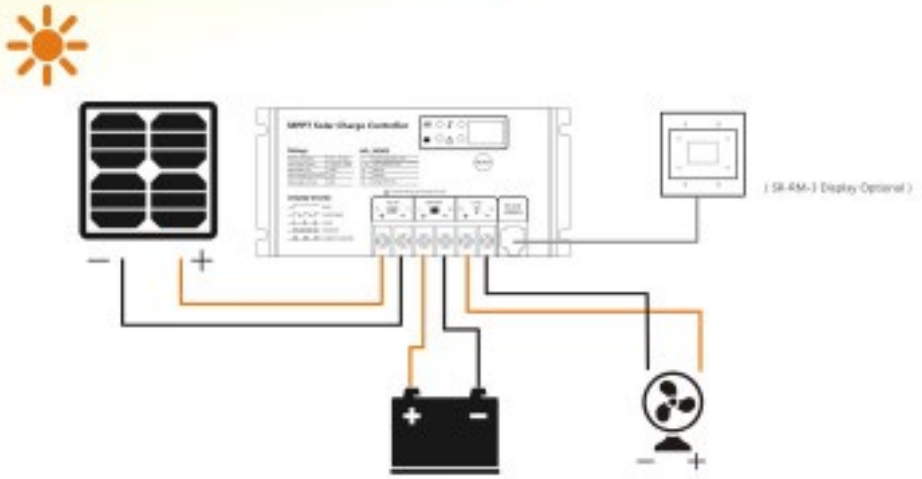

Working State Indication

1.Charge indication: When the solar panel output voltage reaches a certain value, charge indicator start to work. Different flash status represents different charge mode. The specific meaning of charge mode is as the table A below.

2.Battery capacity indication: When the battery is normal, the indicator is on, when it is over discharge, the indicator will slow flash, when the battery is over voltage, the indicator will fast flash.(Table B)

3.Mode indication: When the mode indicator is on, it indicates that the value on the Nixie tube is controller mode. The value will disappear if no key operation within 5s.

4.Fault indication: when the fault indicator is on, it indicates that the value on the Nixie tube is controller fault code; The value will disappear if no key operation within 5s. If fault exists, the indicator will flash.

A. Charging Status Indication Specification:

Serial Number	Diagram	Indicating Status	State of charge
①	BULK	Normally on.	Charge at Max. Power.
②	ACCEPTANCE	Slow flash. (light for 1s, off for 1s, the cycle is 2s)	Boost charging.
③	FLOAT	Single flash. (light for 0.1s, off for 1.9s, the cycle is 2s)	Float charging.
④	EQUALIZE	Fast flash. (light for 0.1s, off for 0.1s, the cycle is 0.2s)	Equalizing charge.
⑤	CURRENT-LIMITED	Double flash. (light for 0.1s, off for 0.1s, reopen for 0.1s, reclose for 1.7s, the cycle is 2s)	Current limited charging.

B. Battery Indication Specification.

Serial Number	LED Status	Battery Status
①	Normally on.	The battery voltage is normal.
②	Slow flash. (light for 1s, off for 1s, the cycle is 2s)	The battery is over discharged.
③	Fast flash. (light for 0.1s, off for 0.1s, the cycle is 0.2s)	The battery is over voltage.

Parameters

Item	Value	
Model	SR-MT2410	
System voltage	12V	24V
Max. input power of solar panel	130W	260W
Transfer efficiency	≤96%	≤97%
Rated charge/ discharge current	10A	
No load loss	<15mA	
Max. input voltage of solar panel	<150V	
MPPT tracing efficiency	>99%	
Over voltage protection	16.5V	33.0V
Limited charge voltage	15.5V	31.0V
Equalizing charge voltage	15.2V	30.4V
Equalizing charge interval	30 days	
Boosting charge voltage	14.4V	28.8V
Floating charge voltage	13.8V	27.6V
Over-discharge recover voltage	12.5V	25.0V
Over discharge voltage	11.0V	22.0V
Boosting charge time	2 hours	
Equalizing charge time	1 hour	
Over temperature protection	Yes	
Light-operated voltage (on)	5V	
Light-operated voltage (off)	6V	
Light-operated delay time	5min	
Working temperature	-35℃~+65℃；	
Weight	430g	
Altitude	≤3000m	
Dimension	143*71*37.4 (mm)	
Installation dimension	139*48(mm)	
Overload protection	Load current≥1.25 times rated current, cut off the load within 10 seconds; Load current≥1.5 times rated current, cut off the load within 5 seconds	
Protections	1.Reverse connection. 2.Inner over temperature. 3.The voltage of PV input terminal is over value. 4.Over load 5.Reverse charging protection at night. 6. TVS lightning protection 7. Waterproof: IP 64	

Appendix B : Solar panel ALPV_85_125M_36_

UNIVERSITÉ DE GENÈVE PVSYST	PVSYST V5.11		13/05/25 10h12

Final year Project
Floating PV

Characteristics of a PV module

Manufacturer, model : **Algerian PV, ALPV 85-125M-36**
Data source : Manufacturer
File : ALPV 85-125M-36B.PAN of 28/11/16 20h24

STC power (manufacturer)	**Pnom**	**85 Wp**	**Technology**	**Si-mono**	
Module size (W x L)	0.545 x 1.225	m²	Rough module area	Amodule	0.67 m²
Number of cells	1 x 36		Sensitive area (cells)	Acells	0.56 m²

Specifications for the model (manufacturer or measurement data)

Reference temperature	TRef	25	°C	Reference irradiance	GRef	1000	W/m²
Open circuit voltage	Voc	21.8	V	Short-circuit current	Isc	5.33	A
Max. power point voltage	Vmpp	17.3	V	Max. power point current	Impp	4.93	A
=> maximum power	Pmpp	85.1	W	Isc temperature coefficient	muIsc	3.7	mA/°C

One-diode model parameters

Shunt resistance	Rshunt	220	ohm	Diode saturation current	IoRef	68	nA
Serie resistance	Rserie	0.24	ohm	Voc temp. coefficient	MuVoc	-73	mV/°C
				Diode quality factor	Gamma	1.30	
Specified Pmax temper. coeff.	muPMaxR	-0.46	%/°C	Diode factor temper. coeff.	muGamma	-0.001	1/°C

Reverse Bias Parameters, for use in behaviour of PV arrays under partial shadings or mismatch

Reverse characteristics (dark)	BRev	3.90	mA/V²	(quadratic factor (per cell))		
Number of by-pass diodes per module		2		Direct voltage of by-pass diodes		-0.7 V

Model results for standard conditions (STC: T=25°C, G=1000 W/m², AM=1.5)

Max. power point voltage	Vmpp	17.4	V	Max. power point current	Impp	4.90	A
Maximum power	Pmpp	85.2	Wc	Power temper. coefficient	muPmpp	-0.46	%/°C
Efficiency(/ Module area)	Eff_mod	12.8	%	Fill factor	FF	0.732	
Efficiency(/ Cells area)	Eff_cells	15.2	%				

PV module: Algerian PV, ALPV 85-125M-36

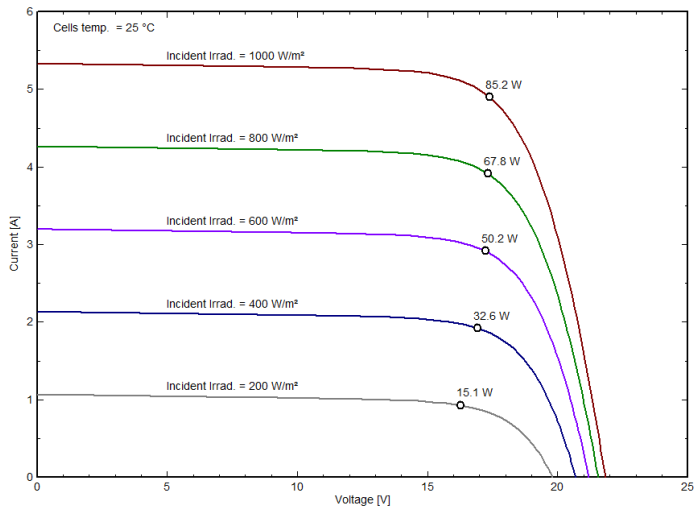

UNIVERSITÉ DE GENÈVE PVSYST	PVSYST V5.11		13/05/25 10h17

Final year Project - Floating PV
ELHAMDI Fatima Zohra - CHAREF KHODJA Imane

Characteristics of a PV module

Manufacturer, model : **Algerian PV, ALPV 85-125M-36**
Data source : Manufacturer
File : ALPV 85-125M-36B.PAN of 28/11/16 20h24

STC power (manufacturer)	**Pnom**	**85**	**Wp**	**Technology**	**Si-mono**		
Module size (W x L)		0.545 x 1.225	m²	Rough module area	Amodule	0.67	m²
Number of cells		1 x 36		Sensitive area (cells)	Acells	0.56	m²

Specifications for the model (manufacturer or measurement data)

Reference temperature	TRef	25	°C	Reference irradiance	GRef	1000	W/m²
Open circuit voltage	Voc	21.8	V	Short-circuit current	Isc	5.33	A
Max. power point voltage	Vmpp	17.3	V	Max. power point current	Impp	4.93	A
=> maximum power	Pmpp	85.1	W	Isc temperature coefficient	muIsc	3.7	mA/°C

One-diode model parameters

Shunt resistance	Rshunt	220	ohm	Diode saturation current	IoRef	68	nA
Serie resistance	Rserie	0.24	ohm	Voc temp. coefficient	MuVoc	-73	mV/°C
				Diode quality factor	Gamma	1.30	
Specified Pmax temper. coeff.	muPMaxR	-0.46	%/°C	Diode factor temper. coeff.	muGamma	-0.001	1/°C

Reverse Bias Parameters, for use in behaviour of PV arrays under partial shadings or mismatch

Reverse characteristics (dark)	BRev	3.90	mA/V²	(quadratic factor (per cell))			
Number of by-pass diodes per module		2		Direct voltage of by-pass diodes		-0.7	V

Model results for standard conditions (STC: T=25°C, G=1000 W/m², AM=1.5)

Max. power point voltage	Vmpp	17.4	V	Max. power point current	Impp	4.90	A
Maximum power	Pmpp	85.2	Wc	Power temper. coefficient	muPmpp	-0.46	%/°C
Efficiency(/ Module area)	Eff_mod	12.8	%	Fill factor	FF	0.732	
Efficiency(/ Cells area)	Eff_cells	15.2	%				

UNIVERSITÉ DE GENÈVE PVSYST | PVSYST V5.11 | 13/05/25 10h17

Final year Project - Floating PV
ELHAMDI Fatima Zohra - CHAREF KHODJA Imane

Characteristics of a PV module

Manufacturer, model : **Algerian PV, ALPV 85-125M-36**
Data source : Manufacturer
File : ALPV 85-125M-36B.PAN of 28/11/16 20h24

STC power (manufacturer)	**Pnom**	**85 Wp**		**Technology**		**Si-mono**	
Module size (W x L)		0.545 x 1.225	m²	Rough module area	Amodule	0.67	m²
Number of cells		1 x 36		Sensitive area (cells)	Acells	0.56	m²
Specifications for the model (manufacturer or measurement data)							
Reference temperature	TRef	25	°C	Reference irradiance	GRef	1000	W/m²
Open circuit voltage	Voc	21.8	V	Short-circuit current	Isc	5.33	A
Max. power point voltage	Vmpp	17.3	V	Max. power point current	Impp	4.93	A
=> maximum power	Pmpp	85.1	W	Isc temperature coefficient	muIsc	3.7	mA/°C
One-diode model parameters							
Shunt resistance	Rshunt	220	ohm	Diode saturation current	IoRef	68	nA
Serie resistance	Rserie	0.24	ohm	Voc temp. coefficient	MuVoc	-73	mV/°C
				Diode quality factor	Gamma	1.30	
Specified Pmax temper. coeff.	muPMaxR	-0.46	%/°C	Diode factor temper. coeff.	muGamma	-0.001	1/°C
Reverse Bias Parameters, for use in behaviour of PV arrays under partial shadings or mismatch							
Reverse characteristics (dark)	BRev	3.90	mA/V²	(quadratic factor (per cell))			
Number of by-pass diodes per module		2		Direct voltage of by-pass diodes		-0.7	V
Model results for standard conditions (STC: T=25°C, G=1000 W/m², AM=1.5)							
Max. power point voltage	Vmpp	17.4	V	Max. power point current	Impp	4.90	A
Maximum power	Pmpp	85.2	Wc	Power temper. coefficient	muPmpp	-0.46	%/°C
Efficiency(/ Module area)	Eff_mod	12.8	%	Fill factor	FF	0.732	
Efficiency(/ Cells area)	Eff_cells	15.2	%				

PV module: Algerian PV, ALPV 85-125M-36

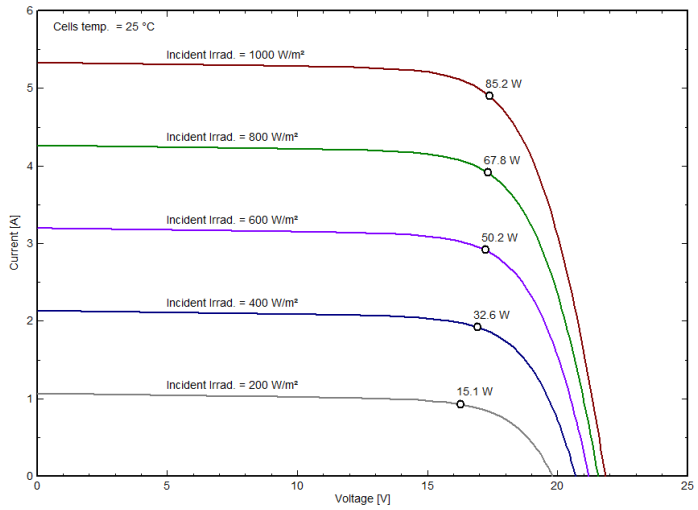

UNIVERSITÉ DE GENÈVE PVSYST | PVSYST V5.11 | 13/05/25 10h17

Final year Project - Floating PV
ELHAMDI Fatima Zohra - CHAREF KHODJA Imane

Characteristics of a PV module

Manufacturer, model : **Algerian PV, ALPV 85-125M-36**
Data source : Manufacturer
File : ALPV 85-125M-36B.PAN of 28/11/16 20h24

STC power (manufacturer)	**Pnom**	**85 Wp**		**Technology**		**Si-mono**	
Module size (W x L)		0.545 x 1.225	m²	Rough module area	Amodule	0.67	m²
Number of cells		1 x 36		Sensitive area (cells)	Acells	0.56	m²
Specifications for the model (manufacturer or measurement data)							
Reference temperature	TRef	25	°C	Reference irradiance	GRef	1000	W/m²
Open circuit voltage	Voc	21.8	V	Short-circuit current	Isc	5.33	A
Max. power point voltage	Vmpp	17.3	V	Max. power point current	Impp	4.93	A
=> maximum power	Pmpp	85.1	W	Isc temperature coefficient	muIsc	3.7	mA/°C
One-diode model parameters							
Shunt resistance	Rshunt	220	ohm	Diode saturation current	IoRef	68	nA
Serie resistance	Rserie	0.24	ohm	Voc temp. coefficient	MuVoc	-73	mV/°C
				Diode quality factor	Gamma	1.30	
Specified Pmax temper. coeff.	muPMaxR	-0.46	%/°C	Diode factor temper. coeff.	muGamma	-0.001	1/°C
Reverse Bias Parameters, for use in behaviour of PV arrays under partial shadings or mismatch							
Reverse characteristics (dark)	BRev	3.90	mA/V²	(quadratic factor (per cell))			
Number of by-pass diodes per module		2		Direct voltage of by-pass diodes		-0.7	V
Model results for standard conditions (STC: T=25°C, G=1000 W/m², AM=1.5)							
Max. power point voltage	Vmpp	17.4	V	Max. power point current	Impp	4.90	A
Maximum power	Pmpp	85.2	Wc	Power temper. coefficient	muPmpp	-0.46	%/°C
Efficiency(/ Module area)	Eff_mod	12.8	%	Fill factor	FF	0.732	
Efficiency(/ Cells area)	Eff_cells	15.2	%				

PV module: Algerian PV, ALPV 85-125M-36

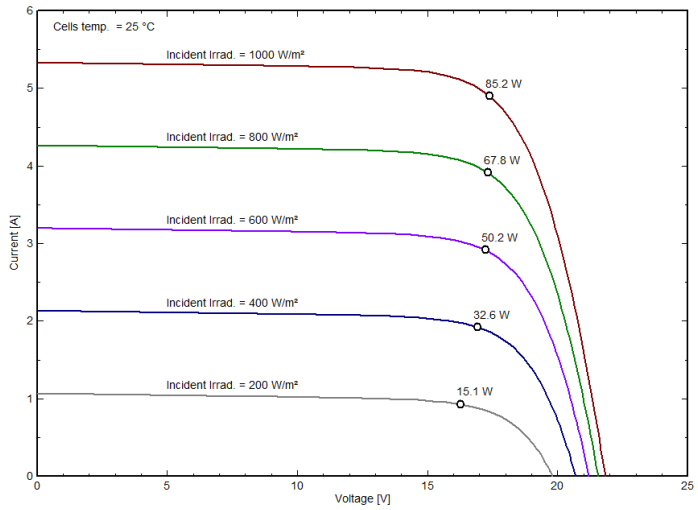

Appendix C: Battery Ritar RA 12-100

Specification

Cells Per Unit	6
Voltage Per Unit	12V
Capacity	100Ah@20hr-rate to 1.75V per cell @25°C
Weight	63.5 lb. (Tolerance ±5%)
Internal Resistance	5m Ω max.
Terminal	Default F12(M8),F15(M6) &L4 Optional
Max. Discharge Current	1000A (5 sec)
Design Life	12 years
Max. Charging Current	30.0 A
Reference Capacity	C_3 75.0Ah C_5 85.0Ah C_{10} 95.2Ah C_{20} 100.0Ah
Float Charging Voltage	13.6 V~13.8 V @ 25°C Temperature Compensation: -3mV/°C/Cell
Cycle Use Voltage	14.6 V~14.8 V @ 25°C Temperature Compensation: -4mV/°C/Cell
Operating Temperature Range	Discharge: -20°C~60°C Charge: 0°C~50°C Storage: -20°C~60°C
Self Discharge	RITAR Valve Regulated Lead Acid (VRLA) batteries can be stored for up to 6 months at 25°C and then recharging is recommended. Monthly Self-discharge ratio is less than 3% at 25°C.Please charged batteries before using.
Container Material	A.B.S. UL94-HB, UL94-V0 Optional.

*Nuts and bolts included.

AGM BATTERY
MAINTENANCE FREE

DC (Deep Cycle) series batteries provide superior high integrity and reliability. It is specially designed for frequent cyclic charge and discharging. By using strong grids, thick plate and specially active material are designed for repeated deep-discharge applications. The DC series batteries offer 30% more cyclic life than the standby series. It is suitable for solar and wind renewable energy storage, mobility and medical equipment and cable TV etc.

ISO 9001 ISO 14001 ISO 45001

UL1989 MH 28539 BSTXD210316008501EC

Dimensions

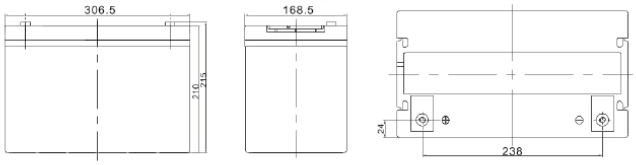

Length	306.5±2mm (12.1 inches)
Width	168.5±2mm (6.63 inches)
Height	210±2mm (8.27 inches)

*The glass mats are placed in between the battery plates, and these glass mats hold the electrolyte.

Constant Current Discharge Characteristics :A(25°C)

F.V/Time	10MIN	15MIN	30MIN	1HR	2HR	3HR	4HR	5HR	8HR	10HR	20HR
1.60V	223.8	180.9	107.8	60.74	36.17	28.17	22.10	18.80	12.06	10.00	5.183
1.65V	206.1	169.1	102.1	58.67	34.96	27.31	21.44	18.21	11.96	9.905	5.155
1.70V	191.0	159.1	96.83	56.79	34.03	26.15	20.78	17.72	11.77	9.714	5.090
1.75V	175.3	149.0	93.01	55.00	32.72	25.48	20.21	17.22	11.58	9.619	5.000
1.80V	159.5	136.4	89.58	52.56	31.60	25.00	19.74	17.00	11.39	9.524	4.952
1.85V	124.8	112.9	75.96	46.91	28.90	23.27	18.51	15.65	10.73	8.952	4.905

Constant Power Discharge Characteristics : W/Cell (25°C)

F.V/Time	10MIN	15MIN	30MIN	1HR	2HR	3HR	4HR	5HR	8HR	10HR	20HR
1.60V	381.0	315.5	195.9	114.0	68.39	53.50	42.59	35.58	23.50	19.61	10.35
1.65V	366.9	306.8	191.3	112.1	66.54	52.17	41.56	34.62	23.31	19.42	10.25
1.70V	342.4	290.4	182.1	108.8	64.88	50.17	40.23	33.76	23.03	19.05	10.16
1.75V	318.6	274.1	175.7	105.8	62.57	48.93	39.29	32.99	22.65	18.86	9.977
1.80V	293.6	253.4	170.0	101.4	61.15	48.65	38.53	32.54	22.28	18.67	9.885
1.85V	232.9	212.9	145.8	91.10	56.31	45.38	36.27	30.10	21.05	17.63	9.792

(Note) The above characteristics data are average values obtained within three charge/discharge cycle not the minimum values.
The battery must be fully charged before the capacity test. The C_{20} should reach 95% after the first cycle and 100% after the third cycle.

DC12-100S(12V100Ah)

RITAR®

Discharge Characteristics Curve

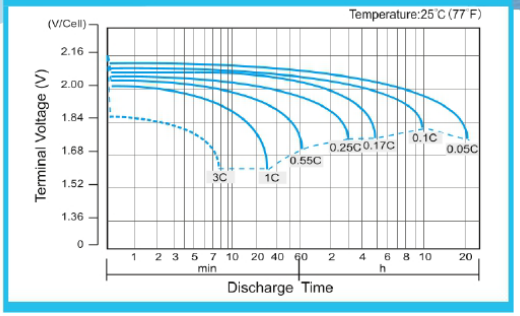

Charge Characteristic Curve for Cycle Use(IUU)

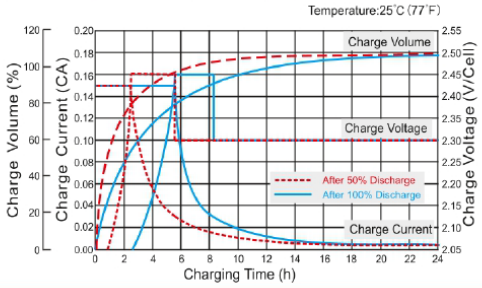

Cycle Life in Relation to Depth of Discharge

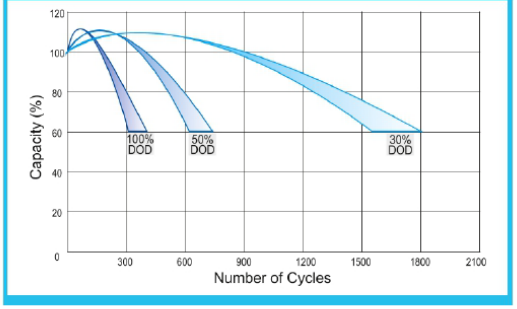

Relationship Between Charging Voltage and Temperature

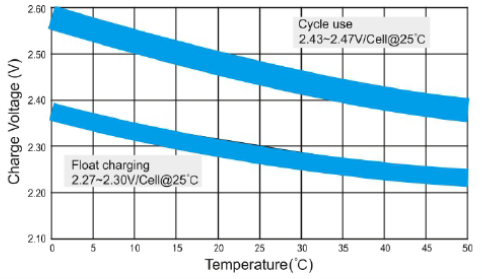

Temperature Effects on Capacity

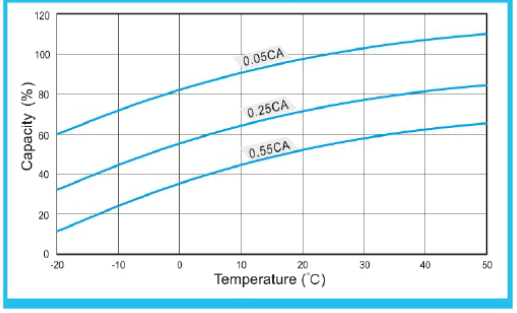

Storage Characteristics

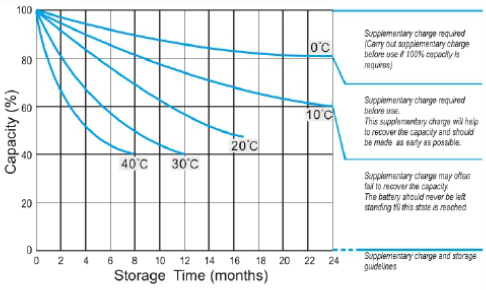

Effect of Temperature on Long Term Life

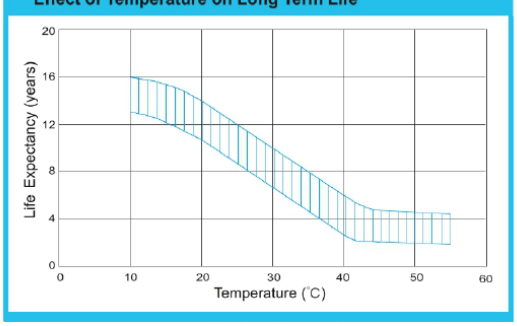

Relationship of OCV And State of Charge(20℃)

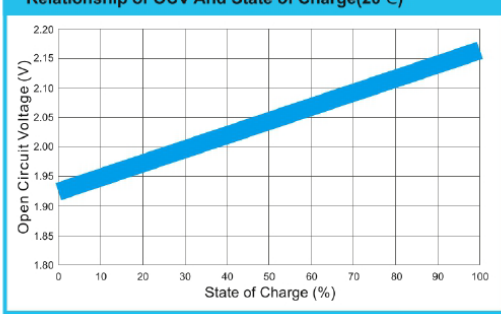

(Note) All above information shall be changed without prior notice, RITAR reserves the right to explain and update the latest information.

HENGYANG RITAR POWER CO.,LTD.
RITAR POWER (VIETNAM) CO.,LTD.
URL: www.ritarpower.com

Add: 10th Floor, Tower C, 1st Building, Software Industry Base, No.81, Xuefu Road, Nanshan District, Shenzhen, Guangdong, China 518057
Tel: +86-755-33981668/83475380 Fax: +86-755-83475180 E-mail: sales@ritarpower.com Version 24B-1-G

Appendix D: Hall effect current sensor LEM LA55

Current Transducer LA 55-P

I_{PN} = 50 A

For the electronic measurement of currents: DC, AC, pulsed..., with galvanic separation between the primary circuit and the secondary circuit.

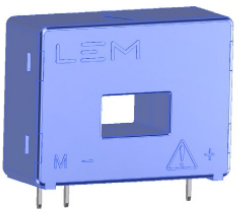

Electrical data

I_{PN}	Primary nominal RMS current			50			A
I_{PM}	Primary current, measuring range			0 … ±70			A
R_M	Measuring resistance		@ T_A = 70 °C		T_A = 85 °C		
			$R_{M\,min}$	$R_{M\,max}$	$R_{M\,min}$	$R_{M\,max}$	
	with ±12 V	@ ±50 A_{max}	10	100	60	95	Ω
		@ ±70 A_{max}	10	50	60 [1]	60 [1]	Ω
	with ±15 V	@ ±50 A_{max}	50	160	135	155	Ω
		@ ±70 A_{max}	50	90	135 [2]	135 [2]	Ω
I_{SN}	Secondary nominal RMS current			50			mA
N_P/N_S	Turns ratio			1 : 1000			
U_C	Supply voltage (±5 %)			±12 ... 15			V
			Min	Typ	Max		
I_C	Current consumption	@ ±15 V	8 + I_S	10 + I_S	12 + I_S		mA

Accuracy - Dynamic performance data

ε	Error @ I_{PN}, T_A = 25 °C	@ ±15 V (±5 %)	±0.65		%
		@ ±12 … 15 V (±5 %)	±0.90		%
ε_L	Linearity error		< 0.15		%
			Typ	Max	
I_{OE}	Electrical offset current @ I_P = 0, T_A = 25 °C			±0.2	mA
I_{OM}	Magnetic offset current [3] @ I_P = 0 and specified R_M, after an overload of 3 × I_{PN}			±0.3	mA
I_{OT}	Temperature variation of I_O	−25 °C … +85 °C	±0.1	±0.6	mA
		−40 °C … −25 °C	±0.2	±1.0	mA
$t_{D\,10}$	Delay time to 10 % of the final output value for I_{PN} step			< 500	ns
$t_{D\,90}$	Delay time to 90 % of the final output value for I_{PN} step [4]			< 1	µs
BW	Frequency bandwidth (−1 dB)		DC … 200		kHz

General data

T_A	Ambient operating temperature		−40 … +85	°C
$T_{A\,st}$	Ambient storage temperature		−40 … +90	°C
R_S	Resistance of secondary winding	@ T_A = 70 °C	80	Ω
		@ T_A = 85 °C	85	Ω
m	Mass		18	g
	Standards		EN 50178: 1997	
			UL 508: 2010	

Notes: [1] Measuring range limited to ±60 A_{max}
[2] Measuring range limited to ±55 A_{max}
[3] Result of the coercive field of the magnetic circuit
[4] For a di/dt = 200 A/µs.

Features

- Closed loop (compensated) current transducer using the Hall effect
- Insulating plastic case recognized according to UL 94-V0.

Advantages

- Excellent accuracy
- Very good linearity
- Low temperature drift
- Optimized response time
- Wide frequency bandwidth
- No insertion losses
- High immunity to external interference
- Current overload capability.

Applications

- AC variable speed drives and servo motor drives
- Static converters for DC motor drives
- Battery supplied applications
- Uninterruptible Power Supplies (UPS)
- Switched Mode Power Supplies (SMPS)
- Power supplies for welding applications.

Application domain

- Industrial.

LEM International SA
Route du Nant-d'Avril, 152
1217 Meyrin
www.lem.com

Current Transducer LA 55-P

Insulation coordination

U_d	RMS voltage for AC insulation test, 50 Hz/1 min	2.5	kV
U_{Ni}	Impulse withstand voltage 1.2/50 µs	5.7	kV
		Min	
d_{Cp}	Creepage distance	5	mm
d_{Cl}	Clearance	5	mm
CTI	Comparative tracking index (group I)	600	

Applications examples

According to **EN 50178 and IEC 61010-1 standards** and following conditions:

- Over voltage category OV 3
- Pollution degree PD2
- Non-uniform field

	EN 50178	IEC 61010-1
d_{Cp}, d_{Cl}, U_{Ni}	Rated insulation voltage	Nominal voltage
Basic insulation	300 V	300 V
Reinforced insulation	150 V	150 V

Safety

This transducer must be used in limited-energy secondary circuits according to IEC 61010-1.

This transducer must be used in electric/electronic equipment with respect to applicable standards and safety requirements in accordance with the manufacturer's operating instructions.

Caution, risk of electrical shock

When operating the transducer, certain parts of the module can carry hazardous voltage (eg. primary busbar, power supply).
Ignoring this warning can lead to injury and/or cause serious damage.
This transducer is a build-in device, whose conducting parts must be inaccessible after installation.
A protective housing or additional shield could be used.
Main supply must be able to be disconnected.

6July2023/Version 19

LEM International SA
Route du Nant-d'Avril, 152
1217 Meyrin
www.lem.com

Dimensions LA 55-P (in mm)

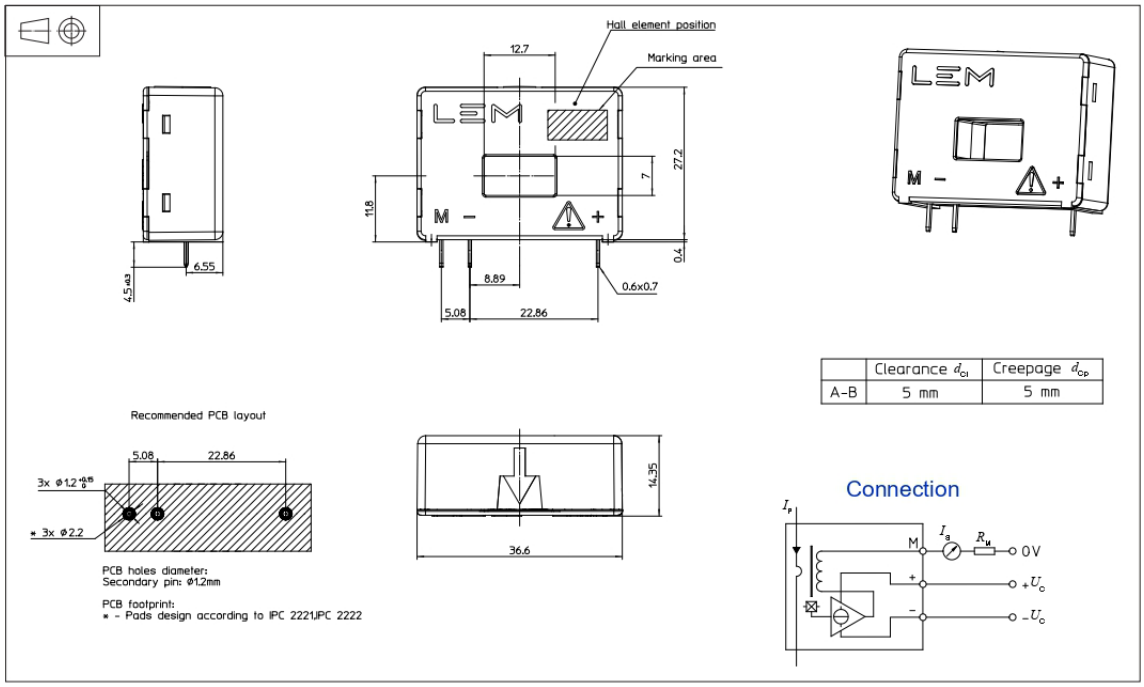

Mechanical characteristics

• General tolerance	±0.2 mm
• Primary through-hole	12.7 × 7 mm
• Fastening & connection of secondary	3 pins 0.6 × 0.7 mm
• Recommended PCB hole	⌀ 1.2 mm

Remarks

- I_S is positive when I_P flows in the direction of the arrow.
- Temperature of the primary conductor should not exceed 90 °C.
- Installation of the transducer must be done unless otherwise specified on the datasheet, according to LEM Transducer Generic Mounting Rules. Please refer to LEM document N°ANE120504 available on our Web site: **https://www.lem.com/en/file/3137/download.**
- Dynamic performances (di/dt and delay time) are best with a single bar completely filling the primary hole.
- In order to achieve the best magnetic coupling, the primary windings have to be wound over the top edge of the device.
- This is a standard model. For different versions (supply voltages, turns ratios, unidirectional measurements...), please contact us.

6July2023/Version 19

LEM International SA
Route du Nant-d'Avril, 152
1217 Meyrin
www.lem.com

Mouser Electronics

Authorized Distributor

Click to View Pricing, Inventory, Delivery & Lifecycle Information:

LEM:

LA 55-P

Appendix E: ACS 712 Current sensor

ALLEGRO microsystems

ACS712

Fully Integrated, Hall-Effect-Based Linear Current Sensor IC with 2.4 kV_{RMS} Isolation and a Low-Resistance Current Conductor

FEATURES AND BENEFITS

- Low-noise analog signal path
- Device bandwidth is set via the new FILTER pin
- 5 µs output rise time in response to step input current
- 80 kHz bandwidth
- Total output error 1.5% at T_A = 25°C
- Small footprint, low-profile SOIC-8 package
- 1.2 mΩ internal conductor resistance
- 2.4 kV_{RMS} minimum isolation voltage from pins 1-4 to pins 5-8
- 5.0 V, single supply operation
- 66 to 185 mV/A output sensitivity
- Output voltage proportional to AC or DC currents
- Factory-trimmed for accuracy
- Extremely stable output offset voltage
- Nearly zero magnetic hysteresis
- Ratiometric output from supply voltage

TÜV America
Certificate Number:
U8V 15 05 54214 038
CB 13 06 54214 026

PACKAGE: 8-Lead SOIC (suffix LC)

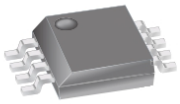

Not to scale

DESCRIPTION

The Allegro™ ACS712 provides economical and precise solutions for AC or DC current sensing in industrial, commercial, and communications systems. The device package allows for easy implementation by the customer. Typical applications include motor control, load detection and management, switch-mode power supplies, and overcurrent fault protection. The device is not intended for automotive applications.

The device consists of a precise, low-offset, linear Hall circuit with a copper conduction path located near the surface of the die. Applied current flowing through this copper conduction path generates a magnetic field which the Hall IC converts into a proportional voltage. Device accuracy is optimized through the close proximity of the magnetic signal to the Hall transducer. A precise, proportional voltage is provided by the low-offset, chopper-stabilized BiCMOS Hall IC, which is programmed for accuracy after packaging.

The output of the device has a positive slope (>$V_{IOUT(Q)}$) when an increasing current flows through the primary copper conduction path (from pins 1 and 2, to pins 3 and 4), which is the path used for current sampling. The internal resistance of this conductive path is 1.2 mΩ typical, providing low power loss. The thickness of the copper conductor allows survival of

Continued on the next page…

Typical Application

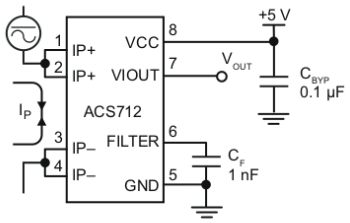

Application 1. The ACS712 outputs an analog signal, V_{OUT}, that varies linearly with the uni- or bi-directional AC or DC primary sampled current, I_P, within the range specified. C_F is recommended for noise management, with values that depend on the application.

ACS712

Fully Integrated, Hall-Effect-Based Linear Current Sensor IC with 2.4 kV_{RMS} Isolation and a Low-Resistance Current Conductor

DESCRIPTION (continued)

the device at up to 5× overcurrent conditions. The terminals of the conductive path are electrically isolated from the signal leads (pins 5 through 8). This allows the ACS712 to be used in applications requiring electrical isolation without the use of opto-isolators or other costly isolation techniques.

The ACS712 is provided in a small, surface mount SOIC8 package. The leadframe is plated with 100% matte tin, which is compatible with standard lead (Pb) free printed circuit board assembly processes. Internally, the device is Pb-free, except for flip-chip high-temperature Pb-based solder balls, currently exempt from RoHS. The device is fully calibrated prior to shipment from the factory.

SELECTION GUIDE

Part Number	Packing [1]	T_A (°C)	Current Sensing Range, I_P (A)	Sensitivity, Sens (Typ) (mV/A)
-S VARIANT [2]				
ACS712ELCTR-20A-S	Tape and reel, 3000 pieces/reel	–40 to 85	±20	100
ACS712ELCTR-30A-S	Tape and reel, 3000 pieces/reel	–40 to 85	±30	66
-T VARIANT [3]				
ACS712ELCTR-05B-T	Tape and reel, 3000 pieces/reel	–40 to 85	±5	185
ACS712ELCTR-20A-T	Tape and reel, 3000 pieces/reel	–40 to 85	±20	100
ACS712ELCTR-30A-T	Tape and reel, 3000 pieces/reel	–40 to 85	±30	66

[1] Contact Allegro for additional packing options.
[2] -S denotes the lead-free construction with tin-silver-based solder bumps.
[3] -T denotes Pb-contained construction with Pb-based solder bumps. Operating performance of -T and -S devices are identical. -T devices are RoHS compliant using allowed exemptions provided in Annex III and IV of Directive 2011/65/EU [Exemptions 7(a), 15, 15(a), as applicable].

ABSOLUTE MAXIMUM RATINGS

Characteristic	Symbol	Notes	Rating	Units
Supply Voltage	V_{CC}		8	V
Reverse Supply Voltage	V_{RCC}		–0.1	V
Output Voltage	V_{IOUT}		8	V
Reverse Output Voltage	V_{RIOUT}		–0.1	V
Output Current Source	$I_{IOUT(Source)}$		3	mA
Output Current Sink	$I_{IOUT(Sink)}$		10	mA
Overcurrent Transient Tolerance	I_P	1 pulse, 100 ms	100	A
Nominal Operating Ambient Temperature	T_A	Range E	–40 to 85	°C
Maximum Junction Temperature	T_J(max)		165	°C
Storage Temperature	T_{stg}		–65 to 170	°C

ALLEGRO microsystems
Allegro MicroSystems
955 Perimeter Road
Manchester, NH 03103-3353 U.S.A.
www.allegromicro.com

ISOLATION CHARACTERISTICS

Characteristic	Symbol	Notes	Rating	Unit
Withstand Voltage [1]	V_{ISO}	Agency rated for 60 seconds per UL 62368-1 (edition 3)	2400	V_{RMS}
Working Voltage for Basic Isolation	V_{WVBI}	Maximum approved working voltage for basic (single) isolation according to UL 62368-1 (edition 3)	420	V_{PK} or V_{DC}
			297	V_{RMS}
Impulse Withstand Voltage	$V_{IMPULSE}$	Tested ±5 pulses at 2/minute in compliance to IEC 61000-4-5, 1.2 µs (rise)/ 50 µs (width)	4000	V_{PK}
Clearance	D_{CL}	Minimum distance through air from IP leads to signal leads.	4	mm
Creepage	D_{CR}	Minimum distance along package body from IP leads to signal leads	4	mm
Distance Through Insulation	DTI	Minimum internal distance through insulation	63	µm
Comparative Tracking Index	CTI	Material Group II	400 to 599	V

[1] 100% Production-tested for 1 second in accordance with UL 62368-1 (edition 3).

Parameter	Specification
Fire and Electric Shock	CAN/CSA-C22.2 No. 60950-1-03 UL 60950-1:2003 EN 60950-1:2001

Allegro MicroSystems
955 Perimeter Road
Manchester, NH 03103-3353 U.S.A.
www.allegromicro.com

Appendix F: B25 Voltage sensor

Voltage Detection Sensor Module 25V

Basics

The Arduino analog input is limited to a 5 VDC input. If you wish to measure higher voltages, you will need to resort to another means. One way is to use a voltage divider. The one discussed here is found all over Amazon and eBay.

It is fundamentally a 5:1 voltage divider using a 30K and a 7.5K Ohm resistor.

Keep in mind, you are restricted to voltages that are less than 25 volts. More than that and you will exceed the voltage limit of your Arduino input.

Basic Connection

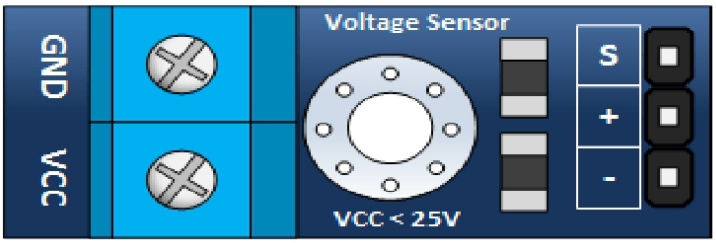

Inputs

- **GND –** This is where you connect the low side of the voltage you are measuring. Caution! : This is the same electrical point as your Arduino ground.
- **VCC:** The is where you connect the high side of the voltage you are measuring

Outputs

- **S:** This connects to your Arduino analog input.
- **– (or minus):** This connects to your Arduino ground.
- **+:** This is not connected. It does absolutely nothing… zilch… nada… jack diddly doo doo.

Schematic

The schematic for this is pretty straight forward. As previously mentioned, its just a couple of resistors. In fact, you could build your own in a pinch.

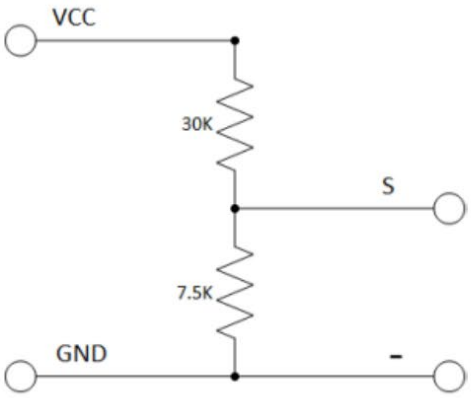

Tutorial

The Connections

Find yourself a 9 volt battery and connect it, your voltage sensor module and Arduino as shown below.

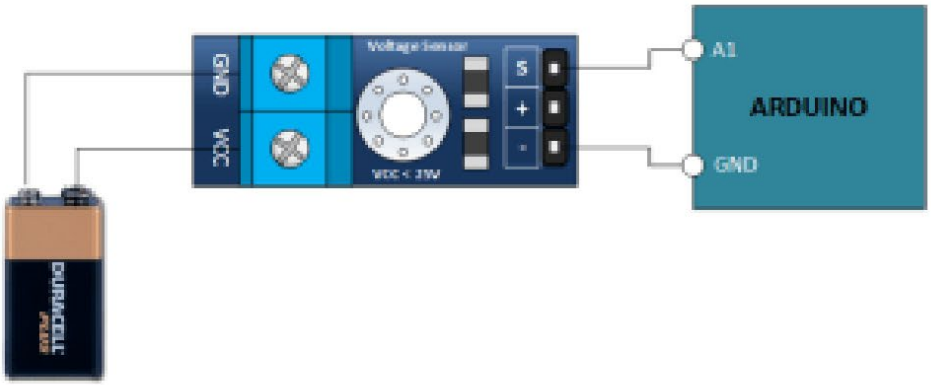

Appendix J: LM35 Temperature sensor

LM35 Precision Centigrade Temperature Sensors

FEATURES

- **Calibrated Directly in ° Celsius (Centigrade)**
- **Linear + 10 mV/°C Scale Factor**
- **0.5°C Ensured Accuracy (at +25°C)**
- **Rated for Full −55°C to +150°C Range**
- **Suitable for Remote Applications**
- **Low Cost Due to Wafer-Level Trimming**
- **Operates from 4 to 30 V**
- **Less than 60-µA Current Drain**
- **Low Self-Heating, 0.08°C in Still Air**
- **Nonlinearity Only ±¼°C Typical**
- **Low Impedance Output, 0.1 W for 1 mA Load**

DESCRIPTION

The LM35 series are precision integrated-circuit temperature sensors, with an output voltage linearly proportional to the Centigrade temperature. Thus the LM35 has an advantage over linear temperature sensors calibrated in ° Kelvin, as the user is not required to subtract a large constant voltage from the output to obtain convenient Centigrade scaling. The LM35 does not require any external calibration or trimming to provide typical accuracies of ±¼°C at room temperature and ±¾°C over a full −55°C to +150°C temperature range. Low cost is assured by trimming and calibration at the wafer level. The low output impedance, linear output, and precise inherent calibration of the LM35 make interfacing to readout or control circuitry especially easy. The device is used with single power supplies, or with plus and minus supplies. As the LM35 draws only 60 µA from the supply, it has very low self-heating of less than 0.1°C in still air. The LM35 is rated to operate over a −55°C to +150°C temperature range, while the LM35C is rated for a −40°C to +110°C range (−10° with improved accuracy). The LM35 series is available packaged in hermetic TO transistor packages, while the LM35C, LM35CA, and LM35D are also available in the plastic TO-92 transistor package. The LM35D is also available in an 8-lead surface-mount small-outline package and a plastic TO-220 package.

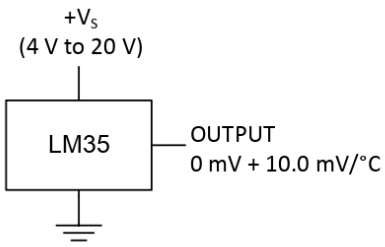

Figure 1. Basic Centigrade Temperature Sensor (+2°C to +150°C)

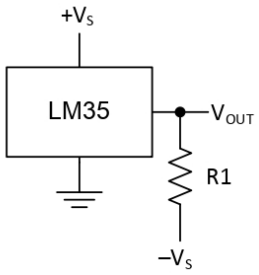

Choose $R_1 = -V_S / 50\ \mu A$
$V_{OUT} = 1500$ mV at 150°C
$V_{OUT} = 250$ mV at 25°C
$V_{OUT} = -550$ mV at −55°C

Figure 2. Full-Range Centigrade Temperature Sensor

These devices have limited built-in ESD protection. The leads should be shorted together or the device placed in conductive foam during storage or handling to prevent electrostatic damage to the MOS gates.

CONNECTION DIAGRAMS

METAL CAN PACKAGE
TO (NDV)

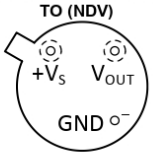

Case is connected to negative pin (GND)

SMALL-OUTLINE MOLDED PACKAGE
SOIC-8 (D)
TOP VIEW

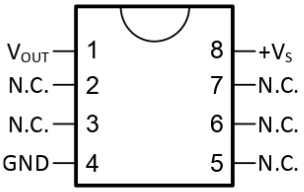

N.C. = No connection

PLASTIC PACKAGE
TO-92 (LP)
BOTTOM VIEW

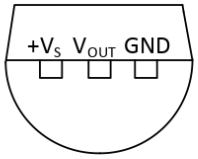

PLASTIC PACKAGE
TO-220 (NEB)

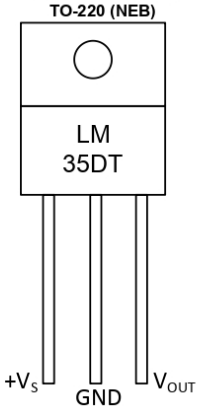

Tab is connected to the negative pin (GND).

NOTE: The LM35DT pinout is different than the discontinued LM35DP

Appendix H: DS18B20

PRELIMINARY

DALLAS SEMICONDUCTOR

DS18B20
Programmable Resolution 1-Wire® Digital Thermometer

www.dalsemi.com

FEATURES

- Unique 1-Wire interface requires only one port pin for communication
- Multidrop capability simplifies distributed temperature sensing applications
- Requires no external components
- Can be powered from data line. Power supply range is 3.0V to 5.5V
- Zero standby power required
- Measures temperatures from -55°C to +125°C. Fahrenheit equivalent is -67°F to +257°F
- ±0.5°C accuracy from -10°C to +85°C
- Thermometer resolution is programmable from 9 to 12 bits
- Converts 12-bit temperature to digital word in 750 ms (max.)
- User-definable, nonvolatile temperature alarm settings
- Alarm search command identifies and addresses devices whose temperature is outside of programmed limits (temperature alarm condition)
- Applications include thermostatic controls, industrial systems, consumer products, thermometers, or any thermally sensitive system

PIN ASSIGNMENT

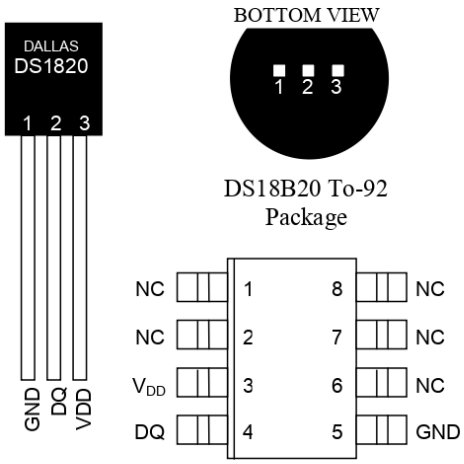

DS18B20 To-92 Package

DS18B20Z
8-Pin SOIC (150 mil)

PIN DESCRIPTION

GND - Ground
DQ - Data In/Out
V_{DD} - Power Supply Voltage
NC - No Connect

DESCRIPTION

The DS18B20 Digital Thermometer provides 9 to 12-bit (configurable) temperature readings which indicate the temperature of the device.

Information is sent to/from the DS18B20 over a 1-Wire interface, so that only one wire (and ground) needs to be connected from a central microprocessor to a DS18B20. Power for reading, writing, and performing temperature conversions can be derived from the data line itself with no need for an external power source.

Because each DS18B20 contains a unique silicon serial number, multiple DS18B20s can exist on the same 1-Wire bus. This allows for placing temperature sensors in many different places. Applications where this feature is useful include HVAC environmental controls, sensing temperatures inside buildings, equipment or machinery, and process monitoring and control.

DETAILED PIN DESCRIPTION Table 1

PIN 8PIN SOIC	PIN TO92	SYMBOL	DESCRIPTION
5	1	GND	Ground.
4	2	DQ	**Data Input/Output pin.** For 1-Wire operation: Open drain. (See "Parasite Power" section.)
3	3	V_{DD}	**Optional V_{DD} pin.** See "Parasite Power" section for details of connection. V_{DD} must be grounded for operation in parasite power mode.

DS18B20Z (8-pin SOIC): All pins not specified in this table are not to be connected.

OVERVIEW

The block diagram of Figure 1 shows the major components of the DS18B20. The DS18B20 has four main data components: 1) 64-bit lasered ROM, 2) temperature sensor, 3) nonvolatile temperature alarm triggers TH and TL, and 4) a configuration register. The device derives its power from the 1-Wire communication line by storing energy on an internal capacitor during periods of time when the signal line is high and continues to operate off this power source during the low times of the 1-Wire line until it returns high to replenish the parasite (capacitor) supply. As an alternative, the DS18B20 may also be powered from an external 3 volt - 5.5 volt supply.

Communication to the DS18B20 is via a 1-Wire port. With the 1-Wire port, the memory and control functions will not be available before the ROM function protocol has been established. The master must first provide one of five ROM function commands: 1) Read ROM, 2) Match ROM, 3) Search ROM, 4) Skip ROM, or 5) Alarm Search. These commands operate on the 64-bit lasered ROM portion of each device and can single out a specific device if many are present on the 1-Wire line as well as indicate to the bus master how many and what types of devices are present. After a ROM function sequence has been successfully executed, the memory and control functions are accessible and the master may then provide any one of the six memory and control function commands.

One control function command instructs the DS18B20 to perform a temperature measurement. The result of this measurement will be placed in the DS18B20's scratch-pad memory, and may be read by issuing a memory function command which reads the contents of the scratchpad memory. The temperature alarm triggers TH and TL consist of 1 byte EEPROM each. If the alarm search command is not applied to the DS18B20, these registers may be used as general purpose user memory. The scratchpad also contains a configuration byte to set the desired resolution of the temperature to digital conversion. Writing TH, TL, and the configuration byte is done using a memory function command. Read access to these registers is through the scratchpad. All data is read and written least significant bit first.

DS18B20 BLOCK DIAGRAM Figure 1

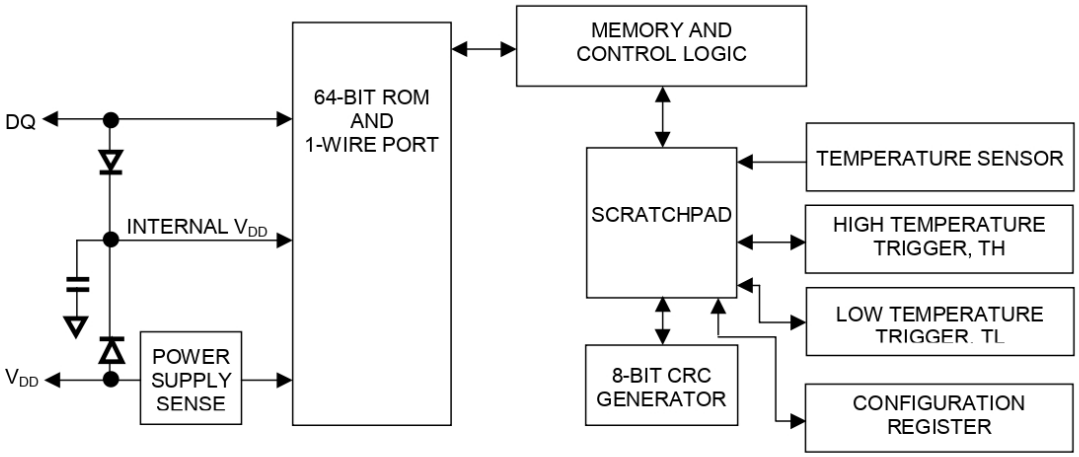

PARASITE POWER

The block diagram (Figure 1) shows the parasite-powered circuitry. This circuitry "steals" power whenever the DQ or V_{DD} pins are high. DQ will provide sufficient power as long as the specified timing and voltage requirements are met (see the section titled "1-Wire Bus System"). The advantages of parasite power are twofold: 1) by parasiting off this pin, no local power source is needed for remote sensing of temperature, and 2) the ROM may be read in absence of normal power.

In order for the DS18B20 to be able to perform accurate temperature conversions, sufficient power must be provided over the DQ line when a temperature conversion is taking place. Since the operating current of the DS18B20 is up to 1.5 mA, the DQ line will not have sufficient drive due to the 5k pullup resistor. This problem is particularly acute if several DS18B20s are on the same DQ and attempting to convert simultaneously.

There are two ways to assure that the DS18B20 has sufficient supply current during its active conversion cycle. The first is to provide a strong pullup on the DQ line whenever temperature conversions or copies to the E^2 memory are taking place. This may be accomplished by using a MOSFET to pull the DQ line directly to the power supply as shown in Figure 2. The DQ line must be switched over to the strong pull-up within 10 μs maximum after issuing any protocol that involves copying to the E^2 memory or initiates temperature conversions. When using the parasite power mode, the V_{DD} pin must be tied to ground.

Another method of supplying current to the DS18B20 is through the use of an external power supply tied to the V_{DD} pin, as shown in Figure 3. The advantage to this is that the strong pullup is not required on the DQ line, and the bus master need not be tied up holding that line high during temperature conversions. This allows other data traffic on the 1-Wire bus during the conversion time. In addition, any number of DS18B20s may be placed on the 1-Wire bus, and if they all use external power, they may all simultaneously perform temperature conversions by issuing the Skip ROM command and then issuing the Convert T command. Note that as long as the external power supply is active, the GND pin may not be floating.

The use of parasite power is not recommended above 100°C, since it may not be able to sustain communications given the higher leakage currents the DS18B20 exhibits at these temperatures. For applications in which such temperatures are likely, it is strongly recommended that V_{DD} be applied to the DS18B20.

Appendix I: Irradiation sensor PYR 20

2 Introduction

PYR20 pyranometer, or solar Radiation Sensor, measures global radiation of both direct and diffusion of solar irradiance. The internal temperature compensation minimizing the error caused by heating of the sensor. Each sensor is calibrated against Eppley Precision Spectral Pyranometer and offers excellent accuracy and consistency. The sensor is applicable for science research, solar power , greenhouse, weather station etc.

- Measurement range to 2000W/m2, Spectral range 400-1100nm
- Output interface with RS485, Voltage or Current
- Temperature compensated
- Level indicator and spring loaded for installation
- Water proof to IP66 can be used outdoor
- High accuracy and consistency with excellent stability
- Reverse power protection and Built-in TVS/ESD protection

Specifications			
Output Interface	Analog Voltage 0-2V (Output resistance ~0ohm)	Analog Current 4-20mA (Load Resistor<500ohm)	RS485 Modbus-RTU
Power Supply	3.9-30V/DC	12-30V/DC	3.9-30V/DC
Power Consumption	7mA@24V DC	30mA@24V DC (with 20mA output signal)	7mA@24V DC
Pyr Range	Range:0-2000W/m2, Accuracy 5%, Resolution:1W/m2		
Spectral Range	400-1100nm		
Direction Error	Percent of reading: ±3% (0 - ±70°); ±10% (±70 - ±85°)		
IP Ratings	IP66		
Operating Temperature	-40~85℃		
Installation	Screw hole * 3		
Cable Length	2 meters, or Customize		
Dimension	75*55*58mm		

3 Wiring diagrams

Type	Wiring diagram
Analog Voltage Output	Red (V+): Power Supply + Black (G): Power Supply - Blue (O1): Analog Output 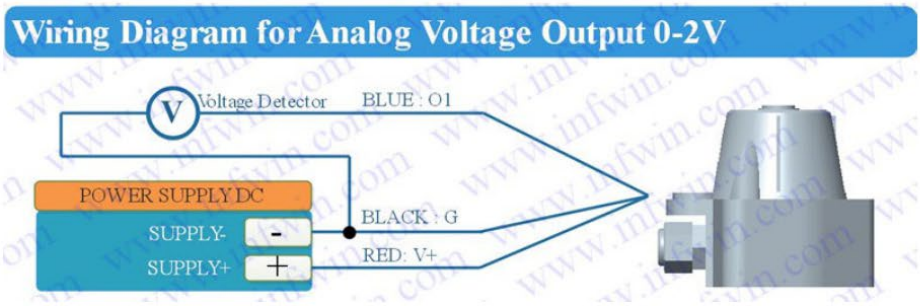
Analog Current Output	Red (V+): Power Supply + Black (G): Power Supply - Blue (O1): Analog Output 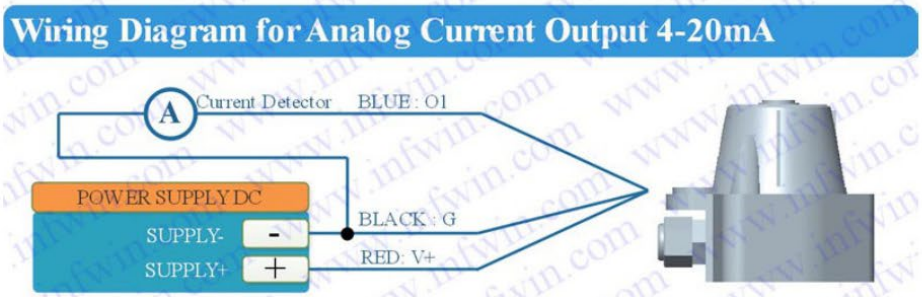
RS485 Modbus	Red (V+): Power Supply + Black (G): Power Supply - Yellow (T+): RS485+/A/T+ White (T-): RS485-/B/T-

Wiring Diagram for RS485 Modbus

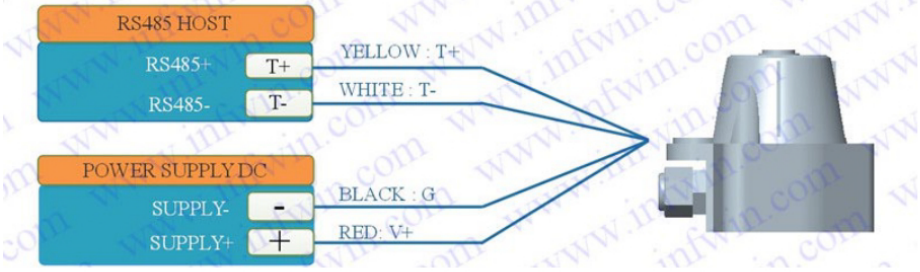

ALL RS485 communication parameters (Mosbus Slave Address, baudrate, parity, databits, stopbits) are set in internal register and can be saved when power down, the factory setting is ADDRESS=1, BAUDRATE=9600bps,PARITY=NONE, DATABITS=8bits, STOPBITS=1bit;

Sometimes you may FORGET the communication settings, In this case, you can open the shield module and press the SET button for more that 3 seconds, then all the communication parameters reset to factory setting, then communicating with the sensor using the factory setting to set your desired settings. Please re-power up the sensor to make the settings effective.